Chem Soc Rev

REVIEW ARTICLE

View Article Online
View Journal

Check for updates

Cite this: DOI: 10.1039/d5cs00531k

Transfer and beyond: emerging strategies and trends in two-dimensional material device fabrication

Gang Huang,†[ab] Ruosi Chen,†[c] Mingxi Chen,†[d] Xianfeng Chen,[bd] Mengting Jiang,[d] Yu Xing,[b] Jiang Wang,[d] Boqun Liang,[e] Qiushi Liu,[f] Xiangdong Li,[g] Chit Siong Lau,[bd] Xiaonan Dong,[hi] Piyush Agarwal,[d] Lin Ke,[d] Syed M Assad,[bd] Jian-Rui Soh,[bd] James Lourembam,[d] Young-Wook Cho,[bd] Qingcheng Liang,*[a] Jian Li,*[j] Xiao Zhang,*[k] Yuan Ma,*[k] Yuerui Lu,*[c] Ping Koy Lam*[bd] and Xuezhi Ma*[bd]

The field of two-dimensional (2D) materials has seen remarkable progress, driven by their exceptional electronic, optical, and mechanical properties. In addition to their intrinsic qualities, 2D materials are atomically thin and readily integrated with a wide range of devices, offering immense potential for next-generation on-chip technologies across various domains, beyond just electronics and optics. Central to the fabrication of 2D devices is the development of effective transfer methods, which are crucial for maintaining clean material interfaces and intact material properties. However, as some of the most fundamental techniques, transfer methods are incredibly diverse, making it challenging to navigate the various approaches. This review provides a comprehensive analysis of the state-of-the-art transfer methods, including a preliminary discussion on high-quality 2D material preparation, along with evaluation of the strengths and weaknesses of various transfer techniques. Furthermore, despite being a foundational field, there are still many significant tasks to be undertaken, with several bottlenecks awaiting breakthroughs. We also highlight emerging trends, such as reconfigurable transfer, all-transfer for chip manufacturing, and the application of transfer techniques to low-dimensional materials across broader research fields, such as chemistry, polariton, tribology, haptics, thermal transport, thermodynamic control, quantum science, neuromorphic computing, electrocatalysts, and energy, offering insights into future directions for 2D material integration.

Received 30th August 2025

DOI: 10.1039/d5cs00531k

rsc.li/chem-soc-rev

Open Access Article. Published on 06 January 2026. Downloaded on 1/16/2026 12:17:14 PM.
This article is licensed under a Creative Commons Attribution-NonCommercial 3.0 Unported Licence.

1. Introduction

Since the groundbreaking mechanical exfoliation of single-layer graphene in 2004,[1] two-dimensional (2D) materials have garnered immense scientific interest due to their exceptional electronic, optical, and mechanical properties. These atomically thin materials exhibit a unique combination of weak interlayer van der Waals (vdW) forces and strong intralayer

[a] School of Materials Science and Engineering, Changchun University of Science and Technology, Changchun, 130022, China. E-mail: liangqingcheng@cust.edu.cn
[b] Quantum Innovation Centre (Q. InC), Agency for Science, Technology and Research (A*STAR), 4 Fusionopolis Way, Kinesis, #05, Singapore, 138635, Republic of Singapore. E-mail: pingkoy@a-star.edu.sg, ma_xuezhi@a-star.edu.sg
[c] School of Engineering, College of Engineering and Computer Science, The Australian National University, Canberra, Australian Capital Territory 2601, Australia. E-mail: yuerui.lu@anu.edu.au
[d] Institute of Materials Research and Engineering (IMRE), Agency for Science, Technology and Research (A*STAR), 2 Fusionopolis Way, Innovis, #08-03, Singapore 138634, Republic of Singapore
[e] Materials Science and Engineering program, University of California-Riverside, Riverside, California 92521, United States
[f] Shanghai Institute of Optics and Fine Mechanics, Chinese Academy of Sciences, Shanghai, 201800, China
[g] Guangzhou Wide Bandgap Semiconductor Innovation Center, Guangzhou Institute of Technology, Xidian University, Guangzhou 510555, China
[h] Life and Health Institute, China Resources Research Institute of Science and Technology Company Ltd, Hong Kong S.A.R., China
[i] School of Biomedical Sciences, LSK Faculty of Medicine, the University of Hong Kong, Hong Kong S.A.R., China
[j] State Key Lab of Analytical Chemistry for Life Science, School of Chemistry and Chemical Engineering, Nanjing University, Nanjing 210023, China. E-mail: jianli@nju.edu.cn
[k] Department of Mechanical Engineering, The Hong Kong Polytechnic University, Hong Kong 999077, China. E-mail: xiao1.zhang@polyu.edu.hk, y.ma@polyu.edu.hk
† Co-first authors.

Open Access Article. Published on 06 January 2026. Downloaded on 1/16/2026 12:17:14 PM.
This article is licensed under a Creative Commons Attribution-NonCommercial 3.0 Unported Licence.

covalent bonds, enabling the stacking of diverse atomic layers into vdW heterostructures without lattice-matching constraints.[2,3] The discovery of additional 2D materials, such as transition metal dichalcogenides (TMDCs) and hexagonal boron nitride (h-BN), has further enriched this material platform, paving the way for multifunctional electronic,[4,5] photonic,[6,7] and quantum devices.[8] Despite their atomic thickness, 2D materials often display pronounced three-dimensional heterogeneity, arising from variations in chemical bonding, interfacial interactions, and spatial defect distributions. These atomic scale nonuniformities can strongly influence material behavior, introducing anisotropic or emergent functionalities.

Gang Huang

Gang Huang is currently a Master's student at the School of Materials Science and Engineering, Changchun University of Science and Technology. His research focuses on the synthesis of low-dimensional semiconductor functional materials and the fabrication of related devices. At Q.InC, he has been involved in research on 2D material transfer and reconfigurable devices.

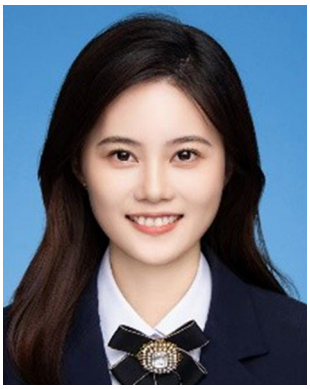

Ruosi Chen

Ruosi Chen is currently a PhD student at the School of Engineering, College of Engineering, Computing & Cybernetics, the Australian National University, Australia. Her research mainly engaged in the electrical and nonlinear optical properties of 2D materials, 2D electronic and optoelectronic devices, and 2D interface engineering combined with their applications in bio-emulation and artificial synapse and neuron fields.

Mingxi Chen

Mingxi Chen received his PhD in Chemistry from Tianjin University in 2021. He joined the Institute of Materials Research and Engineering (IMRE), ASTAR, Singapore the same year as a Scientist. His research focuses on the development of semiconductor materials for advanced electronic and optoelectronic devices.

Qingcheng Liang

Prof. Qingcheng Liang is a Full Professor of micro- and nano-electronic materials and devices at the Changchun University of Science and Technology (CUST). He has rich experiences in thin film transistor manufacturing and testing. In recent years, he has been mainly engaged in research on the preparation and applications of micro- and nano-semiconductor functional materials, devices, including the design and preparation of MXene gas and humidity sensors and photoelectric sensors.

Jian Li

Dr. Jian Li received his B.S. and PhD degrees in Chemistry from Nanjing University. He is currently an associate researcher at Nanjing University. His research focuses on plasmon enhanced chemistry, plasmon enhanced infrared spectroscopy and photo induced force microscopy.

Xiao Zhang

Prof. Xiao Zhang is an Assistant Professor in the Mechanical Department at the Hong Kong Polytechnic University. He is an expert in the fields of electrocatalysis, 2D nanomaterials, and carbon capture and conversion.

This journal is © The Royal Society of Chemistry 2025

Open Access Article. Published on 06 January 2026. Downloaded on 1/16/2026 12:17:14 PM.
This article is licensed under a Creative Commons Attribution-NonCommercial 3.0 Unported Licence.

Consequently, fabrication steps such as transfer, encapsulation, and interface engineering are inherently chemically sensitive processes that demand precise control. Treating these steps as delicate chemical operations is essential for unlocking the full performance and long-term stability of 2D material-based technologies.

To achieve high-performance 2D devices, it is essential to maintain both the intrinsic quality of the 2D materials and the cleanliness and flatness of their interfaces throughout the entire fabrication process. This involves two primary challenges: (1) producing high-quality, wafer-scale 2D films and flakes and (2) integrating them with various device platforms.

Two main approaches exist for producing 2D materials: top-down exfoliation and bottom-up growth. Top-down methods, such as mechanical exfoliation,[9,10] electrochemical delamination,[11] and liquid-phase exfoliation,[12] offer excellent material quality but are often limited by sample size and scalability. In contrast, bottom-up methods, including physical vapor deposition (PVD) and chemical vapor deposition (CVD),[13,14] offer better scalability but face challenges like uncontrolled nucleation, grain boundary formation, and lattice mismatch, which can degrade film quality.[15] Regardless of the approach, the ultimate goal remains the same: to produce large-scale 2D films with high crystallinity, low defect densities, and excellent transferability, enabling their seamless integration into wafer-scale devices. Achieving this goal requires not only precise control over the growth or exfoliation process but also innovative transfer techniques that preserve the chemical and structural integrity of the 2D materials.[16]

As 2D materials transition from fundamental research to practical applications,[17–19] the ability to precisely transfer these atomic-scale layers onto diverse substrates becomes increasingly critical. Effective transfer methods are essential for integrating 2D materials into complex heterostructures, minimizing contamination and preserving exceptional intrinsic properties, all of which are crucial for high-performance electronic, photonic, and quantum devices.

Earlier transfer approaches for building heterojunctions primarily relied on polymer supports, such as polymethyl methacrylate (PMMA). However, these methods often trap contaminants at the interfaces of 2D materials, diminishing the advantages of their unique properties. To overcome these limitations, dry methods such as the clean polydimethylsiloxane (PDMS) stamp method and capillary force assisted methods have been developed, offering improved interface cleanliness and more feasible protocols. After more than ten years of development, transfer methods have been optimized for different application scenarios. However, none of the current transfer methods are perfect and cannot accommodate all requirements at once. Our goal is therefore to provide a

Yuan Ma

Prof. Yuan Ma is an Assistant Professor in the Mechanical Department at the Hong Kong Polytechnic University. He is an expert in the fields of haptics, human-machine mechanical interface, sensors and actuators for wearable electronics, tribology, cross-scale and multi-physics modeling, and the applications of artificial intelligence (AI).

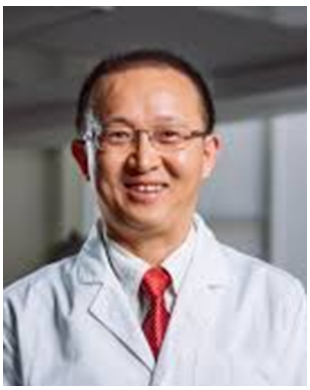

Yuerui Lu

Prof. Yuerui Lu from The Australian National University, who is an expert in nano-optics in 2D materials, especially focused on entangled photon pair generation using 2D materials and their homo- or hetero-structures. He is one of the pioneers in exploring 3R-MoS_2. His research interests also include twist electronics and optics, etc.

Ping Koy Lam

*Prof. Ping Koy Lam is the Chief Quantum Scientist at A*STAR, and a renowned experimental physicist in the research field of quantum information and metrology. His research work includes quantum optical state generation, quantum teleportation, quantum encryption, quantum opto-mechanics, quantum levitation, optical metrology, and quantum communications.*

Xuezhi Ma

*Dr. Xuezhi Ma is a Senior Scientist and group leader at the Quantum Innovation Centre (Q. InC), A*STAR. His background in physics and electrical engineering spans topics on quantum optics, quantum metrology polaritons, near-field optics, optical spectroscopy, nano-photonics, ultrafast optics, nonlinear optics, nanofabrication, 2D materials, and artificial intelligence.*

Open Access Article. Published on 06 January 2026. Downloaded on 1/16/2026 12:17:14 PM.
This article is licensed under a Creative Commons Attribution-NonCommercial 3.0 Unported Licence.

comprehensive review that will serve as a guide for entry-level researchers to get them started quickly and to recommend transfer methods that guarantee high in-plane and out-of-plane quality of 2D materials, while also being easy to use, depending on the application scenario. Additionally, considering that many research groups have their routinely used methods, we aim to introduce some advanced techniques, such as silicon nitride (SiN_x) membrane clean transfer,[20] ultraviolet (UV) tape wafer-scale transfer,[21] and graphene-mediated single-crystal oxide transfer,[22] to experts who typically rely on established techniques.

Beyond the fundamental role of transfer in integrating 2D materials into devices, these processes can also unlock unique physical phenomena by intentionally or unintentionally introducing structural deformations. These deformations, such as bending, twisting, and wrinkling, can serve as powerful tools for manipulating the electronic, optical, and mechanical properties of 2D materials, offering new avenues for device design and fundamental research.

In addition to reviewing established methods, we will explore emerging techniques such as reconfigurable transfer methods and the all-transfer approach for wafer-scale chip fabrication. Most of the currently available transfer methods focus on building a stack of 2D materials like building ''LEGO'' blocks.[23] However, a true ''LEGO'' functionality should also allow for disassembly and reassembly. Reconfigurable transfer methods, which enable the assembly, disassembly, and reassembly of 2D structures, offer a promising direction for exciting applications, such as the ''control variable method'' at the nanoscale. Moreover, the role of transfer methods in the manufacturing of future electrical and optical devices could expand significantly through all-transfer approaches.

The all-transfer strategy, wherein every device component—from active 2D semiconductors to electrodes, dielectrics, and even complete device stacks—is assembled by transfer rather than direct fabrication, marking a paradigm shift in 2D electronics. By eliminating lithography and harsh processing, it preserves intrinsic material quality, ensures pristine interfaces free from disorder and Fermi-level pinning, and enables scalable, low-cost, and high-performance device integration—offering a transformative route toward industrial adoption of 2D materials.

Finally, we have observed that transfer methods are already being applied in a variety of broader fields, such as in chemistry,[24] polaritonic devices,[25] phonon polaritons,[26] tribology,[27] haptics,[28] thermal transport,[29,30] thermodynamic control,[31] quantum devices,[8] neuromorphic computing,[32] electrocatalysts and energy.[33,34] We believe that transfer techniques will continue to play a significant role across many scientific disciplines, offering versatile solutions and broadening their impact in diverse areas of research and technology.

In summary, this review will provide a comprehensive summary on emerging transfer methods for 2D device fabrication. It begins with the preparation of 2D materials, focusing on wafer-scale approaches as a foundation for transfer techniques. We then provide a comprehensive assessment of transfer methods, including dry, wet, capillary force assisted, and emerging strategies such as UV tape-assisted and SiN_x membrane techniques. A radar chart is used to visualize and compare nine representative methods across multiple performance metrics. This section also covers the transfer of 2D and low-dimensional materials on arbitrary substrates, enabling diverse photonic and electronic integrations. In the third section, we explore multifunctionalities made possible by transfer techniques, such as strain, wrinkle, bubble, fold, and twist engineering—which unlock novel properties and device concepts. The perspective section highlights reconfigurable and all-transfer approaches as promising directions for next-generation device manufacturing. Finally, we reflect on the broader impact of transfer methods in fields such as chemistry, wearable electronics, quantum optics, and mechanics, offering insights into their transformative potential.

2. 2D material preparation

The preparation of 2D materials underpins their integration into electronic,[4,5] optoelectronic,[6,7] and quantum devices.[8] A wide spectrum of approaches broadly classified into top-down exfoliation methods, which isolate atomically thin layers from bulk crystals, and bottom-up synthesis techniques, which grow 2D films directly on substrates, have been developed. While the fundamentals of these preparation routes have been extensively reviewed elsewhere,[35–37] our aim is to provide a concise overview that frames the discussion for the central topic of this work: transfer strategies for low-dimensional materials in device fabrication, with a particular emphasis on scalability, wafer-level compatibility, and interfacial control during growth.

The quality and transfer readiness of 2D materials are strongly influenced by both interfacial chemistry, which governs the bonding between layers or between the film and its growth substrate, and surface chemistry, which determines terminal functional groups, surface charge, and defect states. For example, modifying interlayer bonding through ion or molecule intercalation can reduce exfoliation energy, while controlling surface terminations can improve compatibility with downstream processing. Furthermore, the interaction strength between the 2D layer and its substrate, shaped during synthesis, critically affects subsequent transfer efficiency, yield, and cleanliness.

This section therefore outlines the essential principles and representative examples of each preparation route, while highlighting the interplay between growth chemistry, interfacial engineering, and substrate interactions that ultimately dictate transfer performance in device fabrication.

2.1. Top-down methods

Micrometre-sized flakes, peeled off from layered natural minerals or synthetic bulk crystals, marked the beginning of a new era in 2D material research.[3–5,38] Top-down exfoliation methods, such as mechanical exfoliation,[9,10] chemical liquid-phase intercalation,[12] electrochemical exfoliation,[11]

 This journal is © The Royal Society of Chemistry 2025

Open Access Article. Published on 06 January 2026. Downloaded on 1/16/2026 12:17:14 PM.
This article is licensed under a Creative Commons Attribution-NonCommercial 3.0 Unported Licence.

and metal-assisted exfoliation,[39] rely on selectively weakening interlayer vdW interactions while preserving the in-plane chemical bond network. This approach maintains the intrinsic electronic structure, defect distribution, and surface chemical properties of the parent material, providing an ideal platform for studying the intrinsic physicochemical properties of 2D materials.

Effective exfoliation requires precise control over both interfacial chemistries, modifying interlayer bonding, often through ion or molecular intercalation, to reduce exfoliation energy and enhance layer separation and surface chemistry, which governs terminal functional groups, surface charge, and defect states, thereby influencing reactivity and compatibility with downstream device processing.

Traditional mechanical exfoliation offers simplicity and is typically performed by peeling 2D materials from high-quality layered crystals using an adhesion layer.[40,41] However, this method lacks precise control over the cleavage environment.[42] Issues such as random fracture and limited transferable area often arise due to non-conformal contact between the adhesion layer and the 2D material, uneven decoupling between the growth substrate and the 2D material, and uncontrolled bending stress.[43] For example, in 2015, Sutte, Huang *et al.* adopted plasma pretreatment to improve the stripping efficiency and size of 2D materials (Fig. 1a).[44] Before exfoliation, they used oxygen plasma to clean the contaminants adsorbed on the substrate from the environment to increase the adhesion between the substrate and the 2D material, and through thermal treatment, they maximized the contact area between the bulk crystals and the substrate.[39] While this method provides an effective way to exfoliate the high quality and relatively large size 2D flakes (several hundred micrometres),[45] it cannot be easily applied to wafer scale exfoliation.

To achieve larger flakes, emerging exfoliation methods, such as electrochemical exfoliation[46–49] and supercritical fluid exfoliation,[50–52] provide more precise chemical control by tuning thermodynamic (*e.g.*, electrode potential and solvation energy) and kinetic (*e.g.*, ion migration rate and solvent diffusion) parameters. These methods enable the introduction of

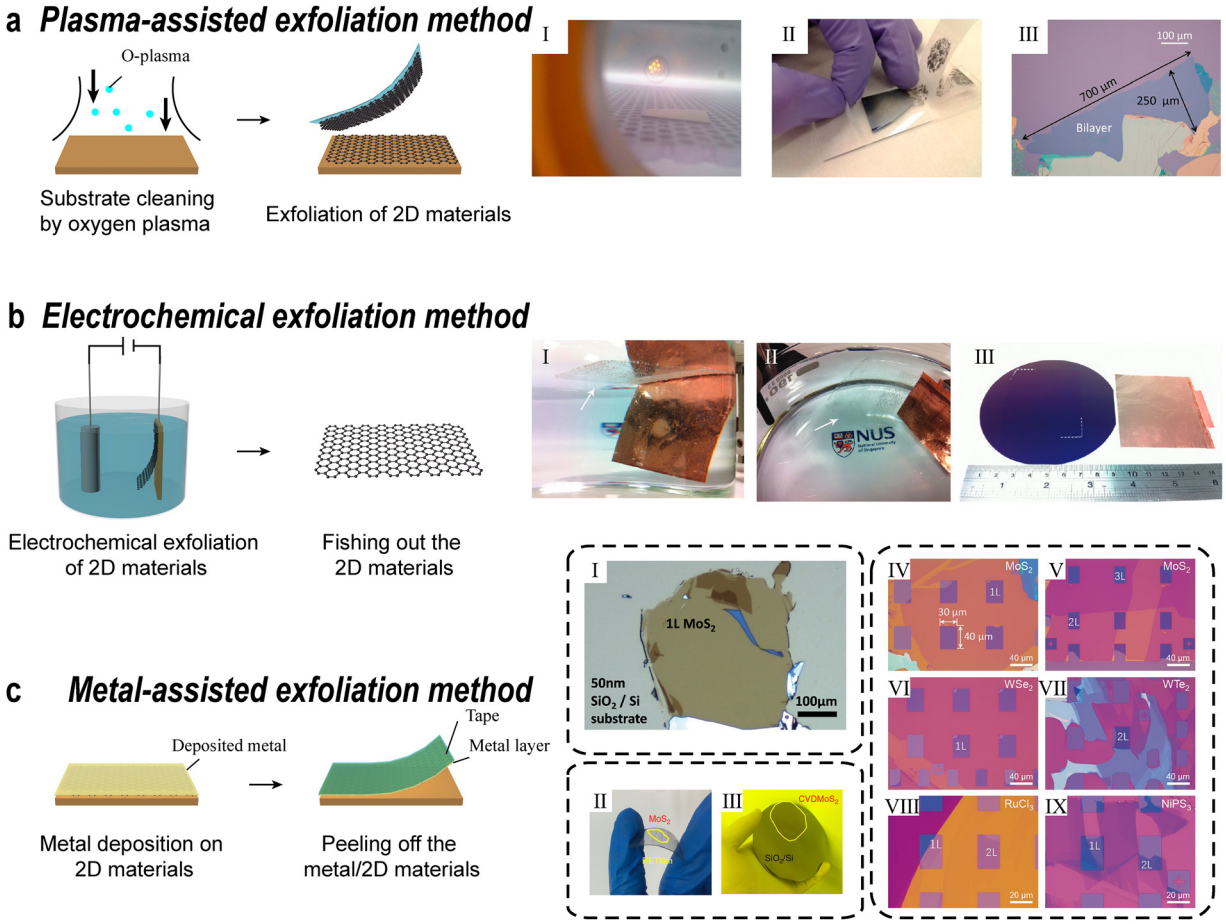

Fig. 1 Exfoliation of 2D materials. (a) Large size 2D material flake exfoliation method enabled by an oxygen plasma cleaned substrate. Reproduced from ref. 44 with permission from American Chemical Society, Copyright 2015. (b) Large area 2D material flake exfoliation by electrochemical methods. Reproduced from ref. 11 with permission from American Chemical Society, Copyright 2011. (c) Metal-assisted exfoliation method. Large flakes of 2D materials can be achieved (I–III). More interestingly, this method also enables the exfoliation with patterning (IV–IX). Adapted from ref. 39 according to Creative Commons Attribution 4.0 International License (CC BY 4.0). Reproduced from ref. 62 with permission from Wiley-VCH, Copyright 2016. Reproduced from ref. 56 with permission from Wiley-VCH, Copyright 2024.

Open Access Article. Published on 06 January 2026. Downloaded on 1/16/2026 12:17:14 PM.
This article is licensed under a Creative Commons Attribution-NonCommercial 3.0 Unported Licence.

specific surface groups or defect states, facilitating more customized material design for electronic, optoelectronic, and quantum device applications.

Liquid-phase exfoliation disperses bulk crystals in solution and induces delamination through either physical (*e.g.*, ultrasonication) or chemical (*e.g.*, electrochemical reactions) methods. While ultrasound can effectively separate layered materials, the violent cavitation bubbles it generates often fracture or degrade the nanosheets, compromising their structural integrity and electronic quality.[53] By contrast, electrochemical exfoliation offers tunable control *via* applied current and cutoff voltage, enabling a more deterministic process. Yet, the bubble-driven reactions readily oxidize and consume copper electrodes, hindering their recyclability and long-term scalability. This intrinsic limitation poses a significant barrier to the broader industrial deployment of electrochemical exfoliation (Fig. 1b).[11]

The metal-assisted exfoliation method is a more efficient exfoliation technique that can yield large flakes (Fig. 1c, Scheme and I–III). It does not require polymer materials as adhesives, thus avoiding the residue of polymers on the surface of 2D materials. Moreover, the metal film has greater mechanical strength and can better protect 2D materials from wrinkling or cracking. Since the development of the Cu-assisted transfer method by Lin *et al.* for the successful transfer of centimeter-sized MoS_2 films,[54] researchers have developed various metal-assisted exfoliation methods, such as Ni,[55] Au,[56] Ag,[57] *etc*.

Au-assisted exfoliation, one representative of metal-assisted approaches, has emerged as a promising strategy for obtaining large-area monolayer TMDCs, owing to the strong adhesive force between gold and 2D flakes.[58,59] However, the effectiveness of this method is highly dependent on the surface roughness of the gold film, which in turn is determined by the underlying deposition substrate.[60] To better understand the mechanism behind Au-assisted exfoliation, researchers conducted first-principles studies comparing the binding energies of Au–MoS_2 and MoS_2–MoS_2 interfaces.[61] It was revealed that the Au–MoS_2 interaction is governed by strong vdW forces rather than true chemical bonding. The role of gold surface roughness was also systematically investigated, showing its critical impact on exfoliation efficiency. Up to now, innovations such as a thermal release tape (TRT) tape have significantly enhanced the success of Au-assisted exfoliation, enabling the verified isolation of over 40 types of 2D materials.[39,62]

One of the most notable aspects of the Au-assisted exfoliation method is its ability to combine patterning with exfoliation, as demonstrated by Bao *et al.* through an Au template-assisted mechanical exfoliation strategy (Fig. 1c(IV)–(IX)).[56] This technique enables the production of atomically thin, large area 2D crystals while avoiding contamination associated with wet chemical processes. Additionally, it addresses the limitations of traditional dry transfer, such as the restricted variety and small size of materials. In addition to gold, silver has also been explored as an intermediate layer for large-area exfoliation of 2D semiconductors.[57] Both gold and silver are currently the most reliable auxiliary materials for assisted exfoliation. However, their high cost remains a major barrier to widespread commercial adoption.

2.2. Bottom-up methods

Compared to exfoliated flakes, which inherently maintain single-crystalline structures with low defect densities and well-preserved intrinsic properties, bottom-up methods offer a more practical pathway for wafer-scale production. However, these methods often struggle to match the exceptional crystal quality of exfoliated samples. To bridge this gap, physical chemistry views have emerged to be critical for improving crystal quality. These include precise control over precursor composition, optimized gas-phase reaction kinetics, surface passivation, selective doping, and *in situ* defect healing. Additionally, ligand-assisted growth, vapor-phase transport, and metal–organic surface modification can reduce grain boundaries and enhance crystallinity.

Recently, techniques including sputtering, molecular beam epitaxy (MBE), atomic layer deposition (ALD), pulsed laser deposition (PLD), and vapor-phase deposition methods, such as CVD, PVD, and metal–organic CVD (MOCVD), have been developed and optimized to bridge the gap between laboratory research and practical applications of 2D materials (Fig. 3a–d). To provide a more intuitive overview, we also present in Fig. 2, a roadmap of the development of 2D material growth techniques, highlighting both their historical evolution and emerging trends. These advancements also lay a solid foundation for further studies on 2D material transfer.[63] Epitaxial growth, a key synthesis strategy, enables atomic or molecular assembly of 2D materials on diverse substrates. Combined with the above preparation techniques, it allows precise control over composition and crystallinity, offering significant potential for producing high-quality, single-crystal, and wafer-scale 2D films.[64,65]

2.2.1. Surface nucleation. The growth of 2D materials begins with the initial nucleation process. When precursors diffuse into the deposition region, they are absorbed by the target substrate and accumulate to form nuclei, which act as ''seeds'' for the initial growth stage (Fig. 3e).[66,67] These ''seeds'' gradually evolve into single crystalline domains, which eventually merge and cover the entire substrate, forming large-area films, where the former serving generally as high-quality single crystal research samples, and the latter as the basis for commercial applications. As the initial stage of 2D material growth, surface nucleation behaviour has attracted extensive attention in both mechanistic exploration and material design, which is crucial for controlling the crystallinity, grain size, and uniformity of 2D material films.[68]

Nucleation commonly occurs at high-energy sites on the surface, such as steps, twists, defects, scratches, and nanoparticles on the substrate. Seeding promoters are commonly used to artificially facilitate the nucleation process. For instance, the substrate modified by reduced graphene oxide (rGO) or perylene-3,4,9,10-tetracarboxylic acid tetrapotassium salt (PTAS) can significantly improve crystallinity, uniformity, and controllability.[69] Recently, Moon *et al.* demonstrated the

 This journal is © The Royal Society of Chemistry 2025

Open Access Article. Published on 06 January 2026. Downloaded on 1/16/2026 12:17:14 PM.
This article is licensed under a Creative Commons Attribution-NonCommercial 3.0 Unported Licence.

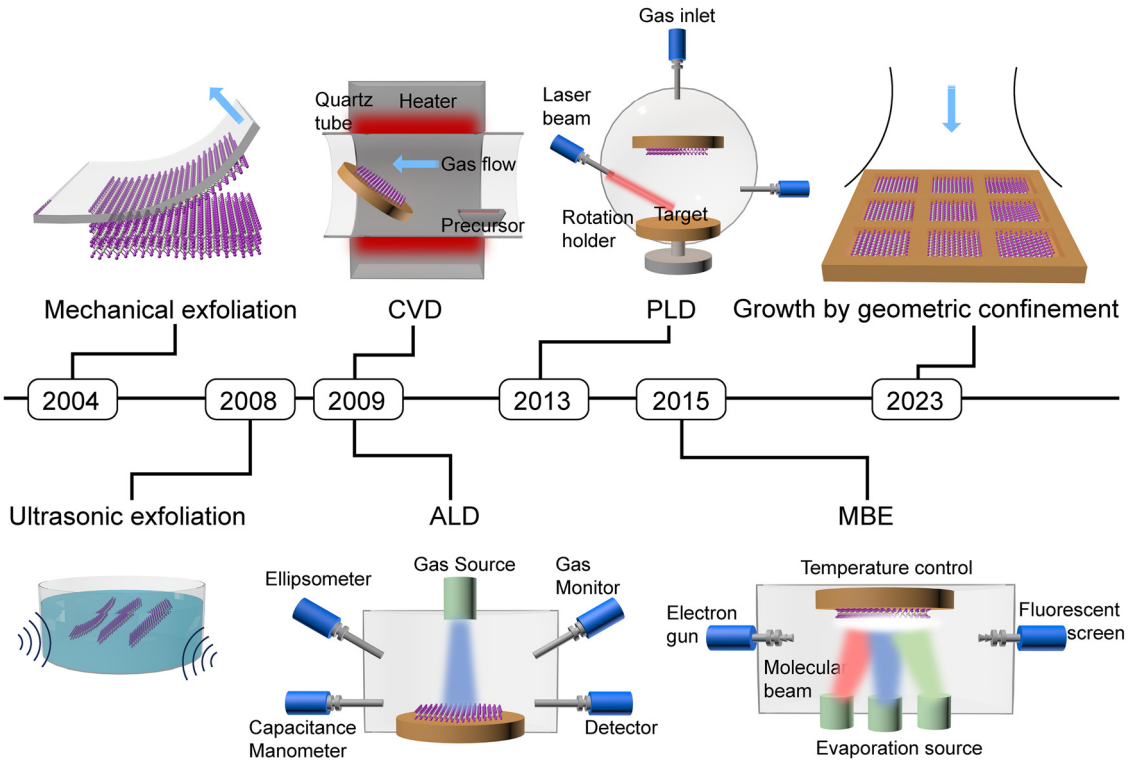

Fig. 2 Growth of the 2D material roadmap.

"hypotaxy method" by using graphene templates to precisely regulate MoS_2 nucleation and thickness (Fig. 2f).[70] This approach enabled the fabrication of wafer-scale, single-crystal MoS_2 layers with high thermal conductivity ($\sim$120 W m^{-1} K^{-1}) and mobility ($\sim$87 cm^2 V^{-1} s^{-1}).

Another approach to controlling nucleation is pre-patterning the substrate to directly obtain patterned 2D materials, thereby eliminating the need for photolithography and etching processes.[71,75–78] For example, Kim and colleagues achieved the growth of single-domain arrays by geometric confinement, adjusting the difference in surface binding energy within the patterned SiO_2 array and confining nucleation to the target area (Fig. 3g).[71,75] By optimizing the array size, they fabricated single-domain arrays with excellent electrical performance, reliably avoiding grain boundaries and the introduction of defects caused by etching post-processing.

Beyond substrate pre-patterning strategies, another widely adopted approach involves the use of low-melting-point precursors, such as metal halides and metal–organic compounds, or molten-salt-assisted processes.[79–81] In pursuit of compatibility with complementary metal-oxide-semiconductor (CMOS) back-end-of-line integration, the semiconductor industry has been striving to confine the growth temperature of 2D materials below 450 °C, a threshold that would substantially accelerate their industrial deployment. Compared with metal oxide precursors, low-melting-point species can generate a higher vapor flux, promote precursor diffusion and facilitate the nucleation of 2D layers at low temperature.[82]

Notable work includes the use of $(NH_4)_2MoS_4$ or metal iodides to achieve the low-temperature, large-area growth of 2D materials.[83,84] Moreover, organometallic precursors such as $Bi(C_6H_5)_3$ and $(CH_3)_2Se_2$ have enabled the synthesis of Bi_2O_2Se thin films at 300–400 °C, dramatically lowering the temperature from conventional values near 1000 °C.[85] Zhu *et al.* employed $Mo(CO)_6$ as a volatile precursor to realize monolayer MoS_2 growth below 300 °C within 60 min, directly on silicon-based CMOS circuits.[86] More recently, Hoang *et al.* further utilized the same precursor to achieve the direct synthesis of a high-crystalline MoS_2 monolayer at temperatures as low as $\sim$150 °C, setting a new record for low-temperature growth and even enabling deposition on flexible polymer substrates (Fig. 3h).[72] In addition, ALD has emerged as a versatile low-temperature technique, offering atomically precise thickness control through self-limiting surface reactions.[87] Recent studies have demonstrated that ALD enables the conformal growth of ultrathin, high-κ dielectrics, such as sub-3 nm Al_2O_3 and HfO_2 films on 2D surfaces, greatly improving interface quality and gate controllability in MoS_2 transistors.[88,89] This breakthrough demonstrates excellent CMOS compatibility and potential for wearable electronics, although the polycrystalline MoS_2 films produced at such low temperatures still require further optimization to meet the mobility standards specified by the International Roadmap for Devices and Systems (IRDS) roadmap.[90,91]

2.2.2. Epitaxial growth. Since nucleation occurs randomly and without orientation in the absence of regulation, the core

Open Access Article. Published on 06 January 2026. Downloaded on 1/16/2026 12:17:14 PM.
This article is licensed under a Creative Commons Attribution-NonCommercial 3.0 Unported Licence.

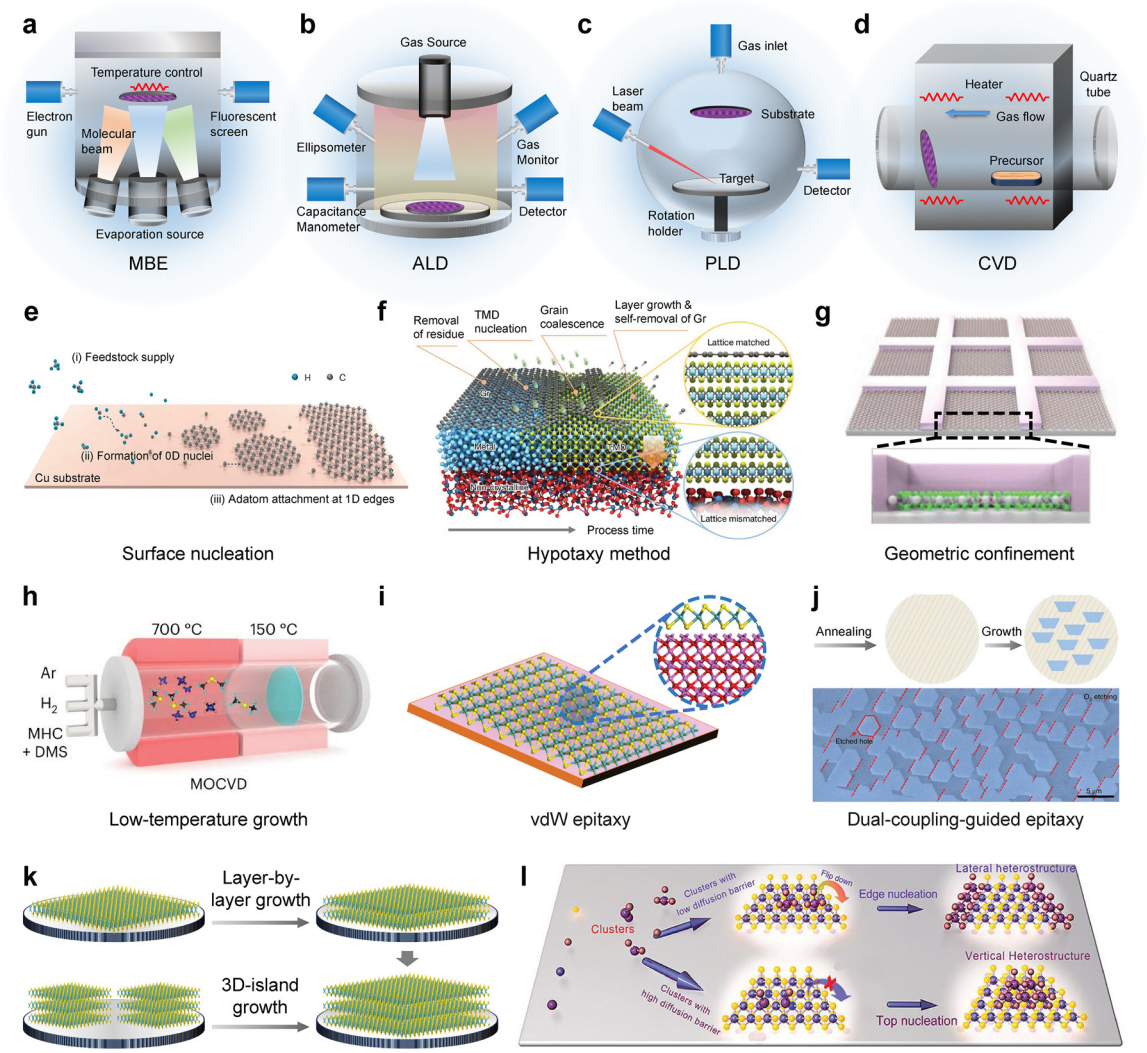

Fig. 3 Growth of 2D materials. (a)–(d) Schematic of 2D material growth techniques by MBE, ALD, PLD, and CVD, respectively. (e) Surface nucleation mechanism of graphene on a Cu substrate. Reproduced from ref. 67 with permission from Springer Nature, Copyright 2024. (f) Growth mechanism of the proposed hypotaxy. Reproduced from ref. 70 with permission from Springer Nature, Copyright 2025. (g) Patterned single crystal 2D material growth *via* geometric confinement. Reproduced from ref. 71 with permission from Springer Nature, Copyright 2023. (h) Low-temperature growth by MOCVD. Reproduced from ref. 72 with permission from Springer Nature, Copyright 2023. (i) Schematic of vdW epitaxy of TMDCs on a sapphire substrate. (j) Dual-coupling-guided epitaxial growth mechanism of WS_2 on a two-inch sapphire wafer. Reproduced from ref. 73 with permission from Springer Nature, Copyright 2021. (k) Layer-by-layer and 3D-island growth of multilayer 2D materials. (l) Schematic of controlled growth for out-of-plane and in-plane heterostructures. Reproduced from ref. 74 with permission from American Chemical Society, Copyright 2022.

of epitaxial growth lies in enhancing the surface binding energy between 2D domains and a single-crystal substrate to dictate their alignment.[92,93] Therefore, this is an ideal strategy for promoting high-quality single-crystal and wafer-sized 2D films. In 1984, Koma *et al.* pioneered this approach by demonstrating the epitaxial growth of Se on Te bulk crystals and $NbSe_2$ on MoS_2, naming it "vdW epitaxy" (Fig. 3i).[94] Unlike traditional 3D material epitaxy, 2D material interfaces lack surface dangling bonds, significantly reducing the lattice constant matching requirements, with surface symmetry becoming the decisive factor. This greatly expanded the heteroepitaxy system and laid the foundation for 2D material growth and transfer.

For example, high-quality graphene and h-BN have been widely reported to be grown on transition metal substrates like Cu and Ni using techniques such as CVD and MBE, or through epitaxial graphitization on the top surface of hexagonal SiC crystals.[95–99] In this case, transition metals act as both the growth substrate and the catalyst for hydrocarbons or borohydrides. Notably, graphene and h-BN share the same lattice structure and have closely matched lattice constants. A large number of experimental observations and theoretical predictions are consistent, showing that they have the maximum binding energy along the Cu(110) direction and tend to grow on Cu(111) and Cu(110). Especially, Cu, due to its very low carbon solubility, is considered an ideal substrate for the preparation of large-scale, high-quality, and uniform monolayer graphene or h-BN. However, graphene has C_{6v} symmetry, while h-BN has lower C_{3v} symmetry, which results in the formation of twin

 This journal is © The Royal Society of Chemistry 2025

Open Access Article. Published on 06 January 2026. Downloaded on 1/16/2026 12:17:14 PM.
This article is licensed under a Creative Commons Attribution-NonCommercial 3.0 Unported Licence.

boundaries when h-BN 2D domains merge, making it more difficult to generate single-crystal films.[64,100]

Unlike graphene, the growth of TMDCs does not require catalytic substrates, instead, Cu or Ni substrates tend to undergo sulfidation. The chemically inert graphene layer and Au film have become the suitable template for epitaxial growth. Shi *et al.* and Gao *et al.* demonstrated the epitaxial growth of MoS_2 on CVD-grown graphene and WSe_2 and Au(111) surfaces, respectively.[101,102] In recent years, researchers have successfully synthesized wafer-sized TMDC single crystals on sapphire substrates. Various methods, such as sulfur-rich conditions, substrate annealing for atomic smoothness, and Ni foam, have been used to adjust the orientation of 2D domains.[103–105] However, the low symmetry of h-BN and TMDCs leads to inverse parallel domains, forming twin boundaries that significantly degrade their electronic properties. To solve this challenge, Wang *et al.* achieved the epitaxial growth of a 10 × 10 cm^2 single-crystal h-BN monolayer on a Cu(110) vicinal surface. By step-edge coupling between the Cu(211) step and h-BN zigzag edges, they attained unidirectional orientation exceeding 99% and proposed the concept of ''step-edge guiding epitaxy''.[106] Yang *et al.*, in 2020, achieved wafer-scale epitaxial growth of single-crystal MoS_2 monolayers on vicinal Au(111) thin films by melting and resolidifying commercial Au foils, attaining unidirectional alignment and seamless stitching.[107] Subsequently, Li *et al.* grew 2-inch MoS_2 single crystals on c-plane sapphire with a miscut orientation towards the *a*-axis. By applying an $\sim 1^\circ$ shear angle along this direction, they induced atomic steps that effectively broke the nucleation energy degeneracy. The resulting field-effect transistors exhibited excellent wafer-scale uniformity and a high mobility of 102.6 $cm^2\ V^{-1}\ s^{-1}$, setting a record for monolayer CVD-grown MoS_2.[108] Inspired by this, Wang *et al.* proposed the concept of ''Dual-Coupling Effect'' to describe the complex synergy between epitaxial relationships and atomic steps and eventually enabled the preparation of large-size single crystal TMDC films, including WS_2, MoS_2, $MoSe_2$, and $NbSe_2$ (Fig. 3j).[73] The epitaxial interaction between WS_2 and vicinal *a*-plane sapphire surfaces gives rise to two preferred antiparallel orientations, while the sapphire step edges disrupt the symmetry of these orientations. These two interactions promote the unidirectional alignment of crystal islands, ultimately resulting in seamless fusion without grain boundaries.

2.2.3. Beyond epitaxial growth. The first key aspect is the significant influence of the layer number on the optical and electrical properties of 2D materials. As the number of layers increases, these materials exhibit higher current density and carrier mobility, along with notable changes in the spectral peak position and intensity. Moreover, twisted Moiré superlattices demonstrate the fractal quantum Hall effect, different topological phases, and unconventional superconductivity.[109–111] The epitaxial growth mechanism of multilayer 2D materials is more complex (Fig. 3k). Growth can occur in a 2D layer-by-layer mode, where a new layer only forms after the previous one is fully covered. For example, Wang *et al.* achieved precise control of up to six layers of MoS_2 by controlling the nucleation density.[112] Another mode is a 3D island growth mode, where multilayer islands form preferentially and gradually merge during subsequent growth. A representative work in this mode is the use of reverse-flow chemical vapor epitaxy, achieving defect-free stacking of bilayer MoS_2.[113] Additionally, large-area multilayer TMDCs can be synthesized by using strategies such as ALD and MOCVD, in which metal oxide precursors undergo sulfurization. For instance, Kalanyan *et al.* presented a pulsed MOCVD method for the controlled growth of MoS_2 films with thicknesses ranging from 1 nm to 25 nm at low temperatures and short deposition times.[114]

Atomically thin 2D materials without interlayer dangling bonds are also ideal building blocks for constructing 2D/2D heterojunctions. Heterostructures can also be directly synthesized *via* bottom-up epitaxy by precisely controlling precursor supply, nucleation sites, and deposition sequence. Wafer-sized vertical heterostructures, such as MoS_2/graphene, MoS_2/WS_2, WSe_2/MoS_2, and $WSe_2/MoSe_2$, have been successfully synthesized using chemical methods.[115–119] Beyond vertical (out-of-plane) structures, TMDCs can also be used to construct atomic-scale lateral (in-plane) heterostructures. Unlike vertical structures, planar epitaxy requires a higher degree of crystal structure matching, where two different 2D single crystals form 1D linear bonding only at the interface (Fig. 3l). The growth of heterostructures as vertical (VHs) or lateral (LHs) depends on the growth kinetics and thermodynamics, with factors such as nucleation energy, diffusion, vdW interaction energies, and edge energy influencing the final structure's stability.[74] For example, Gong *et al.* demonstrated a growth strategy for WS_2/MoS_2 heterostructures, achieving both out-of-plane heterostructures with strong excitonic transitions and in-plane heterostructures with localized photoluminescence enhancement by controlling the growth temperature.[120] Li *et al.* successfully achieved precise control of the heteroepitaxy direction and effective manipulation of the diffusion barrier of active clusters by rationally controlling the metal/chalcogenide ratio in the vapor precursors.[121]

In summary, with the advancement of synthesis techniques, the family of 2D materials has been greatly expanded, with sizes extending from the micron scale in the laboratory to the wafer scale. Epitaxial growth methods have significantly improved the crystallinity, wafer-scale uniformity, optical and electrical properties, and expanded the range of complex 2D materials and heterostructures. However, due to the immaturity of low-temperature growth processes, the next major challenge hindering the commercialization of 2D materials is the high-yield, repeatable, residue-free, wrinkle-free wafer-scale 2D transfer technology.

3. Current 2D material transfer methods

With the development of scalable, high-quality 2D material synthesis techniques, researchers can now routinely obtain both wafer-scale films and high-purity exfoliated flakes.

Open Access Article. Published on 06 January 2026. Downloaded on 1/16/2026 12:17:14 PM.
This article is licensed under a Creative Commons Attribution-NonCommercial 3.0 Unported Licence.

However, realizing the full technological potential of these materials depends not only on their intrinsic quality, but also on the ability to precisely transfer them onto diverse substrates without introducing contamination or structural damage. Transfer processes thus serve as a crucial bridge between material preparation and device fabrication, ensuring that atomic-scale properties are preserved during integration. In this section, we provide a comprehensive overview of current state-of-the-art 2D material transfer methods, highlighting their underlying principles, strengths, and limitations. This discussion aims to equip both newcomers and experts with practical guidance for selecting and optimizing transfer strategies tailored to various applications.

3.1. Philosophy of transfer strategies

The successful transfer of 2D materials relies fundamentally on a careful balance of interfacial forces throughout the process. As illustrated in Fig. 4, the transfer operation consists of two primary steps: (1) detaching the 2D material from the growth substrate using an intermediate medium (the pick-up stage), and (2) releasing the 2D material from the medium onto a target substrate (the release stage). Each stage is governed by the interplay of three key interfacial forces, which can be finely tuned at the molecular level.

$\mathbf{F_1}$: the interaction between the 2D material and the original growth substrate, determined by chemical bonding or physical adsorption (*e.g.*, vdW forces).

$\mathbf{F_2}$: the adhesion between the 2D material and the transfer medium (such as PDMS or polymer layers), regulated by polymer chemistry, surface energy, or electrochemical modulation.

$\mathbf{F_3}$: the adhesion between the 2D material and the target substrate, which can be enhanced through surface treatments (*e.g.*, hydroxylation and amino-silanization) or chemical activity at defect sites.

For efficient pick-up, $\mathbf{F_2}$ should be larger than $\mathbf{F_1}$, allowing the intermediate medium to lift the 2D material from its original substrate. This can be achieved through methods like capillary force-assisted transfer, where water thin film provides the additional adhesion force to enhance the $\mathbf{F_2}$, or polymer-assisted transfer, where the interaction between the polymer and the 2D material is carefully designed to strengthen $\mathbf{F_2}$ by adjusting the temperature.[122] Alternatively, reduce $\mathbf{F_1}$ through other methods until it becomes easy to overcome. For example, use liquid nitrogen to weaken the vdW force between the TMDCs and the growth substrate.[123] If $\mathbf{F_1}$ is too strong to overcome, a common solution is PMMA-assisted wet transfer, where the growth substrate is chemically etched to effectively kill the $\mathbf{F_1}$ to zero.

During the release step, $\mathbf{F_2}$ should be smaller than $\mathbf{F_3}$, ensuring that the 2D material adheres preferentially to the target substrate. A common strategy is to reduce $\mathbf{F_2}$. For example, in the capillary-assisted method, the water vapor that initially serves as a temporary adhesive disappears after pick-up. As the vapor vanishes, the adhesive force drops significantly, resulting in a much lower $\mathbf{F_2}$.

Strategies such as solvation effects (intercalation of water molecules[124,125]), or thermodynamic disturbances (*e.g.*, temperature-induced polymer chain movement[126–129] and differences in thermal expansion coefficients[130]), are employed to weaken $\mathbf{F_2}$, allowing $\mathbf{F_3}$ to dominate and successfully complete the transfer. Furthermore, PDMS has strong adhesion when the peeling speed is fast and weak adhesion when the peeling speed is slow. By slowly releasing the 2D material, it is possible to effectively reduce $\mathbf{F_2}$, thus allowing the 2D material to remain on the target substrate.[9]

In some extreme cases, when the interaction force between the transfer medium and the 2D material is excessively strong and cannot be released without compromising the material quality, the transfer medium is typically removed or dissolved, thereby reducing the $\mathbf{F_2}$ value to zero. For instance, in the case of PMMA or metal transfer media, their inherently high $\mathbf{F_2}$ values necessitate removal by dissolution after the 2D material is brought into contact with the target substrate, rather than relying on the competition of interfacial forces.

By systematically controlling these interfacial forces, as schematically depicted in (Fig. 4), researchers can achieve high-fidelity, clean, and reproducible transfer of 2D materials to a wide variety of substrates, thus bridging the gap between material synthesis and device fabrication. In the following sections, we will elaborate on how this underlying philosophy is implemented across various state-of-the-art transfer methods, illustrating the practical strategies and innovations developed to address the unique challenges of 2D material integration (Fig. 5).

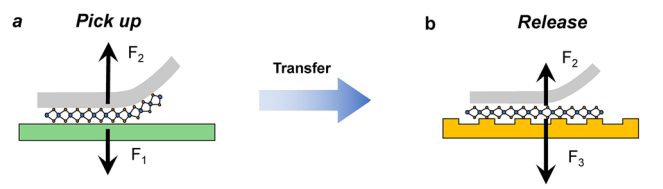

Fig. 4 The philosophy of 2D transfer. (a) The successful pick up requires $\mathbf{F_2} > \mathbf{F_1}$. (b) The successful release process requires $\mathbf{F_3} > \mathbf{F_2}$.

3.2. Transfer methods

3.2.1. The current available transfer methods. Transfer methods for 2D materials can be broadly categorized into three main classes: wet,[131] dry[9] and capillary force assisted hybrid.[124,132,133] The essential principle underlying all these approaches is to ensure that the adhesion force between the handling medium and the 2D material is greater than that between the 2D material and its original substrate. This balance can be achieved either by enhancing the interaction between the 2D material and the handling medium, or by reducing the adhesion between the 2D material and the growth substrate.

Building on this fundamental philosophy, several advanced transfer strategies have emerged in recent years, including the UV tape assisted wafer scale method,[21] the Au assisted method,[39] and the SiN_x membrane assisted method,[20] each offering unique advantages for specific applications.

This journal is © The Royal Society of Chemistry 2025

Open Access Article. Published on 06 January 2026. Downloaded on 1/16/2026 12:17:14 PM.
This article is licensed under a Creative Commons Attribution-NonCommercial 3.0 Unported Licence.

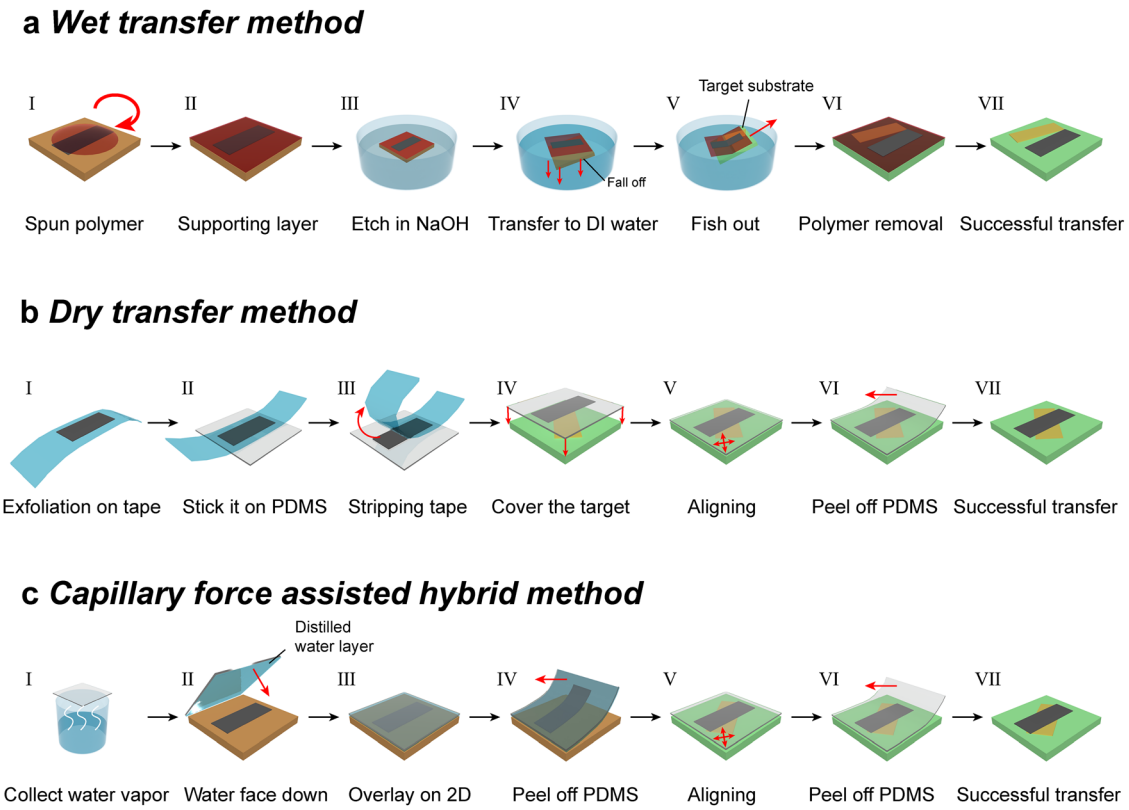

Fig. 5 2D material transfer methods. (a) Wet transfer method: the polymer support layer is spun onto the 2D material, then placed in the etcher, the film breaks off from the substrate and floats on the surface of the solution, and finally the film is fished out using the target substrate in deionized water, and the polymer support layer is removed by solvent dissolution or annealing. (b) The dry transfer method: 2D flakes are stripped directly onto the surface of the PMDS stamp by tape, and then the stamp is pressed to the target position and the PMDS is slowly stripped, and the 2D material is left in the target position. (c) Capillary-force-assisted hybrid: place the PMDS over boiling deionized water so that a thin layer of water condenses on the surface of the PMDS. The PMDS is then attached to the surface of the 2D material, after which the PMDS is quickly peeled off, at which point the 2D material is attached to the PDMS, and then the PMDS is pressed on the target position and the liquid layer is evaporated, at which time the PDMS 2D material is peeled off and left on the target position.

To facilitate a systematic comparison, we present a comprehensive evaluation of each method using radar charts, assessing critical dimensions such as transfer cleanliness, ease of operation, achievable area, completeness, versatility across different types of 2D materials (*e.g.*, CVD-grown *vs.* exfoliated), and potential for multifunctional integration.

Wet transfer. CVD has become the dominant method for producing large-area, high-quality graphene and other 2D materials, primarily on catalytic transition metal substrates such as copper or nickel. Copper is especially favoured due to its low carbon solubility,[134] which enables uniform, single-layer graphene growth with well-preserved crystallinity and excellent electrical properties, closely matching those of mechanically exfoliated graphene.[135]

However, the strong adhesion between graphene and copper introduces significant challenges during transfer.[136] The most widely used solution is the wet transfer method, in which a polymer support layer, most commonly PMMA, is spin-coated onto the graphene/copper substrate. The copper is then chemically etched away, effectively reducing the interfacial force $\mathbf{F_1}$ (between the 2D material and the growth substrate) to zero and allowing easy delamination. Subsequently, the PMMA/graphene stack is floated onto deionized water and transferred to the target substrate. In the final step, dissolving the PMMA support layer in acetone eliminates the interfacial force $\mathbf{F_2}$ (between the 2D material and the transfer medium), ensuring that the graphene adheres preferentially to the target substrate, in accordance with the core transfer philosophy.

The PMMA-assisted wet transfer approach offers notable simplicity and versatility, making it a standard protocol for a wide range of 2D materials. It provides critical mechanical support, protecting fragile monolayers throughout the transfer process. However, this method is not without drawbacks. PMMA residues often persist even after extensive solvent rinsing, leading to contamination, p-type doping, and degraded electrical performance. Additional strain may also be introduced during curing and removal. These factors have spurred research into alternative polymers; examples include paraffin,[137] polystyrene (PS),[138,139] ploy(L-lactic acid) (PLLA) and L-lactide-ε-caprolactone copolymer (PLC),[132] cellulose nitrate (NC),[140] cellulose acetate butyrate (CAB),[141] cellulose acetate

Open Access Article. Published on 06 January 2026. Downloaded on 1/16/2026 12:17:14 PM. This article is licensed under a Creative Commons Attribution-NonCommercial 3.0 Unported Licence.

(CA),[142] and polyvinyl alcohol (PVA).[143] However, they have corresponding disadvantages: paraffin wax can produce clean and large-area graphene, but due to its large expansion coefficient, temperature perturbations introduce greater stress and reduce the mechanical strength of graphene, so in order to improve mechanical strength, the integrity of the transferred 2D material is generally maintained by double-layer PMMA design.[144,145] Polystyrene PS is usually brittle and difficult to apply in large-area transfer graphene applications, so it is necessary to increase its mechanical flexibility and add softener[139] to the polymer to reduce cracks caused by the transfer process to graphene. NC introduces some strain-related characteristics because it is rigid as a polymer and cannot be relaxed by annealing. The overall surface wrinkles of CAB-transferred graphene are much less than those of PMMA transferred graphene, but the electrical properties are not much improved.

To further reduce contamination, polymer-free wet transfer techniques have emerged, using agents like rosin[146] or cyclohexane.[147] While these can lower surface residues, they tend to compromise mechanical strength or introduce other compatibility issues, such as the need for additional protective layers,[148] or process constraints due to pH sensitivity.

In addition to polymer residues, chemical etching agents themselves can introduce unwanted contaminants during wet transfer. To address this, alternative methods have been explored. One promising approach is electrochemical bubble delamination, which generates gas bubbles at the interface between the 2D material and the substrate, physically lifting the film and thereby reducing the need for aggressive chemical etchants.[11] This process can effectively weaken or even ''kill'' the interfacial force $\mathbf{F_1}$, facilitating delamination. However, it requires careful control, as the mechanical stresses generated by bubble formation can damage delicate 2D materials, necessitating continued reliance on a PMMA support layer for protection.[149] Moreover, this technique is only compatible with conductive (metal) substrates, such as those used for graphene and h-BN, and is not suitable for insulating substrates like SiO_2/Si, mica, or sapphire, which is commonly used for TMDCs. Additionally, any remaining etching steps can still damage the original metal substrate, limiting the method's repeatability and scalability. Improvements such as ultrasonic-assisted delamination have been developed to broaden substrate compatibility and accelerate the process,[150] and some studies have focused on designing sacrificial layers or protective coatings to further minimize substrate damage.[151]

In summary, while wet transfer, particularly the widely used PMMA-assisted method, remains the most practical and scalable approach for transferring CVD-grown 2D materials, it continues to face persistent challenges. These include polymer contamination, strain induced during processing, and a lack of spatial precision, as the floating 2D films cannot be aligned accurately on the target substrate. Such limitations are especially problematic for applications demanding strict control over layer positioning, such as vdW heterostructure assembly or optoelectronic device fabrication. These ongoing challenges continue to drive innovation in both transfer protocols and post-transfer cleaning strategies.

Dry transfer methods. The exfoliation of 2D materials typically yields flakes with random locations, varying sizes, and non-uniform thicknesses. As a result, careful identification and precise isolation are required to enable deterministic placement and assembly, especially in advanced device fabrication where spatial accuracy is paramount.

Conventional wet-transfer techniques, which rely on retrieving floating 2D films from a liquid surface, suffer from significant limitations in spatial control and alignment. To overcome these challenges, deterministic dry transfer approaches have been developed. In these methods, 2D flakes are typically picked up by PDMS stamps and positioned with high precision, making them well-suited for constructing vdW heterostructures and other complex architectures.

The fundamental principle of mechanical exfoliation involves applying a force that exceeds the interlayer vdW attraction in the parent crystal, thereby producing atomically thin flakes while preserving in-plane crystallinity. Castellanos-Gomez *et al.*[9] pioneered a dry transfer protocol using PDMS: bulk vdW crystals are mechanically exfoliated using adhesive tape, transferred onto a PDMS stamp, and then aligned and pressed onto the target substrate. The viscoelastic nature of PDMS facilitates both pick-up and release of the 2D material.

Despite its advantages in spatial precision, the PDMS-based approach faces key limitations. The intrinsic adhesion between PDMS and many 2D materials is relatively weak, which hinders its ability to reliably pick up flakes directly from growth substrates.[152] To improve pick-up efficiency, one might increase PDMS stickiness, either by lowering the cross-linker ratio or optimizing the curing process, making it easier to exfoliate flakes.[153] However, a more adhesive PDMS also tends to be ''dirtier'': long-chain polymer fragments are more likely to transfer onto the 2D flake surface, leading to chemical contamination that degrades material and device performance.[154] On the other hand, using a higher cross-linker content or higher curing temperature produces a cleaner PDMS surface but results in lower adhesion, making it more difficult to pick up 2D materials.[155] This trade-off between cleanliness and adhesion presents a major challenge for PDMS-based transfer.

A practical solution to this dilemma is a two-step approach: first, exfoliate the 2D material onto a clean wafer using a ''clean'' (highly cross-linked, well-cured) PDMS, ensuring minimal contamination; then, transfer the desired flake from the wafer onto the target substrate using a more controllable and clean transfer medium. This strategy enables both high interface quality and reliable flake manipulation and has become increasingly popular for applications requiring both ultra-clean surfaces and spatial precision.

In this manner, a variety of alternative polymer supports have been explored. Polypropylene carbonate (PPC)[126] offers tunable adhesion through temperature control, with adhesion remaining high at room temperature but dropping significantly when heated to $\sim$70 °C, which enables effective pick-up and

 This journal is © The Royal Society of Chemistry 2025

Open Access Article. Published on 06 January 2026. Downloaded on 1/16/2026 12:17:14 PM.
This article is licensed under a Creative Commons Attribution-NonCommercial 3.0 Unported Licence.

easy release. PVA exhibits strong adhesion when melted at 90 °C and can be dissolved in water to yield a clean interface;[14,156] however, it often requires additional support layers to ensure flatness and mechanical stability. Polycarbonate (PC) follows a similar principle but requires higher processing temperatures (~150 °C), which may risk oxidation and degrade 2D material quality compared to the milder conditions used for PVA.[127,157]

In addition to polymer-assisted techniques, h-BN has gained prominence as both a pick-up and encapsulation material.[158] Thanks to its atomically flat, chemically inert surface and robust van der Waals interaction with other 2D materials, h-BN is ideal for assembling clean and high-mobility devices.[159,160] For instance, the mobility of graphene field-effect transistors can reach up to 140 000 $cm^2\ V^{-1}\ s^{-1}$ when h-BN is used as the substrate and encapsulant, an order of magnitude higher than conventional SiO_2-supported devices.[160] The h-BN layer also offers a self-cleaning effect, mitigates charge traps, and provides protection against oxidation and environmental damage,[160–165] The typical procedure involves first picking up h-BN with a PPC stamp, then using this h-BN ''handle'' to pick up the target 2D flake by van der Waals adhesion.

While h-BN-assisted dry transfer offers clear benefits in device performance and interface quality, it comes with its own limitations. The transfer area is constrained by the size of the h-BN flake, and after assembly, the h-BN is difficult to remove, making this approach unsuitable for applications where the 2D surface needs to be exposed, such as in chemical functionalization or catalysis.[166] Additionally, the mechanical rigidity of h-BN imposes limitations on flexible device applications and large-area transfer.

In order to achieve large-scale dry transfer, Zhang *et al.* used selenium (Se) as the mediator and PPC as the support layer.[167] They transferred the wafer-level single-layer MoS_2 onto the target substrate using a water-soluble tape. Subsequently, they removed the PPC through reactive ion etching (RIE) and removed the selenium layer in a nitrogen atmosphere for annealing. This resulted in a highly clean MoS_2 surface. Finally, through standard semiconductor processes, field-effect transistors (FETs) and logic circuits were fabricated on the transferred MoS_2 film, achieving a switching current ratio of up to 2.7×10^{10} and an electron mobility of 71.3 $cm^2 \cdot V^{-1} \cdot s^{-1}$. The compatibility with existing semiconductor manufacturing processes was verified.

Overall, while dry transfer methods have revolutionized the deterministic assembly of 2D materials, enabling unprecedented control over spatial arrangement and interface quality, they are still evolving to address persistent challenges. These include improving the pick-up efficiency for large-area or substrate-bound films, minimizing polymer or PDMS contamination, and enabling more flexible, scalable, and reversible integration strategies. Continued innovation in transfer media, temperature control, and van der Waals engineering is expected to further expand the capabilities and application scope of dry transfer technologies for 2D materials.

Capillary force assisted hybrid method. While dry transfer methods enable precise alignment and clean interfaces, they often struggle when depositing 2D materials onto substrates with complex topographies or limited contact area, resulting in insufficient adhesion for reliable release from the PDMS stamp. Conversely, wet transfer methods allow broad substrate compatibility by retrieving 2D flakes floating on a liquid surface but suffer from poor spatial control and potential contamination.

Recognizing the complementary strengths and limitations of these two paradigms, hybrid capillary-force-assisted transfer methods have emerged as a powerful solution, leveraging the best of both approaches. The essence of these techniques is to temporarily use a thin film of evaporative liquid, such as water, acetone, or isopropanol vapor, as an ''instant glue'' between the PDMS stamp and the 2D material during the pick-up process. The capillary force dramatically increases the effective adhesion ($\mathbf{F_2}$) during pick-up, easily exceeding the interfacial force with the growth substrate ($\mathbf{F_1}$), thereby enabling efficient exfoliation even for challenging geometries or hollow substrates. After the liquid evaporates, the adhesion force drops, greatly reducing ($\mathbf{F_2}$), which allows the 2D material to be cleanly released onto the target substrate (where $\mathbf{F_3} > \mathbf{F_2}$), thus providing a dynamically tunable transfer force throughout the process.

A landmark study by Ma *et al.* introduced this concept by condensing a thin layer of water vapor onto a clean PDMS stamp.[124] The water layer provides strong, but transient, capillary adhesion for picking up graphene or TMDCs from SiO_2/Si substrates, previously impossible with standard dry PDMS. Once the water evaporates, the 2D flake can be precisely and gently placed on the target substrate. Critically, because only volatile liquids are used, this process eliminates polymer contamination and avoids post-transfer annealing, preserving the pristine surface and high mobility of the 2D material. Devices fabricated using this approach have demonstrated record-high carrier mobility and minimal charge neutrality point shift, confirming ultra-clean interfaces. Furthermore, by patterning the PDMS stamp into arrays, selective pick-up and deterministic assembly of device arrays or lithography-free fabrication becomes possible.

Building upon this foundation, a recent work further advanced the field by employing a patterned PDMS stamp (micro-post arrays) and introducing a capillary-force-assisted mass transfer printing (MTP) technology.[133] In this approach, an ethanol–water solution is introduced at the interface, which penetrates non-contact regions between the PDMS micro-posts and the 2D film, causing controlled delamination by capillary action. This enables wafer-scale transfer and patterning of monolayer MoS_2 and vdW heterostructures, with transfer yields approaching 99% and negligible device degradation, even for over a million device arrays in a single step. By tuning the type and ratio of the volatile liquids (*e.g.*, water, ethanol, and isopropanol), the method can be adapted to 2D materials sensitive to water (such as black phosphorus) and can even be performed in inert atmospheres inside gloveboxes. The use of ultraclean, patterned PDMS further reduces contamination and enables selective, scalable device integration.

Open Access Article. Published on 06 January 2026. Downloaded on 1/16/2026 12:17:14 PM.
This article is licensed under a Creative Commons Attribution-NonCommercial 3.0 Unported Licence.

A notable advantage of the capillary-force-assisted hybrid approach lies in its use of exceptionally clean, highly cross-linked PDMS stamps, which significantly reduces polymer contamination compared to conventional sticky PDMS-based methods. This is particularly important for preserving the intrinsic electronic properties of high-mobility 2D devices. Furthermore, the capillary medium is highly adaptable: while water vapor often serves as the ''instant glue'' to provide temporary adhesion, the process can easily be carried out with other volatile solvents such as isopropanol (IPA) or acetone vapor, especially in an inert glovebox environment. This versatility enables the transfer of water-sensitive materials, such as black phosphorus, using compatible vapors that prevent degradation. The combined use of ultra-clean PDMS and tunable capillary media ensures a gentle, contamination-free, and highly efficient transfer process across a broad range of 2D materials and device integration scenarios.

In summary, capillary-force-assisted hybrid methods represent a near-ideal solution for 2D material transfer: they offer tunable interfacial forces for efficient pick-up and release, minimize contamination, and are compatible with both large-area and patterned integration, as well as sensitive or air-unstable materials. This new class of techniques address nearly all key challenges of previous wet and dry transfer methods, opening the door to high-throughput, contamination-free, and lithography-free fabrication of advanced 2D material devices.

3.2.2. Emerging advanced transfer methods. A complete transfer process for 2D materials generally consists of two stages: pick-up and placement, governed by the relative adhesion energies between the transfer medium, the 2D material, and the substrate. All emerging strategies discussed in this section are ultimately variations or refinements of this fundamental principle. Recent advances have enabled the emergence of highly versatile and scalable transfer methods, including dielectric (*e.g.*, Sb_2O_3)-assisted transfer,[168] SiN_x film-assisted transfer,[20] and UV tape-assisted transfer,[21] which we highlight as representative cases of wet, dry, and hybrid approaches, respectively, as illustrated in (Fig. 6).

Dielectric-assisted transfer method (wet-approach). To address persistent polymer contamination, Liao *et al.* developed a dielectric-assisted transfer method using epitaxially grown, single-crystal Sb_2O_3 films on graphene/Cu(111) substrates (Fig. 6a).[168] The resulting Sb_2O_3 layers are atomically flat, ultra-thin, and chemically inert, serving as a temporary support for conformal, crack-free transfer of graphene or MoS_2 onto arbitrary substrates. This approach avoids the introduction of polymer residues and preserves interfacial integrity, enabling devices with exceptional performance—graphene FETs with mobilities up to 29 000 $cm^2 V^{-1} s^{-1}$ and MoS_2 FETs with steep subthreshold swings and high on/off ratios. Such dielectric-mediated strategies offer a scalable and contamination-free platform for next-generation 2D electronics.

SiN_x-assisted transfer method (Dry-approach). The SiN_x-assisted transfer method (Fig. 6b) employs a flexible inorganic SiN_x film, typically coated with a metal layer, to pick up and release 2D materials by controlling adhesion through temperature modulation.[20] This method provides extremely clean surfaces and allows precise tuning of adhesion by adjusting the thickness and composition of the metal coating. However, the release stage requires high temperatures (120–150 °C), posing oxidation risks to sensitive 2D materials and necessitating glovebox processing. Additionally, this approach is less effective for graphene grown on copper foil, a common CVD substrate.

UV tape-assisted transfer method (hybrid-approach). The core innovation of the UV tape method is the use of UV illumination to modulate adhesion (Fig. 6c).[21] After attaching the UV tape to the graphene on a copper substrate, UV exposure hardens the adhesive, enabling reliable pick-up. Electrochemical delamination then separates the tape/graphene stack from the growth substrate, after which the stack is aligned and baked onto a SiO_2/Si wafer, followed by gentle peeling of the tape at 80–90 °C, to leave a clean monolayer of graphene. This process is considered a hybrid method because, while it incorporates a liquid step during electrochemical delamination, it does not fully rely on solution etching for release. This technique stands out for its broad applicability, not only to graphene but also to TMDCs and h-BN, and for its compatibility with diverse target substrates, including ceramics, plastics, and even non-planar surfaces. Patterning the UV tape also enables flexible device array assembly, which is highly advantageous for commercial and industrial applications.

In summary, these advanced transfer methods share several key advantages: high material versatility, streamlined operation, large-area and high-quality transfer capability, and minimal interfacial contamination or damage. As shown in Fig. 6, the latest techniques now enable scalable, precise, and contamination-free transfer of 2D materials for state-of-the-art device integration and commercial applications.

Summary. In conclusion, we have systematically evaluated a wide range of 2D material transfer techniques by considering 6 critical criteria: ease of operation, cleanliness, transfer size, completeness, versatility, and multi-functionality, as compared in the radar chart in Fig. 7. A detailed explanation of the scoring criteria and data sources used to construct the radar chart is provided in the SI (Table S1). These metrics, visualized through radar charts, allow for an intuitive comparison of both established and emerging transfer methods. Our analysis underscores that no single technique excels in every aspect; rather, each approach involves trade-offs tailored to specific application needs. Some methods prioritize large-area scalability or process simplicity, while others focus on achieving atomically clean interfaces or multifunctional device integration. This comprehensive benchmarking highlights the dynamic and evolving landscape of 2D material transfer, emphasizing the necessity of method selection based on targeted performance requirements and practical constraints. Continuous innovation and cross-disciplinary optimization will be essential to approaching the ideal transfer protocol for next-generation 2D devices.

This journal is © The Royal Society of Chemistry 2025

Open Access Article. Published on 06 January 2026. Downloaded on 1/16/2026 12:17:14 PM.
This article is licensed under a Creative Commons Attribution-NonCommercial 3.0 Unported Licence.

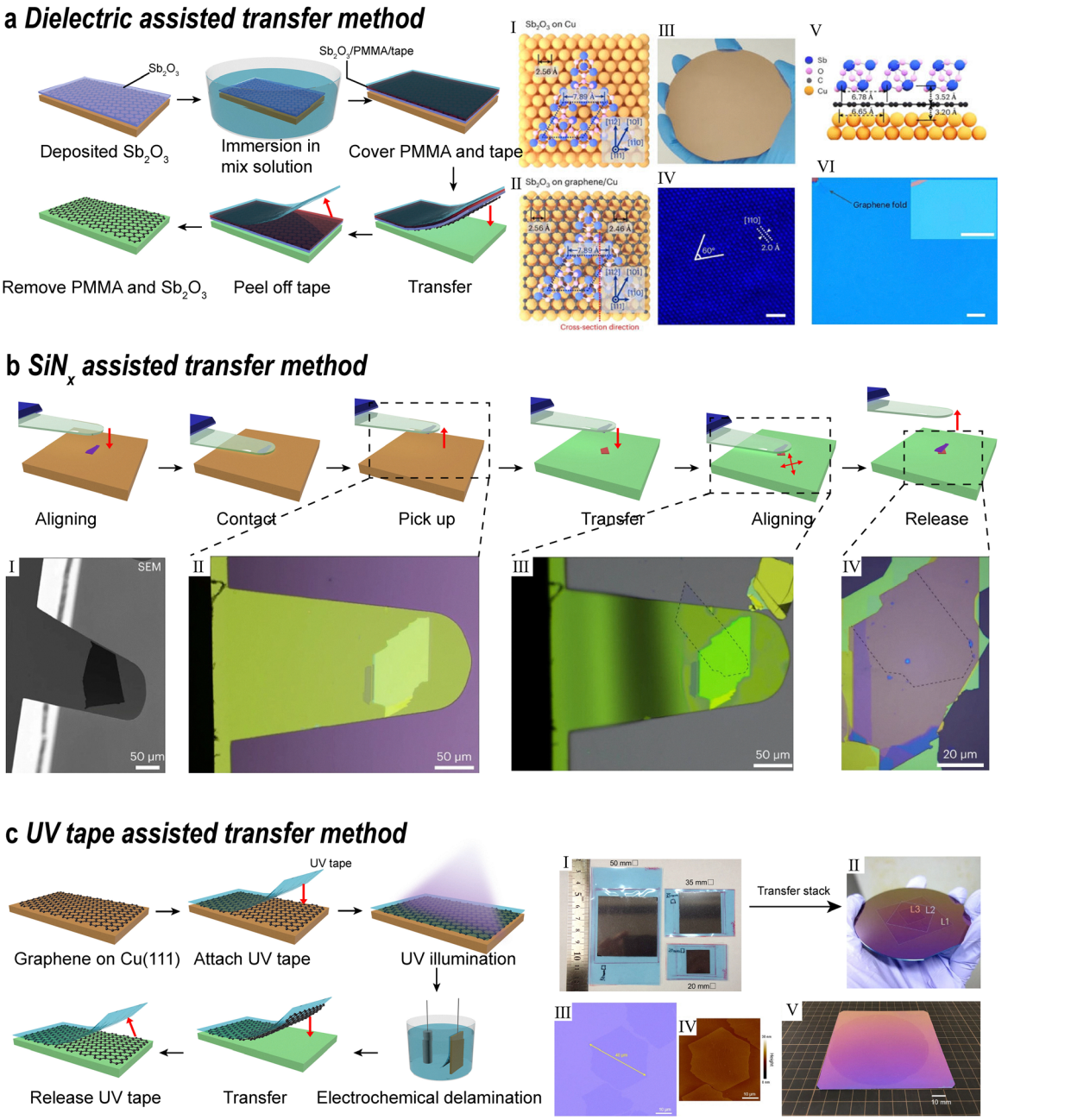

Fig. 6 Recent advanced transfer methods. (a) The dielectric-assisted transfer method. (I and II) The schematic illustration of the lattice symmetry and epitaxial growth of Sb_2O_3 on Cu(111) (I) and graphene-covered Cu(111) (II). (III) The photo of the 4-inch as-deposited s-Sb_2O_3 on graphene-covered Cu(111) wafer. (IV) The z-contrast atomic-level HAADF-STEM image of Sb_2O_3 showing the atomically resolved lattice. (V) The schematic illustration of the atomic structure of Sb_2O_3 grown on graphene-covered Cu(111). (VI) The representative image of the transferred graphene. Reproduced from ref. 168 with permission from Springer Nature, Copyright 2025. (b) The SiN_x membrane-assisted transfer method. Scanning electron microscope (SEM) (I) and optical (II) micrographs of the cantilevers after picking up thick (~40 nm) h-BN crystals. (III) The optical micrograph showing the cantilever in contact with graphene (edges highlighted with a dashed line) on SiO_2. The flexible nature of the cantilevers allows accurate control of the lamination process. (IV) The optical micrograph showing the resulting heterostructure on an oxidized silicon wafer with large uniform areas. Adapted from ref. 20 according to Creative Commons Attribution 4.0 International License (CC BY 4.0). (c) The UV tape-assisted transfer method. (I) Three graphene/Cu(111) substrates with UV tapes, used for large-area three-layer stacked graphene. (II) The photo of the graphene stack made by transferring three sheets of large monolayer graphene. (III and IV) The transferred single-crystal monolayer graphene grains. (III and IV) The optical and atomic force microscopy (AFM) imaging. Adapted from ref. 21 according to Creative Commons Attribution 4.0 International License (CC BY 4.0).

No single transfer method is universally superior in all categories. Instead, each method presents a distinct set of trade-offs tailored for specific research or industrial needs. For applications prioritizing cleanliness and high electronic performance, h-BN pick-up and dielectric-assisted methods are preferred. For large-area and scalable integration, capillary

Open Access Article. Published on 06 January 2026. Downloaded on 1/16/2026 12:17:14 PM.
This article is licensed under a Creative Commons Attribution-NonCommercial 3.0 Unported Licence.

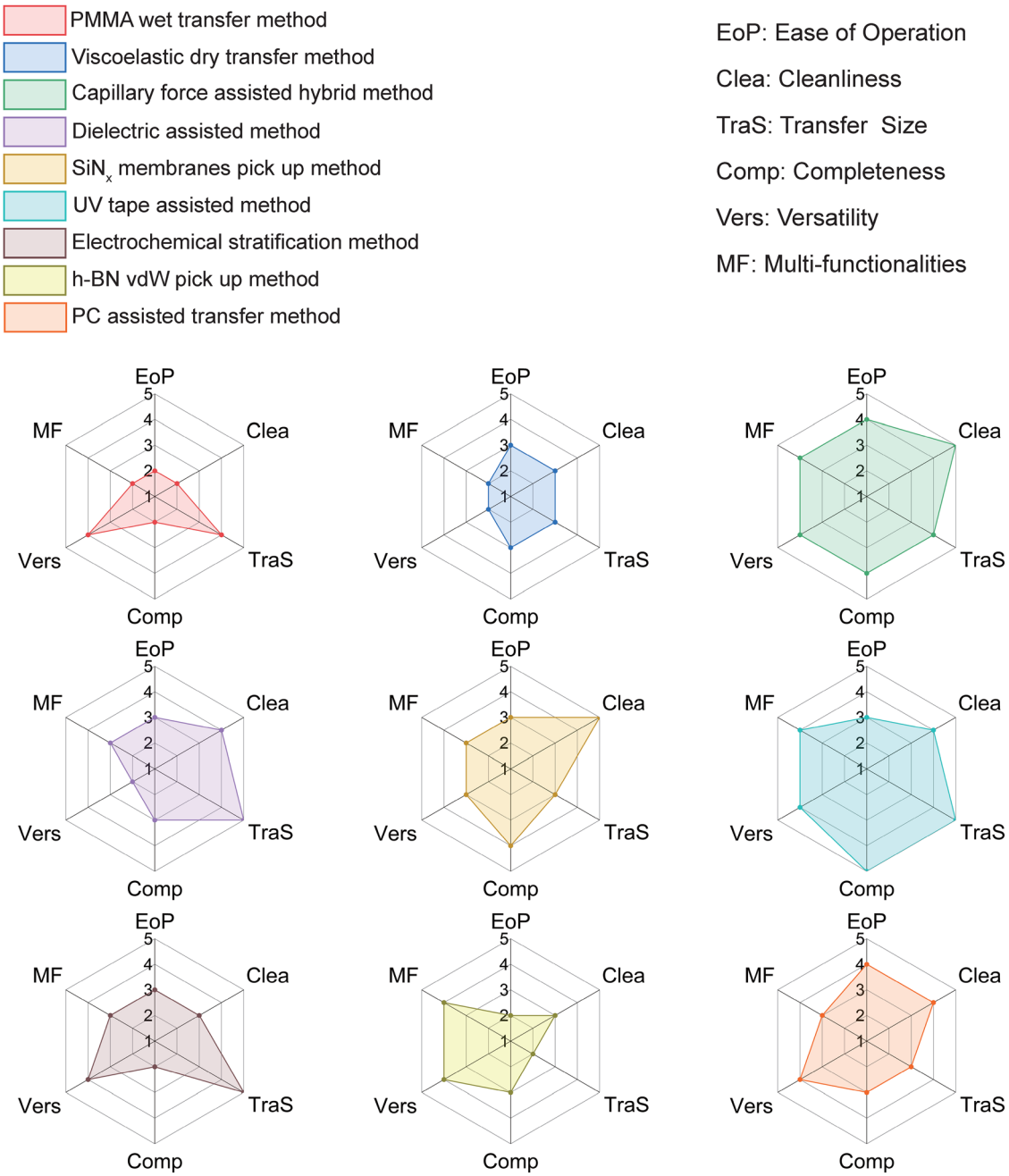

Fig. 7 The radar chart shows the advantages and disadvantages of the selective transfer method. Methods include the PMMA wet transfer method, viscoelastic dry transfer method, capillary force assisted hybrid method, dielectric assisted method, SiN_x membrane pick up method, UV tape assisted method, electrochemical stratification method, h-BN vdW pick up method, and PC assisted transfer method.

force-assisted and UV tape strategies offer major advantages. When process simplicity and versatility are essential, wet transfer remains widely used, despite its drawbacks in interface quality. In addition, we have summarized in the supporting information (Table S2) representative studies of 2D material FETs, compiling device-level metrics such as carrier mobility, contact resistance, threshold voltage shift, noise levels, and long-term cycling stability, to provide readers with direct correlations between transfer strategies and device performance.

3.3. The extension of 2D material transfer

In recent years, the transfer methods for 2D materials have evolved from initially addressing the issues of separating and reconfiguring single-layer or few-layer atomic crystals to becoming a versatile interface engineering technology with wide applicability. The core idea is to precisely control the interaction forces at the material/substrate interface to achieve high-fidelity picking and releasing. This concept has been successfully extended to those non-2D materials, for instance, for the

 This journal is © The Royal Society of Chemistry 2025

Open Access Article. Published on 06 January 2026. Downloaded on 1/16/2026 12:17:14 PM.
This article is licensed under a Creative Commons Attribution-NonCommercial 3.0 Unported Licence.

controlled release of high-refractive-index photonic crystals to achieve precise optical structure assembly;[170] for the transfer of ultra-thin diamond films, thereby expanding their applications in quantum optics and high-power devices;[171] and for the thin films of 3D materials (*e.g.*, silicon-film[172]), providing new ideas for advanced semiconductor manufacturing. More importantly, these transfer methods are not limited to traditional planar substrates but can also be compatible with irregular interfaces with curvatures, steps, or suspended structures, thereby significantly expanding their applicability in heterogeneous integration, flexible electronics, and complex photonic devices. Therefore, starting from ''2D material transfer'', the resulting interdisciplinary methodology has become a key technical foundation in various cutting-edge device manufacturing processes.

3.3.1. Transfer beyond 2D materials. The versatility of transfer techniques developed for 2D vdW materials has catalysed their adoption for a much broader class of materials and devices.[23] As shown in Fig. 8, the fundamental principles underlying 2D material transfer, precise control of interfacial forces and gentle manipulation, have been adapted to enable the integration of metal films, dielectric layers, nanowires, photonic crystal structures, and more onto a variety of target substrates.[170,173,174] This broad applicability makes transfer technology a powerful tool not only for 2D materials research, but also for the scalable fabrication of complex micro- and macro-scale devices, by treating them as low-dimensional material flakes.

A landmark example is the transfer of photonic crystal cavities, treated as van der Waals flakes, as demonstrated by Liu *et al*.[170] Using classical PDMS dry transfer, vertically stacked heterostructures were first assembled on an Si/SiO_2 substrate, after which prefabricated photonic crystals were picked up and precisely transferred onto the 2D stack. This enabled localized enhancement of electroluminescence in the nanocavity, illustrating the power of transfer for multifunctional device integration (Fig. 8a). In addition, transfer techniques have further expanded to one-dimensional and multilayer photonic devices. Yang *et al.* applied an improved transfer printing method for integrating 1D photonic crystal films onto organic translucent photovoltaic devices, using PDMS as a support for roll-to-roll (R2R) compatible, low-temperature transfer.[173] Similar strategies have been extended to membrane reflectors, multi-layer laser cavities, and even wafer-scale transfer of compound semiconductor layers.[175,176] For advanced nanomaterials, such as MXenes, wet transfer protocols have enabled large-area, flexible, and conductive films. Xu *et al.* prepared $Ti_3C_2T_x$ MXenes on glass, then employed PMMA-assisted wet transfer onto diverse targets.[177] In optoelectronics, dry transfer has been used to fabricate transparent conductive electrodes (TCEs) based on Ag nanowires, offering excellent electrical and mechanical properties (Fig. 8b).[178] Even traditional semiconductor wafers have benefited: Wang *et al.* used a combination of wet etching and dry PDMS transfer to assemble ultra-thin silicon wafers onto patterned $PtSe_2$, followed by further device integration steps to realize high-speed UV photodetectors (Fig. 8c).[172] Notably, transfer methods have even enabled the manipulation of robust materials such as diamond. Jing *et al.* devised a single-edge burst stripping technique, using tape to peel off wafer-scale diamond films, which can then be integrated onto various substrates (Fig. 8d).[171] This process produces ultra-flexible, large-area diamond films compatible with strain engineering and flexible sensing.

Overall, these examples underscore the remarkable generality and transformative potential of transfer techniques. By refining steps originally developed for 2D materials, researchers are now able to integrate a diverse array of functional films and nanostructures, ranging from atomically thin layers to macroscale membranes, opening new frontiers in electronics, optoelectronics, and flexible devices by transferring for almost ''everything''.

3.3.2. Transfer on arbitrary devices. Building on the diverse transfer strategies reviewed above, not only for 2D materials but also for complex films and nanostructures, the field has now advanced toward the deterministic integration of 2D materials with functional optical and electronic devices. Leveraging these versatile transfer techniques, researchers can now position 2D materials with high precision onto a wide variety of device architectures, including ring resonators, waveguides, suspended photonic crystals, and heterostructure arrays (Fig. 9). This level of integration is critical for harnessing the unique properties of 2D materials in practical device settings, enabling the realization of advanced functionalities such as dark exciton control,[179] low-threshold nano lasers,[180] electro-optic modulators,[181] and single-photon sources for emerging quantum photonic circuits.[182]

One significant challenge in integrating 2D materials onto functional devices is the inherent non-planarity and structural complexity of many target surfaces. Device architectures such as photonic crystals with pillar or hole arrays, or waveguides with pronounced topography, often present a low fill factor or rough, uneven profiles.[183] As a result, the average interfacial adhesion force ($\mathbf{F_3}$) between the 2D material and the device surface is substantially reduced, making reliable and residue-free transfer particularly difficult. In such cases, conventional transfer methods may fail to achieve uniform contact or clean release. To address this, it becomes essential to adopt transfer strategies that can further minimize the adhesion between the 2D material and the transfer medium ($\mathbf{F_2}$)—for example, through hybrid or capillary force-assisted techniques, substrate heating, or the use of sacrificial layers—thereby ensuring successful transfer even onto substrates with minimal or discontinuous contact area.[132,184] The versatility of 2D materials, stemming from their atomic thickness and vdW interactions, allows them to conform to a variety of substrates, but optimal integration requires careful engineering of interfacial forces tailored to the specific device geometry.

Here, we highlight some representative examples for transfer onto arbitrary substrates, including ring resonators, waveguides and suspend devices. Electro-optic modulation and ring resonators: Datta *et al.* integrated monolayer WS_2 onto a silicon nitride microring resonator using polymer-assisted wet

Open Access Article. Published on 06 January 2026. Downloaded on 1/16/2026 12:17:14 PM.
This article is licensed under a Creative Commons Attribution-NonCommercial 3.0 Unported Licence.

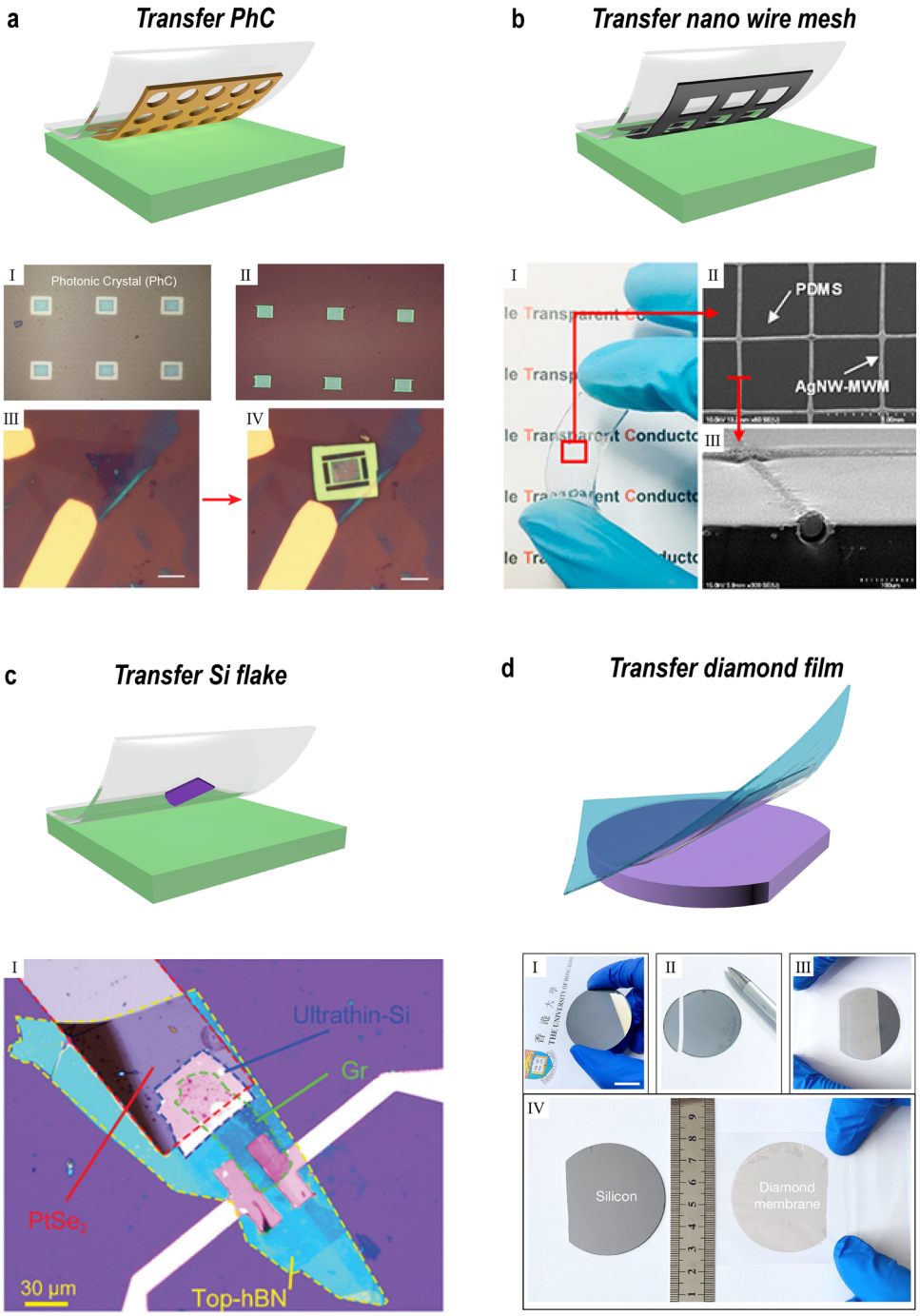

Fig. 8 Transfer beyond 2D materials. (a) The photonic crystals (PhCs). Suspended PhCs are detached from GaP and transferred onto SiO_2/Si substrates, enabling integration with light-emitting vdW heterostructures and cavities. Reproduced from ref. 170 with permission from American Chemical Society, Copyright 2017. (b) Nanowire mesh. A large-area nanowire mesh device is fabricated and transferred, as shown in top-view and cross-sectional SEM images. Reproduced from ref. 178 with permission from American Chemical Society, Copyright 2017. (c) Si flakes. An ultrathin Si flake is transferred onto $PtSe_2$ to form a UV photodetector. Reproduced from ref. 172 with permission from Wiley-VCH, Copyright 2024. (d) Diamond film. An ~1 μm-thick, 2-inch-wide diamond membrane is exfoliated from Si using adhesive tape, leaving the substrate clean and reusable. Reproduced from ref. 171 with permission from Springer Nature, Copyright 2017.

transfer, demonstrating strong light–matter interaction between 2D materials and ring resonators and the electrical tunable opto-device (Fig. 9a).[181] Graphene-based modulators, first demonstrated by Liu *et al.*, were realized by transferring monolayer graphene onto optical fiber waveguides, enabling the development of the first integrated graphene electro-absorption modulator.[185] Besides, single-photon emitters on waveguides: Peyskens *et al.* used dry transfer to place WSe_2 onto silicon nitride photonic integrated circuits, realizing deterministic integration of single-photon emitters (Fig. 9b).[182]

 This journal is © The Royal Society of Chemistry 2025

Open Access Article. Published on 06 January 2026. Downloaded on 1/16/2026 12:17:14 PM.
This article is licensed under a Creative Commons Attribution-NonCommercial 3.0 Unported Licence.

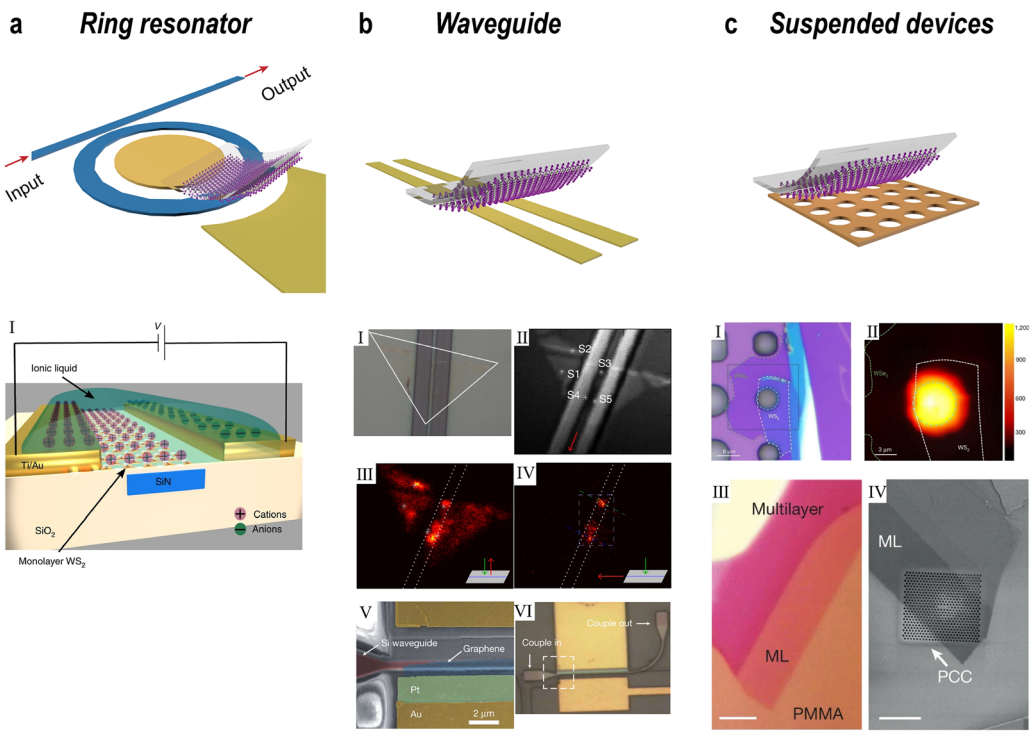

Fig. 9 Transfer materials on arbitrary devices. (a) Transfer to ring resonators. Schematic and device design showing a WS_2 monolayer integrated with a SiN_x ring resonator for ionic-liquid-controlled modulation. Reproduced from ref. 181 with permission from Springer Nature, Copyright 2020. (b) Transfer materials to waveguides. Scheme and experimental demonstration examples of transferred WSe_2 or graphene flakes on waveguides. Adapted from ref. 182 according to Creative Commons Attribution 4.0 International License (CC BY 4.0). Reproduced from ref. 185 with permission from Springer Nature, Copyright 2011. (c) Transfer material on suspended devices. Schematic and device design of transferring the 2D twisted device or monolayer on holes or a hole array (PhC cavity). Reproduced from ref. 180 with permission from Springer Nature, Copyright 2015. Reproduced from ref. 186 with permission form Springer Nature, Copyright 2022.

Sun *et al.* employed mechanical exfoliation and dry transfer to place WS_2/WSe_2 heterojunctions onto circular hole arrays, observing interlayer exciton enhancement in suspended geometries (Fig. 9c).[186] Similarly, dark exciton readout and quantum photonics: Ma *et al.* transferred exfoliated WSe_2 and h-BN films onto silicon nitride PhC using capillary force-assisted clean stamp transfer.[179] This enabled the realization of a dark exciton qubit readout system. Nanolaser has also been achieved by Wu *et al.* through the traditional polymer wet transfer. They integrated WSe_2 onto prefabricated photonic crystal cavities, serving as a gain medium for nanolasing after polymer removal.[180]

3.4. From lab to industry

Building on the laboratory-scale advances outlined in Sections 3.1–3.3, where diverse transfer techniques have been established and several already demonstrated wafer-scale feasibilities, the critical question now is how these methods can evolve into industry-compatible processes. This transition requires not only meeting the stringent requirements of large-area production, high material quality, and yield stability, but also ensuring seamless compatibility with existing semiconductor manufacturing. In this section, we first outline the key criteria for industrial adoption, including scalability, quality, yield, integration, and environmental compliance, before reviewing emerging strategies that address these challenges. In particular, we highlight the convergence of roll-to-roll (R2R) processes with robotics- and artificial intelligence (AI)-assisted automation, which is poised to define the next phase of wafer-scale, high-throughput 2D material transfer.

3.4.1. The requirements of industrialization. To advance 2D material transfer from laboratory demonstrations to commercial deployment, several key requirements must be addressed. These include achieving scalable production capacity, ensuring material quality, maintaining a high yield rate, securing compatibility and integrability with existing semiconductor processes, and meeting environmental compliance. Each of these factors is critical to determining whether transfer methods can support reliable, cost-effective, and sustainable industrial applications.

Production scale. For commercialization, production capacity determines the ability to supply the market, serves as the foundation for seizing market share, and directly affects costs and profits. This is because the scale of output directly determines the allocation of labor and energy costs, thereby influencing the commercial feasibility and being the key factor determining whether something can be commercialized.[187] Although the small-batch process can produce high-quality 2D materials, its production capacity is far from meeting the industrial demand. The inability to efficiently produce these

Open Access Article. Published on 06 January 2026. Downloaded on 1/16/2026 12:17:14 PM.
This article is licensed under a Creative Commons Attribution-NonCommercial 3.0 Unported Licence.

materials has deprived them of price competitiveness and has limited their potential for industrial development.[188]

Material quality. If large-scale production is the ''entrance ticket'' for commercialization, then high quality is the ''long-term pass'' for commercialization. Without high quality, even if a large-scale production capacity opens up the market, it will quickly lose users due to malfunctions and low performance. The quality of the material lattice, grain size, and defect density directly determine the benchmark performance migration rate, saturation current, light response intensity, and noise of electronic/optical devices. For high-end electronic devices, high-quality materials are necessary. Large-scale production capacity and high-quality materials are often a difficult choice.[189] Therefore, there is an urgent need to develop a method that takes into account both the preparation efficiency and the material quality.[190]

Yield rate. Yield directly determines the production cost and resource utilization of products is the key to balancing profits on a large scale and is also the core indicator of material quality stability and is the key to sustainable commercial development. For 2D materials, reducing defects (bubbles, wrinkles, cracks, and residues) has a strong correlation with yield.[187] Therefore, how to avoid material defects and improve yield is another challenge that needs to be overcome for commercial sustainable development. Moreover, different types of defects have various impacts on the performance of the materials, and a complete inspection process needs to be established by combining different testing methods and characterization means.[191]

Compatibility and integrability. For industrialization, compatibility is the foundation for the synergy of the industrial chain. Seamless integration with the existing manufacturing ecosystem is necessary to quickly integrate into the existing industry and reduce implementation costs. The silicon-based industry is already mature enough, while many high-performance 2D materials cannot be integrated with the silicon production lines, facing issues such as mismatched thermal budgets, low alignment accuracy, and incompatibility with other processes.[192] Although the transfer method usually works well in dealing with these issues, it does bring about defect problems, thereby reducing the quality and yield of the materials.[189] Once 2D materials are integrated with the traditional silicon-based industry, they can effectively increase integration density and provide a more advanced platform for next-generation electronic products,[193] especially as silicon technology itself evolves toward multilayer architectures—from 3D FinFETs to gate-all-around (GAA) FETs and ultimately to multi-bridge channel FETs (MBCFETs)—where the incorporation of 2D materials is particularly well suited to future scaling trends.[194]

Environmental compliance. Even if the production line can be compatible with the existing ones and can produce high-quality materials, the environmental protection aspect determines whether commercialization can be permitted by regulations and policies. Besides meeting legal requirements, considering costs as well, many processes use harmful solvents. Therefore, the high cost of waste disposal is another challenge for commercialization.[188] The advantages of R2R and CVD depend on the reusability of the materials.

Addressing these industrial requirements has motivated the exploration of next-generation transfer strategies that combine cleanliness, scalability, and broad material compatibility. Very recently, the team led by Zheng *et al.* proposed a transfer method based on the electrostatic double layer (EDL) repulsion mechanism (EDL transfer), which utilizes the EDL repulsive force formed in ammonia solution to achieve non-destructive separation of vdW materials from the growth substrate.[195] Importantly, this method does not rely on etching reactions. The EDL repulsive force is based on making both the material and the substrate surface negatively charged to form a long-range electrostatic repulsion force, overcoming van der Waals attraction, thereby achieving material exfoliation, avoiding the problems of etching damage, contamination and residue in traditional methods. It not only improves the integrity and interface cleanliness of the material but is also applicable to various 2D materials (TMDs, graphene, h-BN, CNT, *etc.*) and substrates (oxides, metals, nitrides, mica, *etc.*). By adjusting the pH and ionic strength of the solution, the EDL repulsive force can be effectively enhanced to achieve rapid, uniform, wafer-level material exfoliation. Moreover, the entire process is rapid and mild and can achieve centimetre-level exfoliation in just a few seconds.

3.4.2. Large-scale and automated transfer approaches. Building on the requirements outlined above, this section reviews recent advances in large-area and automated transfer methods, focusing on how R2R strategies and AI/robotics-driven systems can enable wafer-scale integration with industrial compatibility.[196–200]

The advent of automation and AI-enabled process control further amplifies this transformation.[201] By enabling precise, reproducible handling of delicate 2D layers, minimizing human error, and allowing real-time process optimization, automated transfer systems not only boost yield and uniformity, but also facilitate the complex multi-step stacking and assembly required for next-generation electronic and optoelectronic devices. These advances are directly aligned with the evolving requirements of the global semiconductor industry, as reflected in the IRDS.[90,91]

In this section, we will highlight how large-scale transfer approaches, especially R2R and AI-driven automated transfer, are poised to unlock the industrial potential of 2D materials, ensuring their successful integration into the semiconductor roadmap and setting the stage for the next wave of electronic and quantum technologies.

Roll-to-roll (R2R) transfer. R2R transfer has established itself as a cornerstone for the large-scale manufacturing of 2D materials, especially in contexts demanding flexible substrates and continuous, high-throughput production (Fig. 10a). In a

 This journal is © The Royal Society of Chemistry 2025

Open Access Article. Published on 06 January 2026. Downloaded on 1/16/2026 12:17:14 PM.
This article is licensed under a Creative Commons Attribution-NonCommercial 3.0 Unported Licence.

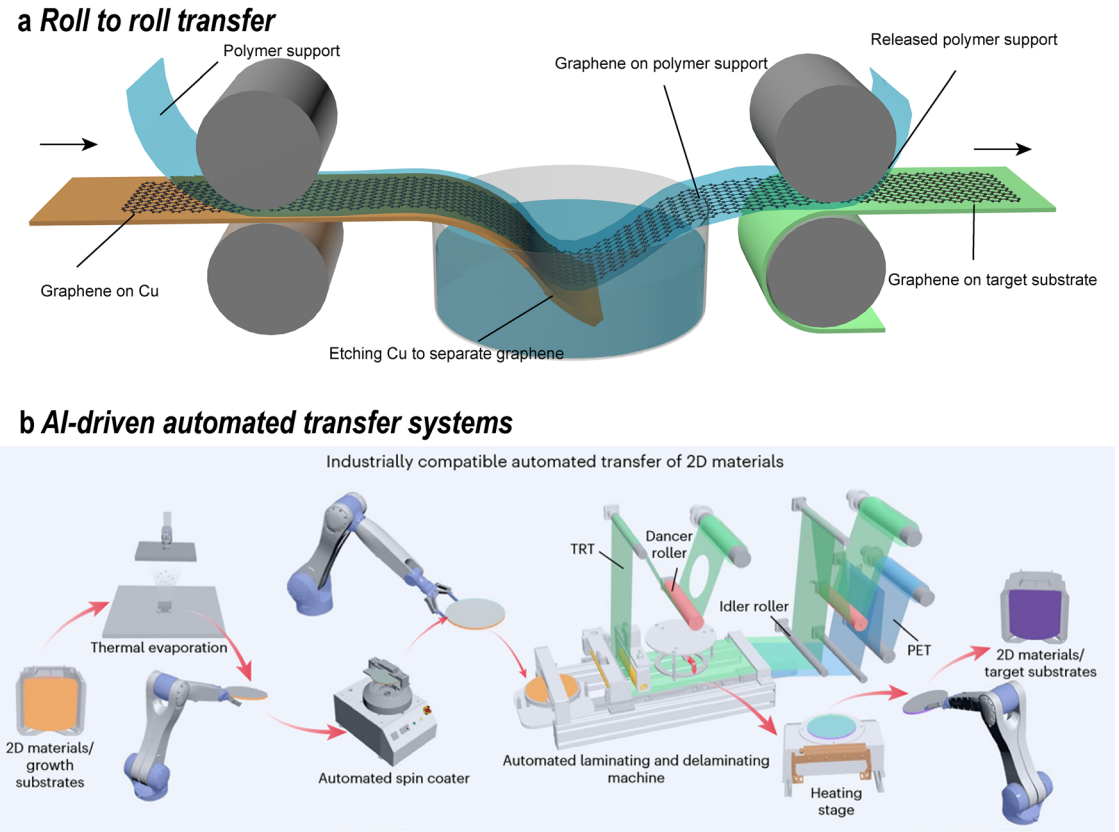

Fig. 10 Large-scale preparation (a). The concept of the roll-to-roll (R2R) transfer. (b) The concept and design of AI-driven automated transfer systems. Reproduced from ref. 201 with permission from Springer Nature, Copyright 2025.

typical R2R process, 2D materials such as graphene or MoS_2 are first synthesized on metal foils, most commonly copper or nickel, and subsequently transferred onto flexible polymer supports such as polyethylene terephthalate (PET) or polyimide (PI) *via* continuous mechanical lamination.

Early breakthroughs in this field were exemplified by Bae *et al.* who achieved the transfer of 30-inch graphene films using a wet-etching process to remove the copper growth substrate, followed by direct lamination onto polymer films.[200] Subsequent advancements by Kobayashi and colleagues introduced photocured epoxy resin adhesives, which substantially improved transfer yield and enabled the production of graphene films up to 100 meters in length, marking a significant step towards true industrial-scale production.[202] For TMDs like MoS_2, whose vapor-phase growth chemistry complicates direct R2R integration, hybrid wet/dry R2R strategies have been devised, allowing for the continuous transfer of large-area MoS_2 layers with high crystallinity and device-grade performance.

Despite these substantial advances, the R2R paradigm presents technical challenges, particularly those inherited from wet-transfer processes, namely, polymer residue contamination, difficulties in maintaining interface cleanliness, and the single-use nature of etched metal substrates. These issues can degrade the electrical and mechanical properties of the transferred 2D layers, limiting their utility in high-performance devices. Recent innovations, such as dry R2R methods that enable precise control of peel tension and speed, are mitigating these limitations and yielding higher-quality films. Additionally, techniques like electrochemical delamination and etchant-free hot water separation have enabled the reuse of metal growth substrates and reduced the risk of ionic contamination, further enhancing process sustainability and scalability.

Nevertheless, R2R transfer remains largely confined to 2D materials and substrate combinations compatible with continuous roll architectures. Translating these advances to rigid wafers or arbitrary substrates presents ongoing challenges, particularly in terms of alignment, uniformity, and defect minimization over meter-scale areas. Achieving pristine interfaces free from mechanical defects such as wrinkles, tears, and bubbles remains a critical area of technical development for the next phase of industrial integration.

AI-driven automated transfer systems: towards scalable and reproducible manufacturing. The development of AI- and robotics-assisted transfer systems represents a major step toward industrial-scale, high-throughput manufacturing of 2D materials and their heterostructures. Traditional manual or semi-automated transfer methods are inherently limited by human-induced variability, poor control over strain and adhesion, and the risk of contamination, ultimately restricting scalability, reproducibility, and device yield.

Open Access Article. Published on 06 January 2026. Downloaded on 1/16/2026 12:17:14 PM.
This article is licensed under a Creative Commons Attribution-NonCommercial 3.0 Unported Licence.

Liu Zhongfan's team recently reported a fully automated transfer platform that addresses these bottlenecks by integrating advanced robotics, programmable feedback control, and precision engineering of interfacial forces[201] (Fig. 10b). Their approach introduces a tunable Al/Al_2O_3 adhesion layer, enabling programmable internal strain and precise delamination/lamination control. Combined with robotics for handling, spin-coating, lamination, and peeling, the system achieves crack-free, residue-free, and highly uniform wafer-scale transfer of CVD-grown graphene, h-BN, MoS_2, and their vdW heterostructures.

Notably, the system demonstrates a production capacity of up to 180 wafers per day, with >99% intactness and carrier mobilities for transferred graphene exceeding 14 000 $cm^2 V^{-1} s^{-1}$ across a 4-inch wafer, with performance metrics comparable to or even surpassing those of manually exfoliated materials. The automated, solution-free process eliminates harsh chemical etchants and minimizes environmental impact, as verified by comprehensive life cycle assessment (LCA).

AI- and robotics-assisted transfer systems set new benchmarks for precision and repeatability in 2D materials integration, as these platforms tightly regulate tension, speed, and pressure during each transfer step, dramatically reducing defects such as cracks, bubbles, and wrinkles that often plague manual approaches and ensuring high device reliability at scale.[201] The resulting material and substrate flexibility is notable: automated workflows can seamlessly handle graphene, h-BN, MoS_2, and complex heterostructures, with compatibility across a broad spectrum of substrates, including Si, SiO_2/Si, HfO_2, and Al_2O_3. Layer-by-layer stacking and heterostructure assembly become both programmable and highly reproducible. From an industrial viability standpoint, these automated solutions achieve high throughput, robust wafer-to-wafer consistency, and ultra-low contamination, effectively bridging the gap between academic demonstrations and practical manufacturing for photonics, electronics, and quantum technologies.[203] Importantly, sustainability is enhanced by minimizing liquid-phase waste and reducing labour costs, yielding a more environmentally friendly and economically attractive process than traditional chemical-based transfers. Nevertheless, challenges remain, including adapting these platforms to rigid, non-rollable substrates, automating multi-material assembly, and developing closed-loop, AI-driven defect detection to ensure quality and scalability for future industrial applications.

In summary, the emergence of automated, AI-assisted transfer and analysis platforms represents a paradigm shift in the scalable production of 2D materials.[204,205] These systems will be foundational to integrating 2D materials into the semiconductor roadmap and unlocking their full commercial potential in next-generation flexible, transparent, and quantum electronic devices.

3.5. Summary and perspectives

In this section, we summarized the landscape of 2D transfer methods, covering wet, dry, and hybrid strategies, together with scalable innovations such as dielectric-assisted, SiN_x film-assisted, and UV tape-assisted transfer. These approaches demonstrate that transfer has evolved from an auxiliary step into a central technology, directly determining interface cleanliness, scalability, and device fidelity. Despite remarkable progress, major challenges remain in achieving residue-free interfaces, wafer-level uniformity, and compatibility with industrial processes. Looking forward, breakthroughs in intrinsically clean transfer, reconfigurable stacking, and automated wafer-scale assembly will be crucial for bridging laboratory demonstrations with semiconductor manufacturing, thereby enabling 2D materials to play a transformative role across electronics, photonics, and quantum technologies.

4. Strategies for mitigating environmental sensitivity in 2D materials

The atomically thin nature of 2D materials renders them exceptionally sensitive to external environmental perturbations. Ambient factors such as oxygen and humidity readily induce degradation pathways, while transfer processes inevitably introduce polymer residues, interfacial contamination, and mechanical stress. These perturbations obscure intrinsic electronic and optical responses, underscoring the need for rigorous interfacial protection and defect control. In this chapter, we highlight three critical aspects: (i) environmental influences and encapsulation strategies, (ii) transfer-induced contamination and strain, and their diagnostic identification, and (iii) post-transfer treatment by mechanical and chemical cleaning. Altogether, these perspectives establish a framework for preserving the intrinsic functionality of 2D materials and guiding their reliable integration into advanced devices.

4.1. Environmental influences and encapsulation strategies

For 2D materials, the external environment is of crucial importance because contaminants will inevitably be introduced onto the material surface. On one hand, the van der Waals surfaces of 2D flakes are atomically clean; on the other hand, these pristine surfaces readily attract trace contaminants from the ambient environment, leading to the formation of an interfacial contamination layer.[206]

Specifically, water and hydrocarbons in the air can quickly contaminate the surface of 2D materials, causing the hydrophilic surface of 2D materials to become hydrophobic.[207,208] By controlling the relative humidity of the environment at a lower humidity level, the density of tiny water droplets in the air can be reduced, and materials with hydrophilicity will not adsorb the moisture in the air.[209] In our laboratory experience, environmental humidity has a profound influence on the stability of exfoliated 2D flakes. For instance, in Singapore, where the relative humidity often exceeds 50–60%, freshly exfoliated flakes exhibit markedly shorter lifetimes compared to those prepared under the much drier conditions in Canberra, Australia (lab humidity is ~30%). The higher ambient moisture

 This journal is © The Royal Society of Chemistry 2025

Open Access Article. Published on 06 January 2026. Downloaded on 1/16/2026 12:17:14 PM.
This article is licensed under a Creative Commons Attribution-NonCommercial 3.0 Unported Licence.

promotes surface adsorption and interfacial oxidation, accelerating degradation and leading to faster loss of optical and electronic integrity. This observation highlights the critical role of environmental control in preserving the intrinsic properties of 2D materials during storage and device fabrication.

In addition to humidity, the oxidation is another obvious factor that can downgrade the 2D flack qualities.[210] When oxygen undergoes chemical adsorption with the material, an irreversible oxidation reaction occurs, forming localized states at the surface or defects, becoming electron/hole scattering centers or traps, reducing the mobility and causing threshold drift, ultimately leading to a decline in the performance of the device.[211–216] For example, when graphene is oxidized or PMMA is left with carbon, non-radiative recombination increases, photoluminescence (PL) is quenched, the spectral line broadens or an additional background appears.[214]

Moreover, the oxidation of 2D materials is strongly accelerated under certain environmental conditions. Elevated temperatures can enhance oxygen diffusion and reaction kinetics, leading to rapid degradation of materials such as MoS_2 and black phosphorus (BP) through the formation of oxides or suboxides.[217–219] High humidity further exacerbates oxidation, water facilitates oxygen-water redox chemistry and aids defect-assisted hydrolysis/oxidation pathways, producing hydroxylated species that speed up layer etching and chemical degradation, a particularly severe problem for hydrophilic materials such as BP.[219] Therefore, controlling ambient temperature, oxygen partial pressure and relative humidity during transfer and post-processing, together with timely encapsulation, is essential to limit irreversible oxidation and to preserve intrinsic electronic and optical properties.

4.1.1 Encapsulation strategies. Because nearly all atoms in 2D materials are directly exposed to the environment, their surfaces readily interact with oxygen, water vapor, and other airborne species, leading to rapid degradation of their electrical and optical performance. Encapsulation with inert materials such as h-BN has therefore become one of the most effective strategies for maintaining stability and device lifetime.[220] By isolating the active layers from the ambient, h-BN capping prevents oxidation, adsorbate doping, and moisture infiltration, while simultaneously offering a clean, atomically flat interface.

The significance of such encapsulation was first demonstrated by Dean *et al.*, who found that the direct contact between graphene and the substrate introduced significant impurity scattering and reduced carrier mobility.[160] By inserting h-BN as both a substrate and a capping layer, they obtained graphene devices with substantially improved performance, reflected in narrower charge neutrality peaks and higher induced charge densities under magnetic fields. This work laid the foundation for van der Waals heterostructure research and firmly established h-BN encapsulation as a gold standard in 2D material device fabrication.

However, while h-BN encapsulation greatly improves stability, its effectiveness is often compromised in practical device configurations (Fig. 11a). When the encapsulation layer is laminated over topographically uneven regions, particularly over thick metal electrodes, differences in rigidity, adhesion, and surface energy create local voids and interfacial gaps. These nanoscale pockets allow oxygen and water molecules to infiltrate, weakening the encapsulation and leading to localized doping, oxidation, or delamination over time. Such microcavities not only degrade contact reliability but also introduce trapped charge regions that deteriorate long-term device stability.[221]

To address these challenges, three complementary strategies have been developed (Fig. 11b–d): thinning the electrodes, forming 1D edge contacts, and introducing *in situ via* contacts.

Thinner electrode strategy (Fig. 11b): the most straightforward approach is to reduce the electrode thickness to minimize the step height at the metal/h-BN interface.[222] Conventional electrodes, often tens of nanometers thick, can be replaced by ultrathin gold layers a few nanometers in thickness, or even by atomically thin conductive films such as few-layer graphene or emerging 2D metals like Au or Ga.[223–225] These atomically flat electrodes ensure conformal contact between the top

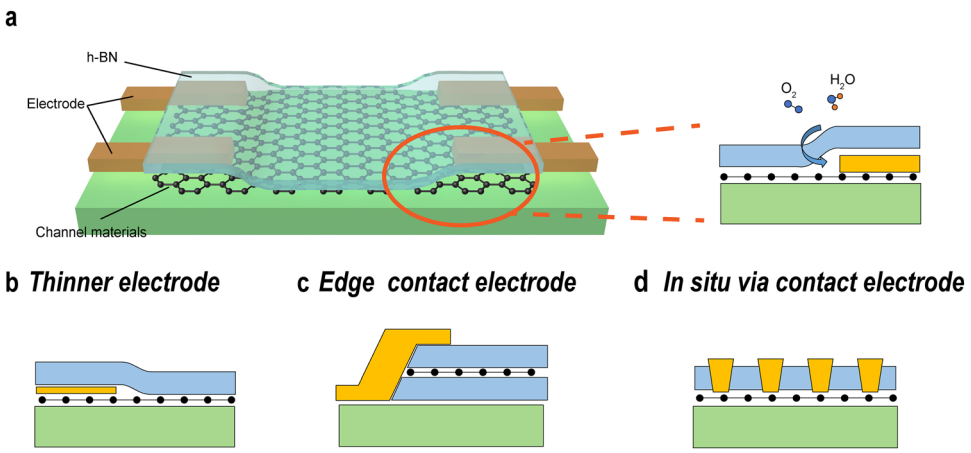

Fig. 11 2D material encapsulation engineering. (a) The h-BN encapsulation strategy and its limitation: moisture or oxygen may seep in through the gap. (b) Thinner electrode. (c) Edge contact electrode. (d) *In situ via* contact electrode.

Open Access Article. Published on 06 January 2026. Downloaded on 1/16/2026 12:17:14 PM.
This article is licensed under a Creative Commons Attribution-NonCommercial 3.0 Unported Licence.

encapsulation and the active 2D channel, suppressing the formation of voids and interfacial strain. Recently, Zhao *et al.* developed a vdW compression technique capable of compressing metals such as Bi, Ga, In, Sn, and Pb to the atomic-thin limit (~1 Å) between MoS_2 anvil layers,[226] offering a new pathway for creating perfectly matched ultrathin contacts compatible with encapsulation processes.

In addition, graphene can also serve as an encapsulation material. Mirzayev demonstrated a suspended 0D/2D heterostructure in which graphene layers were encapsulated and used to replace metal electrodes.[227] This structure integrated C_{60} molecules between the two layers of graphene in a buckyball sandwich structure. The graphene layers protected the C_{60} molecules from damage caused by microscope vacuum and radiation, allowing for a direct study using STEM and imaging at the atomic resolution. Gyeon *et al.* used $PtSe_2$ films as electrodes/contacts to fabricate FET devices and prepared a FET array with $PtSe_2$ channels.[228] The on/off ratio under p-type behavior reached approximately 10^3. This demonstrates that the electrode material can not only be used for semiconducting properties but also as an electrode or contact metal in certain devices.

Edge contact strategy (Fig. 11c): an alternative route to preserve interfacial integrity is to contact the 2D channel along its exposed edge rather than the top surface. Wang *et al.* first demonstrated this one-dimensional edge contact configuration, in which graphene encapsulated within h-BN was etched to expose its edges before metallization.[169] This geometry eliminates the need for metal deposition on top surfaces, achieving both full encapsulation and excellent electrical coupling. The resulting devices exhibited record-high room-temperature mobilities of up to 140 000 $cm^2 V^{-1} s^{-1}$, attributed to the reduced contact-induced disorder and absence of trapped interfacial residues.

In situ via contact strategy (Fig. 11d): building upon the edge-contact concept, Telford *et al.* proposed integrating pre-patterned metal vias within the h-BN encapsulation layer itself, forming direct vertical contacts to the 2D channel beneath.[229] This approach avoids local delamination caused by electrode topography, enabling intimate coupling with minimal contamination. Li *et al.* later advanced this technique using *in situ* through-hole metallization to embed contacts within h-BN, achieving excellent reproducibility, mechanical robustness, and long-term reliability.[230] Such *in situ via* architectures are particularly promising for scalable, wafer-level integration, offering compatibility with industrial semiconductor processing.

In addition to the h-BN based encapsulation, graphene or even the functional devices themselves can serve as the protection layers. Recently, Bai *et al.* utilized a photonic crystal defect cavity (1D PhC defect cavity) to enhance and stabilize the second harmonic generation (SHG) performance of $NbOCl_2$.[220] By placing a thin $NbOCl_2$ sheet between the upper and lower TiO_2/SiO_2 stacked mirrors to form a vertical resonant cavity, the incident light strongly resonates within the $NbOCl_2$ layer, resulting in a 12-fold SHG enhancement. Moreover, the outer photonic crystal cavity served as a physical encapsulation layer, ensuring that the SHG signal of $NbOCl_2$ did not show significant attenuation for 10 months in a room-temperature air environment.

In summary, although encapsulation remains essential for preserving the intrinsic properties of 2D materials, achieving defect-free sealing across realistic device geometries requires precise engineering of contact topology and interfacial conformity. Strategies such as ultrathin or 2D-metal electrodes, 1D edge contacts, and *in situ via* embedding have collectively pushed encapsulation performance to new limits. Altogether, these advances form the technological basis for achieving air-stable, durable, and high-mobility 2D electronic and optoelectronic systems.

4.2. Transfer-induced undesired effects

4.2.1. Effects of contamination and defects on intrinsic properties. Even after employing advanced transfer techniques, post-transfer processing remains essential for achieving clean and high-performance 2D material devices. Due to their atomic thinness, 2D materials are highly sensitive to both external contaminants (such as polymer residues) and internal structural distortions (such as wrinkles, cracks, and bubbles), all of which can significantly degrade their intrinsic physical and electronic properties.

Chemical contamination and residues. Among various transfer strategies, wet transfer, especially PMMA-assisted methods, remains widely used, yet polymer residues and surface contaminants continue to pose major challenges. PMMA residues, for example, act as p-type dopants and scattering centers on graphene, reducing carrier mobility and overall performance.[231,232] In addition, the transfer process itself may cause structural defects such as tearing or bubbling.[97,159] Zheng *et al.* further showed that PMMA can chemically react with etching agents (*e.g.*, HF, KOH, NaOH, and $FeCl_3$) during transfer, leaving insoluble residues that persist even after acetone rinsing.[195] In contrast, transfers using ammonia-based etchants resulted in almost residue-free surfaces, highlighting that chemical compatibility between the polymer and etchant is crucial. Residues not only lower mobility but also modify the optical response, introducing nonradiative recombination centers, redshifts in PL peaks, and spectral broadening due to local strain and disorder. In multilayer TMDCs, residual PMMA can suppress interlayer coupling, causing their optical features to resemble those of monolayers until annealing restores proper interlayer interactions.

Etching-based wet transfer introduces additional concerns.[233] Metal ions (K^+ and Na^+) from common etchants can unintentionally dope 2D semiconductors and are incompatible with CMOS processes. In large-area MoS_2 transfers, such residues increase surface roughness and contact resistance while degrading carrier mobility. Liu *et al.* recently demonstrated that incomplete rinsing steps can leave residual PMMA islands on graphene, creating localized charge traps and potential fluctuations that alter both Raman and PL signatures.[234] These

Open Access Article. Published on 06 January 2026. Downloaded on 1/16/2026 12:17:14 PM.
This article is licensed under a Creative Commons Attribution-NonCommercial 3.0 Unported Licence.

findings underline that polymer residues and interfacial impurities remain one of the most persistent obstacles in 2D material transfer.

Structural and interfacial defects. Beyond chemical contamination, physical stress introduced during transfer can also compromise material integrity. The surface tension and capillary forces in liquid-based transfers often induce wrinkles, cracks, and trapped bubbles. Wrinkles cause anisotropic carrier scattering and mobility reduction, while localized strain bends the band structure, forming quantum-dot-like emission hotspots and modifying PL energy and intensity.[235] Cracks and twin boundaries disrupt charge transport and Raman symmetry.[235] Meanwhile, interfacial bubbles not only enlarge the physical gap between layers but also generate localized charge puddles, degrade optical absorption, and reduce overall device mobility.[236]

During the transfer process, particularly in wet transfer, surface tension and capillary forces inevitably introduce local stress within the 2D material, leading to the formation of wrinkles, cracks, and interfacial bubbles. Such structural distortions significantly influence electrical and optical performance. Wrinkles and cracks increase resistance and carrier scattering, resulting in anisotropic conductivity and reduced carrier mobility.[237,238] The strain accumulated along folds can also bend the local band structure of TMDCs, generating ''quasi-quantum-dot'' emission hotspots that alter the local PL energy and brightness, and in some cases, cause reconfiguration of the energy levels at the deformed regions.[239,240] Internal crystal defects, including twin boundaries and irregular grain boundaries, further disturb Raman responses and disrupt lattice symmetry.[241] Interfacial bubbles, on the other hand, enlarge the physical separation between adjacent layers, degrading optical coupling and introducing non-radiative recombination centers. These trapped voids increase PL and absorption interface states, diminish overall membrane response,[242] and deteriorate charge transport by lowering field-effect mobility.[243]

4.2.2. Identification and characterization of transfer-induced contaminants. Apart from environmental exposure, contamination can be introduced at nearly every step of the transfer process, from polymer supports and etching agents to residues originating from the growth substrate itself. Identifying the sources of these pollutants and optimizing each process step are therefore essential to minimizing contamination at its origin.[244]

Optical microscopy, along with a range of non-contact spectroscopic techniques, provides the most rapid and convenient means of assessing the quality of transferred films.[238] Raman spectroscopy and photoluminescence (PL) mapping are particularly effective for detecting contamination and local strain or doping. For instance, variations in the D, G, and 2D bands of graphene, or shifts in excitonic peak positions in TMDCs, can indicate the presence of carbonaceous residues, strain accumulation, or charge-transfer doping.[245] While these optical probes can distinguish between physical adsorption and charge doping, they are less effective at identifying the chemical composition of contaminants.[246,247]

X-ray photoelectron spectroscopy (XPS) complements optical methods by providing information on elemental composition and bonding states. Characteristic peaks such as C 1s, O 1s, C–O, and C═O reveal organic residues (*e.g.*, PMMA fragments) or oxidation products.[247] However, XPS suffers from limited spatial resolution and must often be combined with local probes. Photothermal-induced resonance (PTIR) offers a nanoscale alternative, capable of mapping the infrared spectra of surface pollutants with nanometer-scale resolution and high mass accuracy.[248]

Morphological methods such as atomic force microscopy (AFM) and scanning electron microscope (SEM) remain indispensable for identifying nanoscale residues, wrinkles, or bubbles through surface roughness mapping.[249] Advanced photoelectron and work-function imaging techniques, such as X-ray photoemission electron microscopy (XPEEM), further enable correlation between surface chemistry and electronic structure.[247] Cathodoluminescence (CL), when combined with SEM or scanning transmission electron microscopy (STEM), allows high-resolution optical characterization of encapsulated TMDs and h-BN heterostructures.[250]

Finally, secondary ion mass spectrometry (SIMS) provides high spatial and depth resolution, coupled with broad chemical sensitivity across elements, isotopes, and molecules, serving as a powerful complement to the above approaches.[251]

In summary, these characterization tools form a comprehensive framework for diagnosing contamination in transferred 2D materials, bridging structural, chemical, and electronic perspectives to guide cleaner and more reliable transfer protocols.

4.3. Post-transfer treatment by mechanical and chemical cleaning

To address these challenges, various post-processing techniques have been developed (Fig. 12), each targeting removal of organic residues, improving interfacial flatness, and eliminating interlayer bubbles:

4.3.1. Physical mechanical cleaning. Physical cleaning, as a straightforward and simple cleaning method, is widely used to remove contaminants from the surfaces of 2D materials. Examples include annealing, plasma treatment, electrostatic adsorption, AFM scanning or nano-mechanical scraping. Thermal annealing (Fig. 12a) in controlled atmospheres is a widely adopted strategy, wherein post-acetone heating decomposes and desorbs PMMA residues, while simultaneously reducing oxygen-containing species covalently bound to graphene. Nevertheless, excessive thermal budgets may induce structural defects or further degrade PMMA into reactive radicals. At the same time, it may increase the coupling between the 2D material and the substrate, resulting in excessive doping of the 2D material and a significant reduction in mobility.[252]

The electrostatic-assisted cleaning approach (Fig. 12b), achieved by placing a statically charged cloth above the contaminated region, enables non-destructive PMMA removal at

Open Access Article. Published on 06 January 2026. Downloaded on 1/16/2026 12:17:14 PM.
This article is licensed under a Creative Commons Attribution-NonCommercial 3.0 Unported Licence.

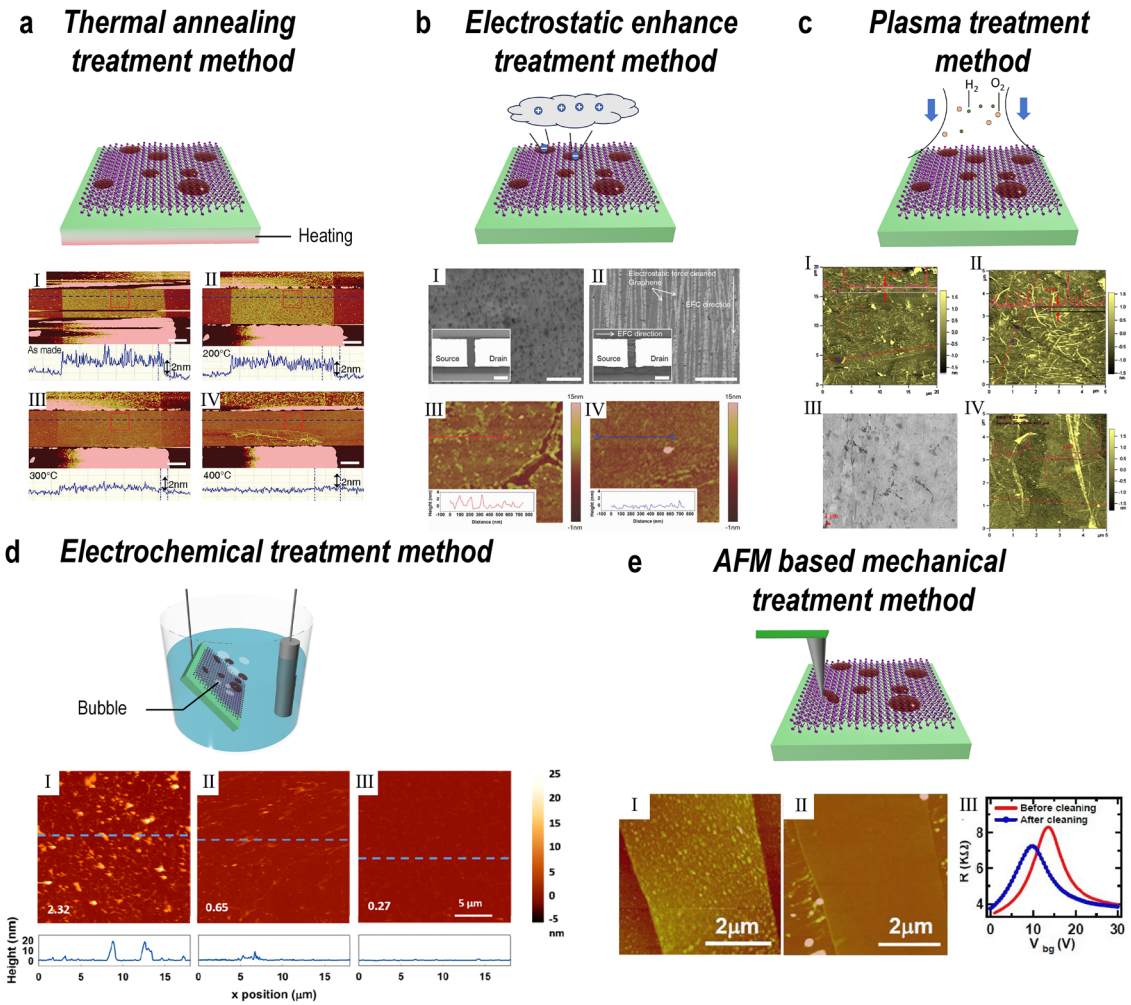

Fig. 12 Post-processing for clean strategies. (a) The thermal annealing method: thermal annealing gradually reduces surface roughness and removes residues at elevated temperatures. Reproduced from ref. 252 with permission from American Chemical Society, Copyright 2011. (b) The electrostatic force-assisted method: electrostatic force cleaning enables PMMA removal and yields cleaner graphene compared to solvent treatment. Reproduced from ref. 255 with permission from Wiley-VCH, Copyright 2013. (c) The plasma treatment method: plasma treatment produces large-area clean graphene films with preserved monolayer integrity. Reproduced from ref. 256 with permission from Elsevier, Copyright 2012. (d) The electrochemical treatment method: electrochemical treatment eliminates residues through electrolytic cleaning, lowering surface roughness. Reproduced from ref. 257 with permission from IOP Publishing, Copyright 2017. (e) The AFM-based mechanical treatment: AFM sweep ("nano-broom") mechanically removes fabrication residues, improving device characteristics. Reproduced from ref. 258 with permission from IOP Publishing, Copyright 2011.

room temperature through electrostatic attraction. Plasma treatments (Fig. 12c), employing oxygen, hydrogen, or mixed gas chemistries (*e.g.*, H_2–N_2 and H_2–Cl_2), offer highly effective removal of persistent organic and silicon-derived contaminants that survive conventional solvent cleaning or annealing. However, prolonged exposure can etch or unintentionally dope the 2D lattice. AFM/nanoprobe-based mechanical cleaning (Fig. 12e) allows localized and direct debris removal using atomic force microscope tips, particularly flexible or nanowire-coated probes, without substantial chemical modification. The combined "nano-ironing" approach, integrating thermal annealing with tip-assisted cleaning, further enhances surface planarity while minimizing oxidation and scratching. Although these methods of cleaning two-dimensional materials through mechanical force are more effective, they share a common drawback: the cleaning area is small, making them difficult to apply to large-scale cleaning of 2D materials.

4.3.2. Chemical wet cleaning. Chemical wet cleaning removes surface contaminants and polymer residues from 2D materials through solvent dissolution or electrochemical reactions. Common techniques such as solvent cleaning and electrochemical bubbling are widely adopted in laboratories and large-area material cleaning due to their simplicity and scalability. However, the dissolution of polymers like PMMA in organic solvents is a complex process involving diffusion, swelling, and partial denaturation of long-chain molecules. As a result, complete removal is often difficult, and residual fragments frequently remain on the 2D surface. Therefore, wet cleaning is typically combined with other post-processing treatments. For instance, acetone vapor dissolution is often

 This journal is © The Royal Society of Chemistry 2025

Open Access Article. Published on 06 January 2026. Downloaded on 1/16/2026 12:17:14 PM.
This article is licensed under a Creative Commons Attribution-NonCommercial 3.0 Unported Licence.

followed by thermal annealing to eliminate trace residues. Jeong *et al.* further optimized this approach by introducing a UV-assisted pre-treatment step, in which ultraviolet irradiation breaks the ester side chains of PMMA, weakening its adhesion to graphene. Subsequent cleaning with isopropanol, acetone, and methyl isobutyl ketone efficiently removes the polymer layer, achieving cleaner surfaces and improved electronic performance.[253]

Electrochemical cleaning (Fig. 12d) employs a voltage-driven water decomposition process to generate hydrogen bubbles that physically lift polymer residues off the surface. Although this technique is effective, precise control of the applied potential is necessary to prevent local delamination or structural damage.

Despite their maturity, chemical cleaning methods still face limitations such as incomplete residue removal, potential secondary contamination, and possible chemical damage to sensitive 2D lattices. These challenges have driven the search for more efficient and non-destructive alternatives. Recently, Fu *et al.* demonstrated an ultraviolet-based method to repair degraded sapphire substrates.[254] Air exposure leads to hydrolysis of sapphire, disrupting epitaxial alignment and degrading its use as a growth template. However, by irradiating the substrate with 320–400 nm UV light for 30 minutes followed by heat treatment, its crystalline order can be fully restored. Using this repaired sapphire, 2-inch wafer-scale WS_2 films were grown with exceptional uniformity and crystallinity, achieving $>95\%$ device yield and mobility fluctuations below 20%.

In summary, despite significant progress, no post-treatment can guarantee complete removal of PMMA or other organic residues. High-temperature or plasma treatments may only partially eliminate pollutants and can introduce new structural defects or chemical doping. Mechanical and electrochemical approaches offer promising alternatives but still carry risks of physical or chemical damage to delicate 2D structures.

Therefore, while post-processing greatly improves cleanliness and device performance, it often adds complexity and new sources of variability. The persistent challenge of achieving truly residue-free and undamaged interfaces underscores the urgent need for the development of fundamentally contamination-free, clean transfer methods as the field moves forward.

4.4. Summary

In summary, despite significant advances in cleaning and interface engineering, no post-treatment can guarantee the complete removal of PMMA or other organic residues. High-temperature annealing or plasma treatment may reduce contamination but often introduces new structural defects or unintentional doping. Mechanical and electrochemical approaches offer promising alternatives, yet they still risk damaging delicate 2D lattices. Consequently, post-processing—while improving cleanliness and performance—adds operational complexity and new sources of variability.

We must therefore acknowledge that post-transfer treatments can only partially restore interfacial quality and cannot fully reverse contamination or stress accumulation. Rather than relying on repair after transfer, the focus should shift toward preventing contamination at its source. This calls for the development of fundamentally clean, residue-free transfer methodologies using self-depolymerizing or volatile media, functionalized 2D support membranes, and automated, AI-driven platforms that minimize human variability. In parallel, *in situ* monitoring systems, based on Raman spectroscopy, optical interferometry, or electron microscopy, should provide real-time feedback to ensure closed-loop optimization. Collectively, these advances will enable reproducible, contamination-free integration of 2D materials at the wafer scale, bridging laboratory precision with industrial manufacturability.

5. Transfer enabled 2D material multifunctionality engineering

The atomically thin nature of 2D materials endows them with remarkable mechanical flexibility, making them uniquely susceptible to a range of deformations, such as bubbles, wrinkles, bending, folding, and twisting, during transfer and device integration. In the previous sections, we emphasized the criteria for achieving high-quality transfer, with particular focus on minimizing defects, bubbles, strain, and contamination. Yet, the same mechanical compliance that presents challenges for defect-free integration also offers unprecedented opportunities for engineering new functionalities.

The deliberate manipulation of 2D material morphology and stacking, whether by inducing controlled wrinkles, bubbles, strain fields, or twist angles, has emerged as a powerful toolkit for tailoring electronic, optical, and vibrational properties. Twist stacking, in particular, introduces a novel degree of freedom for tuning interlayer interactions and band structure in 2D materials.[259] By precisely controlling the relative rotational angle between stacked layers, researchers can engineer moiré superlattices that give rise to emergent phenomena such as correlated insulating states, unconventional superconductivity, and tunable optical responses.[260–262] Unlike traditional bulk materials, the atomically thin nature of 2D systems allows for deterministic fabrication and fine-tuning of these twist angles, unlocking rich new physics and functionalities for both fundamental research and device innovation.

In this section, we review the strategies and multifunctional applications enabled by transfer-induced engineering, focusing on wrinkles and bubbles, bending and folding, strain, and twist stacking. We summarize recent advances in the controlled creation, characterization, and utilization of these structural features, highlighting their impact on the physical properties and device performance of 2D materials.

5.1. Wrinkle and bubble engineering

Due to their atomic thickness, 2D materials such as graphene are exceptionally prone to wrinkling and bubbling during synthesis and transfer. Graphene, which has attracted significant attention since its isolation from graphite, exhibits a high

Open Access Article. Published on 06 January 2026. Downloaded on 1/16/2026 12:17:14 PM.
This article is licensed under a Creative Commons Attribution-NonCommercial 3.0 Unported Licence.

density of folds and wrinkles when unsupported, and this tendency increases with decreasing thickness.[263] During transfer, as soon as the 2D material makes contact with a substrate, often far from atomically flat, strong vdW interactions cause immediate adhesion, imprinting the underlying surface morphology onto the film and inevitably inducing ripples, folds, and bubbles.[264] Additional deformations may also arise from handling and from intrinsic factors such as thermal expansion mismatch: for example, CVD-grown graphene often displays pronounced wrinkles due to compressive strain arising from differential contraction with the metal growth substrate.[140,265] These surface irregularities can significantly alter the electronic and structural properties of the 2D material.[266,267]

The formation and control of wrinkles during transfer have been systematically studied. Wang *et al.* investigated wrinkle evolution in wedge transfer using a CAB polymer support.[263] By floating the polymer/graphene stack on water and gradually lowering the water level, pre-existing wrinkles act as drainage channels, guiding the outflow of water and thus influencing the final wrinkle orientation and density (Fig. 13a). Notably, the hydrophilicity or hydrophobicity of the substrate strongly affects wrinkle formation—hydrophobic substrates suppress wrinkles, whereas hydrophilic substrates promote them.

Wrinkle engineering is not limited to graphene. Other 2D materials, such as transition metal oxides and dichalcogenides, also form wrinkles under stress.[268] For example, buckling-induced delamination can introduce strong uniaxial strain in $NbOI_2$, with the folded region reaching 3.1% strain and showing a 35-fold increase in SHG efficiency (the absolute SHG efficiency is larger than 0.2%) compared to flat areas (Fig. 13b).[269]

Han *et al.* proposed that strain is not only a by-product in 2D transfer materials, but also a key means to control the stability and functionality of 2D materials phases.[270] They transferred the In_2Se_3 film onto an uneven substrate, generating controllable local wrinkles, which transformed it from the β phase (ferroelectric) to the α phase (antiferroelectric), thereby enhancing the carrier mobility, improving the on–off ratio and memory performance during the process.

Bubbles, another popular out-of-plane deformation, are prevalent in wet transfer processes.[271,272] These microstructures can be deliberately engineered using droplet-assisted transfer. By introducing a water droplet during pick-up, MoS_2 can be separated from a hydrophilic SiO_2/Si substrate and aligned onto an h-BN layer. Controlled annealing at 130 °C merges small bubbles into larger ones, significantly increasing their aspect ratio and associated local strain. In these bubble

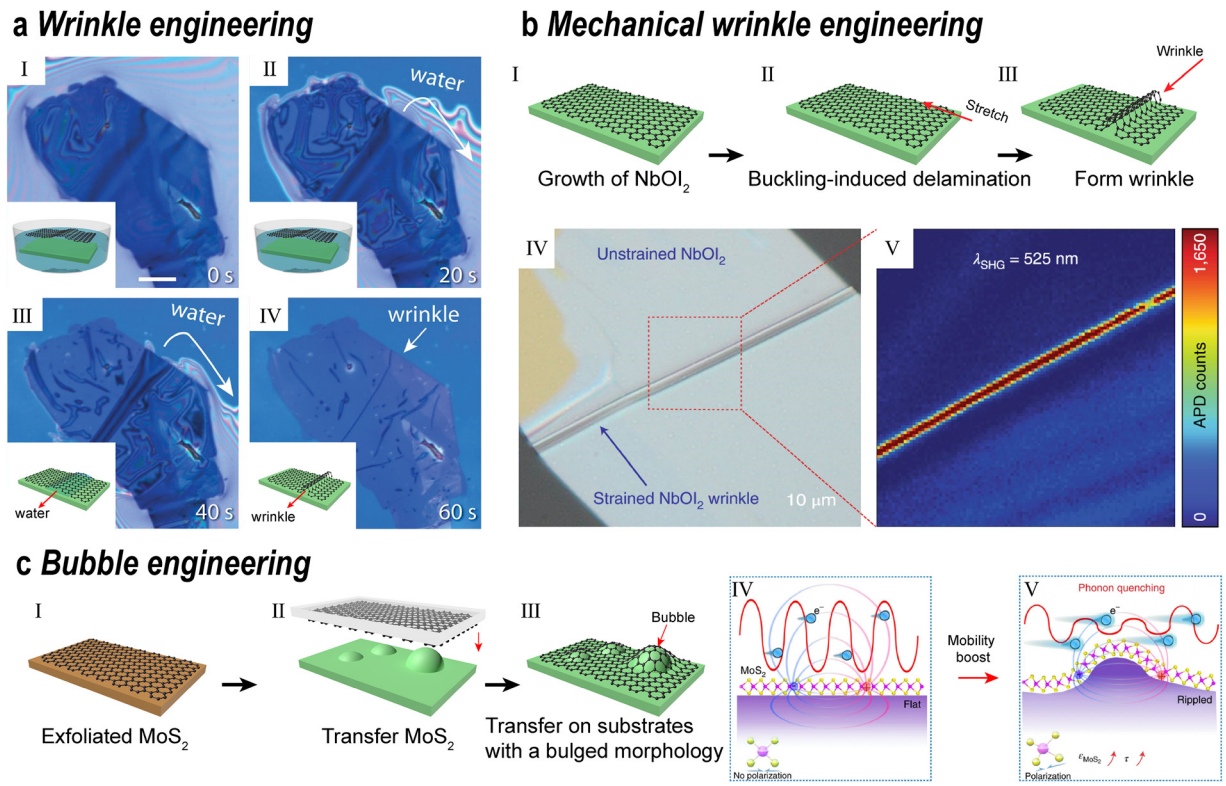

Fig. 13 Transfer 2D material for wrinkle and bubble engineering. (a) The liquid phase wrinkle approach. The formation of graphene wrinkles is controlled by the wedge transfer method. Reproduced from ref. 263 with permission from AIP Publishing, Copyright 2012. (b) The mechanical wrinkle approach: the schematic and experimental demonstration of the mechanical method to achieve wrinkles on 2D flakes. The enhanced second-harmonic generation (SHG) signal has been achieved in $NbOI_2$ flakes with wrinkle-induced strain. Reproduced from ref. 269 with permission from Springer Nature, Copyright 2022. (c) The bubble engineering: bubbles improve the mobility of r-MoS_2. Reproduced from ref. 276 with permission from Springer Nature, Copyright 2022.

This journal is © The Royal Society of Chemistry 2025

Open Access Article. Published on 06 January 2026. Downloaded on 1/16/2026 12:17:14 PM.
This article is licensed under a Creative Commons Attribution-NonCommercial 3.0 Unported Licence.

regions, PL intensity can be enhanced by more than fourfold, owing to a strain-induced funnel effect that concentrates excitonic energy in the high-strain region.[273–275]

Beyond strain from direct handling, transferring 2D materials onto rough or patterned substrates can also induce controllable lattice distortions. For example, Ng *et al.* transferred MoS_2 onto a high-roughness, convex substrate by mechanical exfoliation, producing lattice distortion that enhances dielectric screening and suppresses electron–phonon scattering, thereby boosting charge carrier mobility (Fig. 13c).[276]

Overall, while wrinkles and bubbles are often considered defects, careful engineering of these features, through substrate selection, transfer technique, or post-processing, enables tunable modulation of the mechanical, electronic, and optical properties of 2D materials, opening new avenues for functional device applications—instead of relying on chemical doping, new functions are achieved through mechanical/interface design.

5.2. Folding engineering

The remarkable mechanical flexibility of 2D materials allows for extreme bending and folding under vdW forces.[277] When sufficiently bent, adjacent regions of the material can adhere and form folded structures, first observed in mechanically exfoliated graphene sheets.[278] Folding not only arises naturally during transfer and manipulation, but also becomes a powerful, rapid method for constructing twisted 2D homojunctions and complex heterostructures. Given the critical importance of twist engineering, which has evolved into one of the most significant branches of 2D materials research, we devote a dedicated section to this topic later in Section 5.4.

Folding of 2D materials can generally be categorized into two primary strategies: solution-based folding and mechanical folding. In solution folding, liquid-mediated processes, such as selective delamination, capillary action, or surface tension, are employed to induce controlled bending and folding, often with precise control over twist angle and geometry.[279,280] For example, solution-based methods can use substrate patterning or interfacial engineering to direct the formation and orientation of folds, enabling the fabrication of tailored structures with unique optoelectronic properties. In contrast, mechanical folding utilizes direct physical manipulation, such as applying a local force with a probe, stamp, or engineered substrate, to bend, fold, or stack 2D layers deterministically. Recent advances in mechanical manipulation have enabled sophisticated 3D operations, such as those demonstrated by Wakafuji *et al.* using temperature-controlled PDMS/PVC stamps, which permit folding, sliding, rotation, and precise repositioning of 2D flakes (Fig. 14b).[281]

These folding strategies have been exploited for self-aligned device assembly and multifunctional property modulation. For example, Liu *et al.* achieved precise alignment in large-area 2D transistors through mechanical folding of graphene/h-BN/MoS_2 heterostructures,[282] while Zhang *et al.* used paraffin-induced compression folding (PCF) to introduce strain and enhance photoluminescence in MoS_2.[283] Additionally, surface engineering methods, such as patterning substrates into hydrophilic and hydrophobic zones, enable further control over folding geometry and twist angle, as demonstrated by Wang *et al.*[284]

In summary, both solution-based and mechanical folding approaches provide tunable control over the structure and properties of 2D materials, offering a robust toolkit for engineering novel architectures and multifunctional devices.

5.3. Strain engineering

Strain engineering is a powerful strategy for modulating the properties of 2D materials. Owing to their atomic thickness and exceptional in-plane Young's modulus,[267] 2D materials such as graphene exhibit outstanding flexibility—allowing them to bend and fold easily—yet they remain comparatively resistant to in-plane stretching.[285–287] Nevertheless, even small to moderate uniaxial strains can substantially alter the electronic band structure by distorting the lattice, shifting Dirac points in graphene and enabling new functionalities.[288] Importantly, strain directly modifies the lattice constants of 2D materials, leading to changes in phonon dispersion and vibrational properties.[289–291] As a result, strain not only tunes electronic and optical transitions, but also governs thermal conductivity, phonon lifetimes, and energy dissipation pathways. In fact, the possibility of achieving stretchable strains of up to $\sim$20% in graphene has given rise to the field of ''straintronics,'' opening avenues for electronic and optoelectronic property control beyond conventional semiconductors.[292,293]

One method for realizing and transferring strained 2D materials involves engineering strain prior to transfer. For example, Zhang *et al.* transferred monolayer strained graphene onto a rigid substrate by initially stretching the graphene on a flexible PDMS support and maintaining a 1.5% tensile strain during transfer.[294] To prevent cracking due to stress relaxation, a formalin resin layer was introduced to enhance adhesion and protect the graphene. Buffer droplets on the target substrate provided additional capillary force, facilitating the final transfer of strained graphene. Electrical characterization of back-gated FETs demonstrated increased resistance in strained graphene, attributed to lattice symmetry breaking and altered carrier concentration.[295]

Strain effects in other 2D materials have also been systematically studied. Conley *et al.* examined uniaxial strain in monolayer MoS_2 by bending the substrate, observing a pronounced decrease in PL intensity under $\sim$1% strain---signifying a transition from a direct to an indirect band gap.[296] Guo *et al.* further explored strain transfer efficiency by cyclically stretching and relaxing PDMS substrates bearing uniaxially strained graphene.[297] Their work highlighted the challenges of maintaining tensile strain, as interfacial slippage can limit the effective transfer, while compressive strain often induces wrinkles, bubbles, or overlaps (Fig. 15a).

Raman spectroscopy provides a sensitive, non-destructive probe of strain in 2D materials, especially through the analysis of phonon modes. Mohiuddin *et al.* used high-resolution Raman measurements to monitor the photonic response of

Open Access Article. Published on 06 January 2026. Downloaded on 1/16/2026 12:17:14 PM.
This article is licensed under a Creative Commons Attribution-NonCommercial 3.0 Unported Licence.

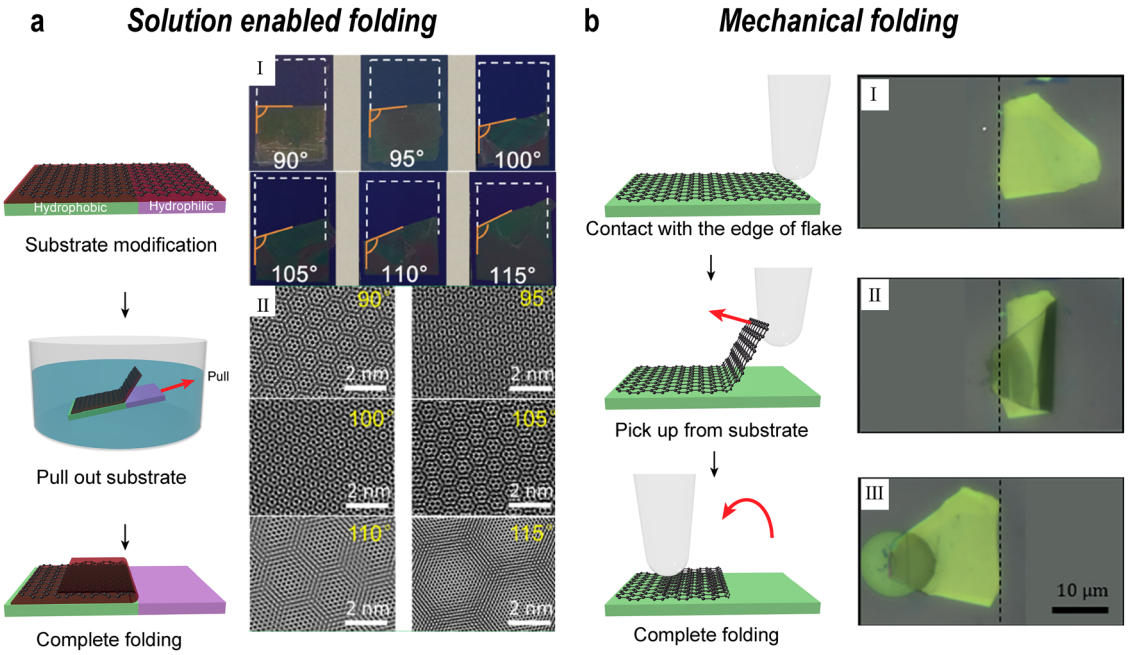

Fig. 14 2D material transfer for folding engineering. (a) The solution-enabled folding: folding of graphene with an arbitrary angle can be achieved using a solution-based method. Reproduced from ref. 284 with permission American Chemical Society, Copyright 2017. (b) The mechanical method for folding: mechanical approaches, such as the AFM probe-based method, can achieve the folding of 2D flakes with arbitrary angles. Reproduced from ref. 281 with permission from American Chemical Society, Copyright 2020.

monolayer graphene under uniaxial strain, observing clear splitting of the G peak into strain-direction-sensitive G^+ and G^- components, consistent with first-principles predictions.[298] These shifts directly reflect changes in lattice constants and phonon energies. Quantification of the Grüneisen parameter and polarization-dependent intensities further enabled mapping of crystallographic orientation and mechanical coupling in graphene devices (Fig. 15b).

Beyond simple mechanical stretching, stress can be engineered to assist in device transfer. Shin *et al.* demonstrated a dry transfer printing process in which platinum (Pt) films deposited under controlled stress conditions could be selectively detached from the substrate by bending.[299] Contacting the strained Pt film with PDMS during substrate bending enabled facile pick-up and flexible device fabrication.

In summary, these approaches illustrate the versatility and promise of strain engineering in 2D materials, not only for tuning electronic, photonic, and optical properties, but also for facilitating new transfer and integration strategies critical for device applications.

5.4. Twist engineering

Since the first discovery of unconventional superconductivity in bilayer graphene at a twist angle close to the magic angle (1.1°),[109] extensive research based on twist devices has been carried out in the past few years.[300–303] 2D crystals exhibit strong in-plane covalent bonding, which ensures excellent mechanical stability within the plane and gives rise to quantum confinement effects.[304] Moreover, the 2D layers are connected by relatively weak vdW forces rather than chemical bonding, facilitating precise interlayer distortion. VdW stacked structures can effectively avoid chemical and structural defects caused by atomic diffusion and lattice mismatch at the interface that are common in traditional stacked structures.[305] When stacking atomic layers, Moiré patterns are created due to tiny mismatches, leading to large periodic potential energies for electrons and excitons. In 2D vdW stacked structures, the interlayer asymmetry can be customized by modulation of misalignments or lattice mismatches.[306] For instance, in a double-layer stacked homostructure, misalignment is the only determining factor for custom Moiré fringes due to the same lattice constant of the adjacent atomic layers, while the Moiré fringes in the heterojunction can be caused by twist angles or lattice mismatch.

In order to study the quantum physics of twist devices, the twist angles should be precisely controlled, because even a slight change in twist angles is adequate to generate a completely new electronic spectrum.[109] A smaller twist angle will create a larger Moiré lattice,[307] and a ''mini-Brillouin zone''. This is the origin of many physical phenomena, such as flat bands and reconstruction of energy band structures, leading to some novel quantum behaviors. For example, unconventional superconductivity,[109,308,309] ferromagnetism,[310] and Mott-like insulating states[311] were found in twisted bilayer graphene (tBLG). Among the other twisted structures, the most common one is stacked and twisted by h-BN and graphene to produce the Moiré superlattice. Since there is a small lattice mismatch between the two materials (δ −1.7%),[312] a near-zero twisted angle can significantly change the band structure of graphene, resulting in many interesting phenomena, including the

This journal is © The Royal Society of Chemistry 2025

Open Access Article. Published on 06 January 2026. Downloaded on 1/16/2026 12:17:14 PM.
This article is licensed under a Creative Commons Attribution-NonCommercial 3.0 Unported Licence.

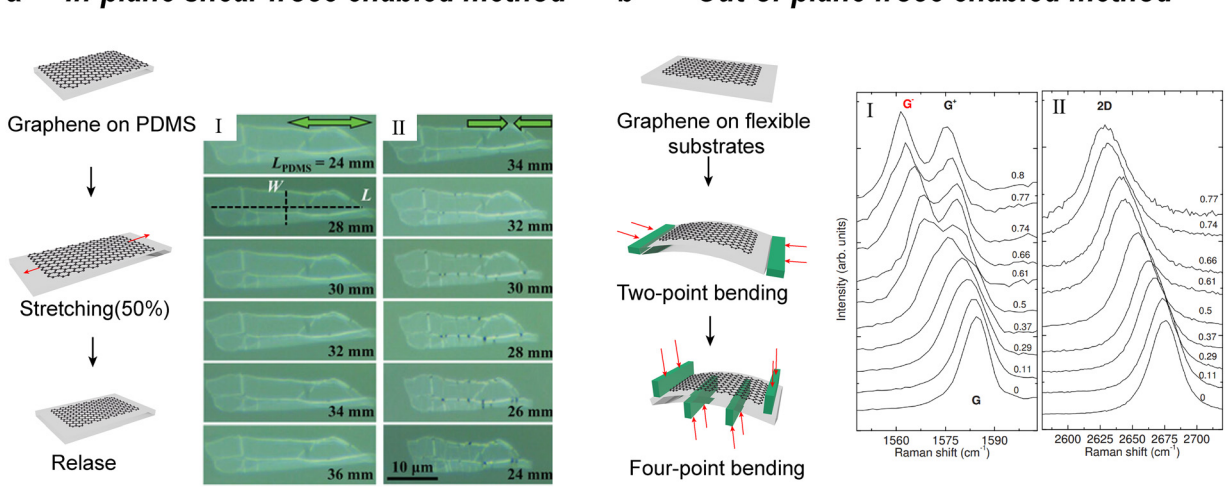

Fig. 15 Transfer 2D material for strain engineering. (a) The in-plane shear force enabled method.[297] The ~1.5% tensile strain was achieved on a graphene flake by stretching the PDMS substrate. Adapted from ref. 297 according to Creative Commons Attribution 4.0 International License (CC BY 4.0). (b) The out-of-plane force enabled method.[298] Tensile strain of a 2D flake can also be achieved by bending the substrate out-of-plane direction. Reproduced from ref. 298 with permission from American Physical Society, Copyright 2009.

famous Hofstadter Butterfly,[110,313–316] Mini Dirac Cone[317] as well as the Quantum Hall effect.[318] In addition to twisted double layer graphene[319] on h-BN, superconductivity and Mott-like insulating states have also been found in three layers of graphene[320,321] on h-BN. These fascinating and exotic electronic behaviors are controlled by the modulation of twisted angles.[322] In this section, we will focus on the method philosophy for fabricating twist devices. The efficient twist methods to fabricate 2D stacked structures with high quality and precise twist angles will be introduced, including the etching-assisted transfer methods and etching-free dry transfer methods.

5.4.1. Etching-assisted transfer methods. Etching-assisted methods employ etching techniques to selectively remove the 2D materials or the substrates during the device preparation process, for example, partial removal of 2D materials on the substrate by plasma etching. In fabrication of twist devices, oxide etch solution is commonly used to etch the SiO_2/Si substrate to obtain a floating polymer/2DM, which can minimize the risk of damage to the material. In this part, current etching-assisted transfer methods for fabrication of twist devices are presented, including the laser-assisted cutting and stacking method and liquid separating and stacking method.

The laser assisted cutting-rotation-stacking technique was first proposed by Chen *et al.* to achieve a high-precision controlled twist angle of 0.1°.[303] The detailed preparation process of the laser cutting method is shown in Fig. 16a. Firstly, a PMMA thin film is spin-coated as a supporting layer. Then, a femtosecond laser is used to cut the 2D flake and produce the parallel straight edges, which can be considered as the guideline to precisely control the rotation angles. After the precutting process, two separate pieces of the same 2D flake (noted as layer one and layer two) with a supporting layer are detached from the substrate after etching by an oxide etching solution. Then, layer one is transferred to a new substrate followed by immersing the substrate in acetone to remove the PMMA film above it, while layer two is flipped over and aligned with layer one with an accurate rotation angle. The twisted homojunction with a clean surface can be achieved after a thermal annealing process. The twist angles of the homojunctions can be extracted from the angular difference of the cutting edges. In addition to the laser cutting technique, the AFM tip can also be used to precut the 2D single crystal materials and produce the reference parallel edges.[323] One thing that should be noted is that contamination may be introduced between the interface of the stacked structure during the wet etching process. An etching-free dry transfer method would be preferable to create the twist stacked structures after the laser cutting process, that is, one of the separate pieces of the same 2D flake is directly picked up by a polymer stamp and kept stationary, while the other flake on the substrate is rotated by a specific angle, and then a homojunction with a specific twist angle can be fabricated by reassembling the separated 2D flakes.[324]

A liquid layer separating and stacking method reported by Puretzky *et al.* similarly requires etching the substrate and transferring the floating 2D flakes supported by a PMMA film,[325] as depicted in Fig. 16b. In this strategy, the substrate with the as-synthesized 2D flakes is precut into two parts. Half of the substrate is coated with PMMA, and a floating PMMA/2DM film can be obtained after etching the substrate. Then, the floating PMMA/2DM film is transferred to a funnel filled with DI water, and meanwhile, the other half of the substrate with 2D flakes is transferred to the bottom of the funnel. As the DI water gradually drains, the floating PMMA/2DM film would slowly approach and finally adhere to the bottom substrate when the DI water is completely drained. The twist angle of the homojunction stacked by liquid layer separation can be defined by the intersection angles of the triangles. This method can create a broad range of twist angles without the aid of a

Open Access Article. Published on 06 January 2026. Downloaded on 1/16/2026 12:17:14 PM.
This article is licensed under a Creative Commons Attribution-NonCommercial 3.0 Unported Licence.

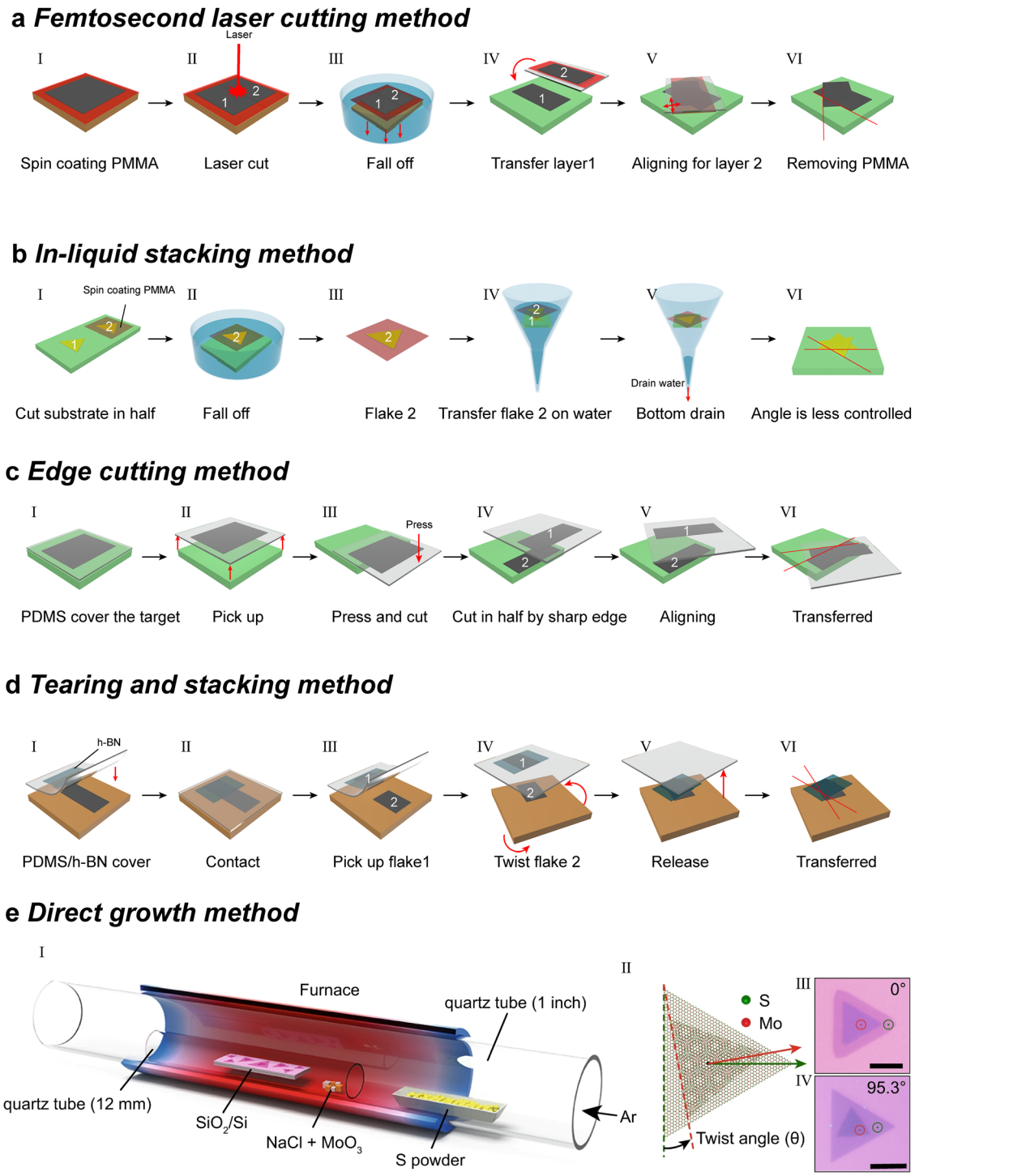

Fig. 16 Etching-free twisted method. (a) The femtosecond laser cutting method. Twisted bilayer graphene is fabricated by coating graphene with PMMA, cutting it into two parts, and releasing a PMMA/graphene film through etching. One piece is transferred to a new substrate, while the other is inverted and stacked at a controlled twist angle. PMMA removal and annealing yield the final structure. (b) The in-liquid stacking method. The substrate with a 2D flake is cut into half; one half is floated on water and transferred onto the other half by bottom draining, forming a twisted bilayer with a less controlled angle. (c) Edge cutting method: the 2D film is first picked up with a PDMS stamp and split into half by pressing at the substrate edge, leaving one half on the substrate and the other on PDMS. By rotating the PDMS and realigning, the detached half is released back, forming the desired twisted bilayer structure. (d) The tearing and stacking method: a 2D flake on a substrate is cut into two parts. One half is coated with PMMA, etched to release a floating PMMA/2D film, and aligned onto the other half by water drainage. After acetone removal and annealing, the stacked structure forms a twisted bilayer 2D flake at the target angle. (e) The direct growth method for 2D twisted structures. Adapted from ref. 330 according to Creative Commons Attribution 4.0 International License (CC BY 4.0).

This journal is © The Royal Society of Chemistry 2025

Open Access Article. Published on 06 January 2026. Downloaded on 1/16/2026 12:17:14 PM.
This article is licensed under a Creative Commons Attribution-NonCommercial 3.0 Unported Licence.

microscope. However, this liquid stacking method is typically applicable to the stacking of 2D materials grown by CVD, since it is difficult to precisely locate a specific 2D material or an exact cutting line when cleaving the substrate without microscopic monitoring. Besides, due to the uncontrollable alignment process, it's challenging to ensure a precise twist angle of the stacked structures.

5.4.2. Etching-free transfer methods. Instead of the etching-assisted transfer methods mentioned above, etching-free transfer methods are more favourable in fabrication of twist devices on account of the simpler operation procedure and cleaner stacking interface. In this section, some mainstream etching-free transfer methods for preparation of twist devices are reviewed, including peel-off transfer methods and CVD direct growth methods.

In the past few years, numerous studies on dry peel-off transfer techniques have been carried out.[124,127,326] The edge cutting technique reported by Sun *et al.* is an efficient dry peel-off method to fabricate $m{\cdot}2^N$ stacked layers by only N sequential stacking operations, where m refers to the layer number of the initial 2D material, and N is the stacking rounds.[327] The detailed preparation process of the edge cutting method is presented in Fig. 16c. Firstly, the intact 2D flake is covered and picked up by a PDMS film. Then, one half of the 2DM is pressed to the edge of the substrate and separated from the other half after the PDMS supporter being picked up again. A twist stacked structure with a precise twist angle can be attained through aligning the cutting line and restacking the separated flakes. This dry peel-off method is promising for fabrication of high-quality twist devices due to the etching-free process and high-precision angle alignment. Nevertheless, uneven force applied to the PDMS film may result in the fracture of the 2D materials, especially in the case of monolayer or few-layer materials. Besides, different adhesion forces between the 2DM/2DM and 2DM/substrate interfaces may cause wrinkles, or ruptures, or tensile strain within the 2DM as well.

A tear-and-stack technique is another commonly used peel-off technique to fabricate twisted devices with accurate crystal axis alignment. The specific procedures of the tear-and-stack method are displayed in Fig. 16d. The PDMS handle can be prepared by drop-casting the prepolymer mixture of PDMS and a curing agent on a planar PDMS mold. The hardness of the polymer handle can directly affect the contact force. Take an epoxy handle as an example, since the PDMS handle is softer than the epoxy one, so the former handle can achieve weaker contact force.[326] The hardness of the PDMS handle can be controlled by regulating the baking time of the prepolymer mixture. After preparation of the PDMS handle, PVA or PPC can be coated on the handle to pick up the h-BN flake. Herein, since the adhesion force between h-BN and other 2D materials is much larger than that between the SiO_2/Si substrate and 2D materials, the intact 2D flake will be torn apart and detached from the SiO_2/Si substrate due to the strong adhesion force induced by h-BN. Then, the remaining graphene on the substrate can be rotated with a specific angle assisted by a reference rotary alignment mask and picked up by the h-BN with the other torn half of the graphene. Compared with the laser cutting or AFM tip cutting techniques, the tear-and-stack method requires more simplified procedures since the cutting step is omitted. Additionally, the adhesion of the handle can be controlled by coating different adhesive polymers on it, such as poly(bisphenol A carbonate) (PC),[324,328] PMMA,[326] PVA,[329] or PPC.[45] Moreover, with the h-BN as the adhesive layer, the cleanliness of the stacking structure can be improved compared to other transferring methods, which require the dissolution of organic polymer support films. However, h-BN cannot be removed after the fabrication of stacking structure with a precise angle, which may not be applicable for the study of chemical reaction on the 2D heterostructures. The dimension of the transferred materials is also restricted by the size of h-BN.

Among all the methods for fabricating twisted devices, the CVD direct growth method can be used to fabricate large-area, high-quality twisted structures with a large range of twist angles. As illustrated in Fig. 16e(I), a one-step reconfiguring nucleation CVD method for growing twisted bilayer MoS_2 with a wide range of rotational angles from 0° to 120° has been proposed by Xu *et al.*[330] The growth of a high-quality twisted bilayer MoS_2 is achieved by controlling the gas flow rate and the molar ratio of the mixed MoO_3/NaCl. The twist angles of the bilayer homostructures can be easily defined by the angular difference between the edges of the triangular monolayer, as depicted in Fig. 16e(II). The optical microscopy images of the as-synthesized twisted bilayer MoS_2 are shown in Fig. 16e(III) and (IV). This CVD method can prepare twisted bilayer homostructures with large sizes and a wide range of twist angles. On the other hand, the twist angles are randomly formed during the CVD process, and it's hard to reproduce the twisted structures with specific pre-designed angles.

In summary, we have reviewed several techniques for the fabrication of twisted devices in detail in this section, such as the laser cutting and stacking method, liquid separating and stacking method, peel-off dry transfer methods (*i.e.*, the edge cutting and stacking method and tear-and-stack method), and CVD direct growth method. Different fabrication methods have their own advantages and disadvantages. For example, etching-assisted transfer methods can reduce the damage risk of the 2D materials due to the existence of the supporting layer, while the etching process may induce contamination between the interface of the twist structures. Dry peel-off transfer methods can create stacked structures with a cleaner interface and higher twist accuracy through a simpler operation procedure, but these methods are only suitable for preparation of 2D homo/heterojunctions with small lateral sizes. CVD direct growth methods can prepare large-scale twisted homostructures; however, the twisted angles are random and unpredictable, and the possibility of reproducing the twisted bilayer with specific angles is extremely low. Therefore, an appropriate method should be chosen based on the specific experimental requirements.

Recently, several *in situ* twist fabrication strategies have emerged. Given their potential significance, we will discuss these developments in detail in the next section.

Open Access Article. Published on 06 January 2026. Downloaded on 1/16/2026 12:17:14 PM.
This article is licensed under a Creative Commons Attribution-NonCommercial 3.0 Unported Licence.

6. Reconfigurable transfer technology

The fabrication of vdW heterostructures by stacking and twisting atomically thin materials has revolutionized the design of multifunctional devices for various fields. This approach is often likened to building with ''LEGO'' blocks, given the remarkable flexibility and control researchers now have over the composition, sequence, and geometry of 2D layers---without the usual constraints of lattice matching or interface chemistry. However, a key distinction remains, while true LEGO toys can be freely disassembled and rebuilt into new forms, most current vdW assembly methods are fundamentally one-way.[23] Once stacked, these heterostructures become essentially ''locked in'', the individual layers cannot be easily disassembled, re-twisted, or reconfigured without risking damage or introducing significant residues.[331]

This lack of reconfigurability presents major limitations for both fundamental research and device prototyping. Each assembled stack is unique, with its own defects, contamination, and interface history, making it difficult to perform variable-controlled studies or reproducibly explore phenomena such as magic-angle superconductivity, moiré minibands, or twist-angle-dependent excitonic effects.[332] In practical device development, the inability to ''reset'' or reuse the same 2D building blocks hinders rapid iteration, multi-functionality, and efficient material usage. The capability to reconfigure, ''hot swap,'' or adjust layers and contacts would enable tremendous flexibility in next-generation electronics and quantum devices.

Recent advances have begun to address these challenges with the development of reconfigurable transfer methods, techniques that enable not only precise assembly, but also *in situ* adjustment, disassembly, and realignment of the constituent layers. These approaches make it possible to tune twist angles or registry continuously, dynamically rearrange layer order, or even reverse device fabrication steps. However, many current implementations still rely heavily on polymer support layers, which are difficult to remove completely and often leave behind residues. These residual polymers can severely limit the utility of reconfigured structures, particularly in surface-sensitive applications such as near-field optical microscopy or chemical catalysis, where a pristine, exposed top surface is essential.[180,333,334]

In this chapter, we review the emerging landscape of reconfigurable transfer technologies. We discuss their fundamental working principles, highlight strategies for minimizing or eliminating polymer contamination, and propose potential routes toward achieving ideal or quasi-ideal reconfigurable transfer. Finally, we explore *in situ* approaches that extend beyond conventional transfer, enabling dynamic manipulation and on-demand transformation of 2D assemblies for next-generation quantum and optoelectronic applications.

6.1. Polymer-assisted reconfigurable transfer technology

Recent progress in vdW engineering has led to the development of reconfigurable transfer methods, approaches that go far beyond conventional stacking by enabling *in situ* adjustment, selective disassembly, and realignment of individual layers within a heterostructure.

One influential technique, as demonstrated by Tao *et al.*, utilizes atomically flat, high-adhesion polymers such as PVA or PMMA as handling support layers, as shown in Fig. 17a.[333] This method enables the full disassembly of fabricated vdW stacks back into their original building blocks, while preserving their structural integrity and allowing subsequent restacking or re-twisting in any desired sequence or orientation. Unlike traditional PDMS- or PPC-based methods, which either lift entire stacks or lack layer selectivity, this polymer-mediated approach offers a much greater control: each 2D layer can be separated, characterized (for example, *via* AFM or Raman), and then reassembled with deliberate choice of stacking order, contacts, or twist angle. Furthermore, they demonstrated this by reconfiguring a MoS_2 device from n-type to p-type operation, or from back-gate to dual-gate architectures, simply by changing the stacking sequence and contact strategy. Even more complex assemblies, such as four-layer floating-gate memories, were split and recombined, enabling a single set of 2D flakes to serve in multiple, entirely different device roles. However, it should be emphasized that in this method a polymer mediator, such as PMMA or PVA, is intentionally retained on the 2D layers, since its presence is essential for manipulation and repeated disassembly. While the dry process minimizes mechanical damage, the exposed surface cannot be accessed until the polymer is removed, which restricts certain applications.

Another approach is offered by dynamic twist control, as demonstrated by Yang *et al.*[334] (Fig. 17b). Their approach employs a precision glass slide, a PDMS hemisphere ''gel manipulator,'' and a pre-patterned PMMA patch to grip and rotate specific layers within a pre-assembled heterostructure, all while observing under an optical microscope. This enables continuous, *in situ* tuning of the twist angle or lateral registration between layers, without removing the stack from the device substrate. The technique exploits the superlubricity present at incommensurate 2D interfaces, allowing layers to be slid or rotated with minimal force until ''locking'' at a magic angle is achieved. However, it is important to note that, similar to the disassembly approach, this method fundamentally depends on the use of a PMMA polymer handle for manipulation. The PMMA patch remains attached to the 2D flake throughout the process and cannot be fully removed without compromising the ability to reconfigure the stack. While PMMA handles can be patterned, detached, and reapplied as needed to target different layers or configurations, a thin polymer residue is inevitably left on the manipulated flakes. As such, although the method is highly reproducible and enables dynamic, reversible control of the twist angle, even for ultra-thin or fragile flakes, the presence of polymer limits the accessibility of atomically clean surfaces, which is a critical consideration for certain advanced optical or chemical measurements. Nonetheless, this reconfigurable strategy significantly broadens the experimental capabilities for exploring magic-angle physics, moiré

 This journal is © The Royal Society of Chemistry 2025

Open Access Article. Published on 06 January 2026. Downloaded on 1/16/2026 12:17:14 PM.
This article is licensed under a Creative Commons Attribution-NonCommercial 3.0 Unported Licence.

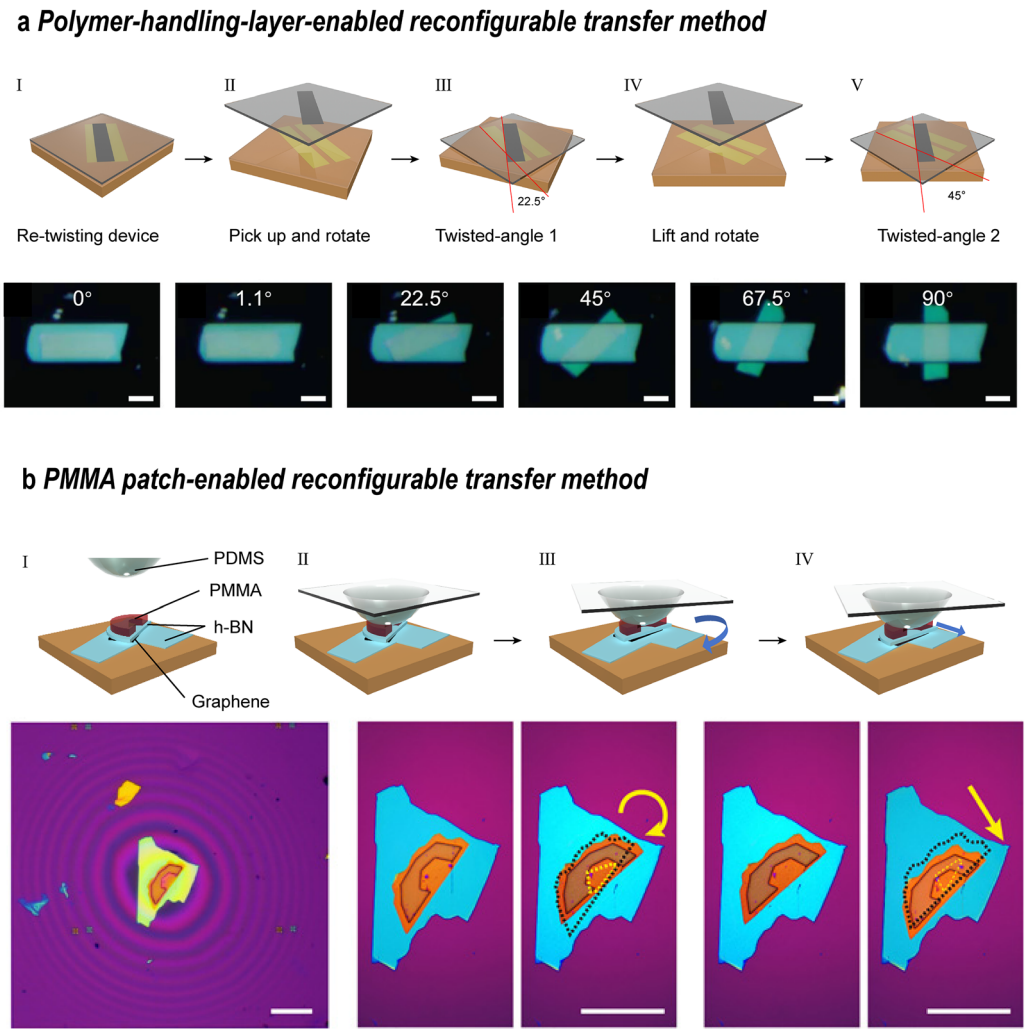

Fig. 17 Reconfigurable transfer methods for reconfigurable twist devices. (a) The polymer-handling-layer-enabled reconfigurable transfer method. Disassembling and reassembling to build a twisted vdW structure have been demonstrated. Adapted from ref. 333 according to Creative Commons Attribution 4.0 International License (CC BY 4.0). (b) The PMMA patch-enabled reconfigurable transfer method. The PMMA patch deposited on the top of the sheet is brought into direct contact with PDMS as an operating handle to achieve the purpose of accurately controlling the twist angle between materials. Adapted from ref. 334 according to Creative Commons Attribution 4.0 International License (CC BY 4.0).

superlattices, and other emergent correlated states, all within a single device platform.

Altogether, these reconfigurable transfer methods represent a major step forward for the field of 2D materials. They fundamentally change device assembly from a one-shot, irreversible process to a flexible and reversible platform, allowing researchers to correct misalignments, optimize stacking sequences and explore a wide range of device architectures using the very same set of 2D components. This versatility enables systematic and variable-controlled investigations, such as studies of twist-angle dependent phenomena or rapid prototyping of multifunctional devices, while minimizing the waste of high-quality 2D flakes, particularly when sourcing flakes with identical properties such as thickness, doping type, and strain. The ability to repeatedly disassemble and reconfigure stacks, combined with the dry, polymer-mediated approach, helps to preserve interfacial quality and device integrity, as demonstrated by AFM, electronic transport, and Raman measurements.[333,334] Moreover, these methods are broadly applicable, extending to various families of 2D materials (including graphene, TMDCs, h-BN, and black phosphorus), a range of metals and dielectrics, and even complex multilayer or hybrid device architectures. *In situ* strategies are especially powerful, offering dynamic, high-resolution access to twist angle control and emergent moiré physics within a single device.

Nonetheless, a significant limitation persists as current reconfigurable transfer techniques still rely on carrier polymers such as PMMA or PVA for manipulation and stacking. These polymers are difficult to fully remove and inevitably leave behind thin residues, limiting the ability to obtain atomically clean, exposed surfaces. This issue is particularly problematic for applications that demand pristine surfaces, such as near-field optical characterization,[165,245,249,335,336] surface-sensitive

Open Access Article. Published on 06 January 2026. Downloaded on 1/16/2026 12:17:14 PM.
This article is licensed under a Creative Commons Attribution-NonCommercial 3.0 Unported Licence.

chemical reactions, or catalysis.[245,249,337–341] Addressing these challenges will require the development of new, ''polymer-free'' reconfigurable transfer processes that maintain atomic cleanliness while retaining the flexibility to build, disassemble, and reassemble arbitrary device architectures.

Despite these outstanding obstacles, the advent of reconfigurable transfer technology is already redefining what is possible in 2D materials research and device engineering. For the first time, the device geometry, stacking sequence, and twist angle are all accessible as continuously tunable and reversible parameters. This emerging capability enables systematic experimentation and multifunctional device concepts that were previously unattainable with traditional, static assembly methods and will likely serve as a foundation for the next generation of quantum, photonic, and electronic innovations built from vdW materials.

6.2. Beyond the transfer: *in situ* reconfigurable methods

The need for truly reconfigurable of vdW assembly and dynamic control over stacking geometry has grown increasingly urgent. While recent reconfigurable transfer methods enable disassembly and restacking of 2D heterostructures, these processes are still fundamentally sequential and constrained by the uniqueness of each stack's building blocks.[333] Moreover, most existing approaches cannot deliver continuous, *in situ* control of twist angle or stacking configuration after assembly, leaving a gap between true ''LEGO-like'' reversibility and the requirements of modern quantum materials research.

To bridge this gap, *in situ* reconfigurable methods have emerged as a transformative next step. These techniques enable direct, real-time manipulation of the twist angle or layer registry within a vdW heterostructure, even after fabrication is complete and the device is wired. Such *in situ* tuning allows researchers to systematically explore the evolution of electronic, optical, and quantum properties as a function of twist, strain, or lateral displacement. Unlike conventional stacking methods that ''lock in'' the structure after assembly, in-situ approaches make it possible to dynamically ''retune'' the same device platform, opening new opportunities for both discovery and optimization.

A leading implementation of this concept uses AFM to physically rotate individual layers within a heterostructure with nanoscale precision. For example, Ribeiro-Palau *et al.* realized a dynamically adjustable twist angle in an h-BN/graphene/h-BN stack by stacking a prefabricated h-BN flake atop graphene and then rotating the top h-BN layer *in situ* with an AFM tip (Fig. 18a(I)–(III)).[342] This setup enables real-time control over the interlayer twist angle, allowing systematic investigation of how quantum transport and moiré phenomena depend on stacking geometry. Similarly, Yao and colleagues used AFM-based manipulation in h-BN homojunctions (Fig. 18a(IV) and (V)),[343] achieving highly tunable SHG responses and revealing ''locking'' at specific stacking angles due to enhanced interlayer friction.

Despite the power of these *in situ* twist methods, the intricate microscopic phenomena at the twisted interfaces of vdW devices often escape conventional characterization. While scanning tunneling microscopy (STM) is effective for probing local electronic properties, it remains limited to single-point measurements and cannot easily capture the spatial evolution of quantum phases or interference phenomena involving multiple tunnelling paths.[344,345]

To address these limitations, the quantum twist microscope (QTM) was proposed as a conceptual breakthrough (Fig. 18b).[346] The QTM utilizes an AFM cantilever functionalized with a vdW heterostructure (*e.g.*, platinum, h-BN, and graphene), which forms an atomically sharp and tunable interface with a second 2D material on a substrate. When the cantilever tip is contacted and rotated with sub-milliradian precision, QTM enables local tunnelling experiments that probe the electronic structure, momentum dispersion, and the presence of electrons in multiple spatial locations—all in one measurement. The strong coupling of wavefunctions at the vdW interface allows direct mapping of both charged and neutral excitation spectra, with simultaneous control over magnetic field, carrier density, and displacement fields. While the capabilities of QTM are extraordinary, its technical complexity and cost currently limit widespread use to only a handful of advanced laboratories.

Most current *in situ* twist experiments, however, rely on AFM tip manipulation, which necessitates that the top device layer be patterned or engineered to serve as a mechanical handle. To overcome this, Tang *et al.* introduced a universal MEMS-based actuation platform (MEGA2D, Fig. 18c).[347] This system uses microfabricated silicon columns and pyramidal features for precise, chip-integrated rotational and vertical control of stacked 2D materials. Not only does MEGA2D allow for *in situ* tuning of the twist angle, but it also enables control over interlayer separation *via* substrate spacers—facilitating studies of both proximity and spatially modulated coupling. This platform also opens new possibilities for systematically investigating additional stacking parameters such as lateral translation, stretch, tilt, and shear, vastly expanding the configurational landscape for 2D materials research.

6.3. Summary and perspectives

In summary, these advances highlight the unique power and promise of *in situ* reconfigurable platforms. By providing real-time, dynamic, and often non-destructive control over stacking geometry, these methods allow researchers to probe emergent quantum phenomena, optimize device performance, and access previously unreachable regions of the vdW heterostructure phase space.

To promote these technologies from preliminary demonstrations to wider application, the following issues need to be addressed:

High costs: implementing *in situ* twist requires the use of high-precision AFM equipment. However, in the laboratory, the popularity of high-precision AFM is still very low. Moreover, the new MEMS devices or dedicated QTM systems are very costly, and their maintenance and calibration also require a lot of resources. Modular, small-sized, low-cost MEMS platforms should be developed to promote standardized, reusable sample

Open Access Article. Published on 06 January 2026. Downloaded on 1/16/2026 12:17:14 PM.
This article is licensed under a Creative Commons Attribution-NonCommercial 3.0 Unported Licence.

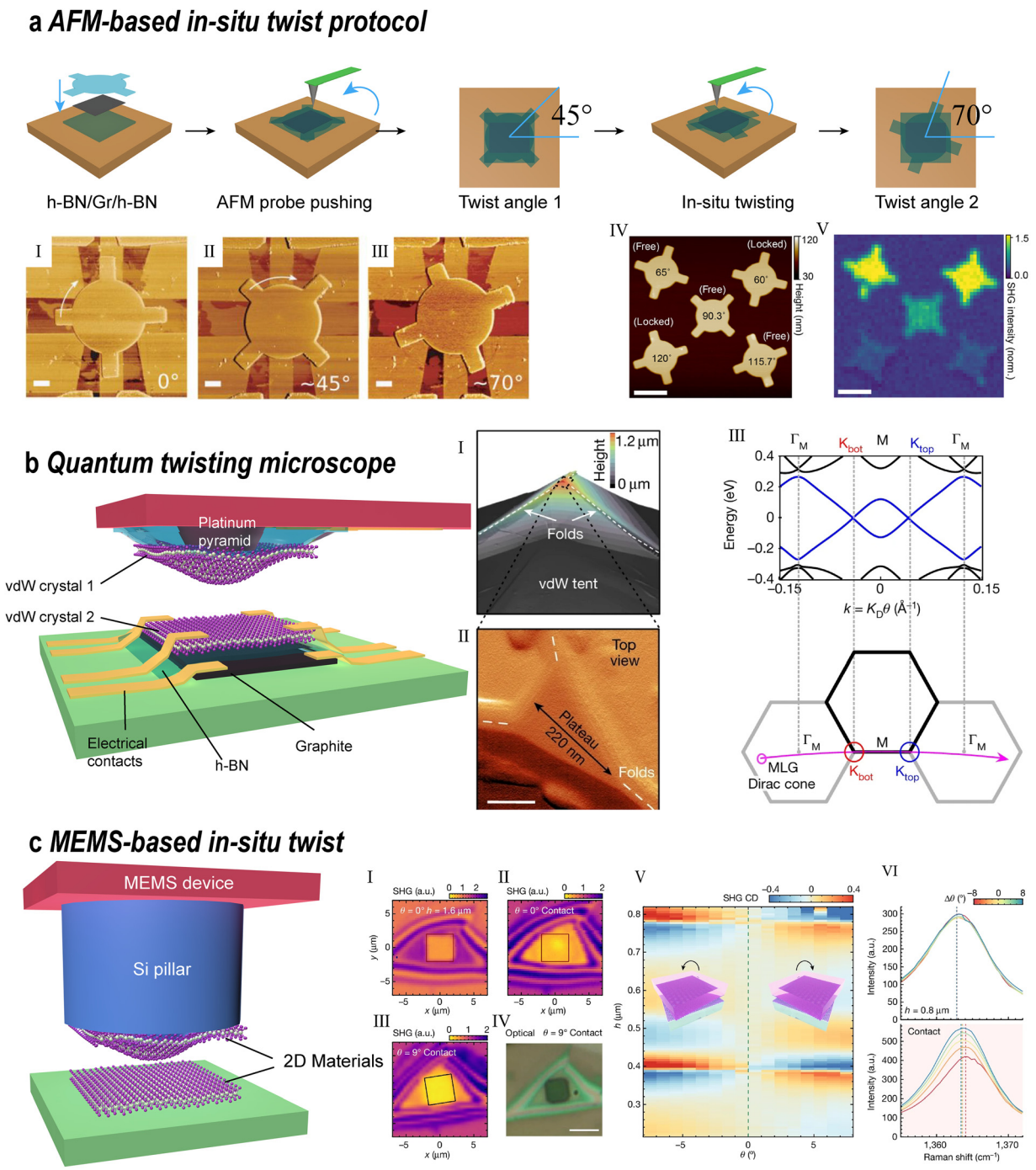

Fig. 18 Method for *in situ* adjustment of twisted devices. (a) The AFM-based *in situ* twist protocol. 2D materials are continuously pushed through AFM. The graphene is first placed on top of the h-BN, and then the preformed h-BN structure is transferred to the top of the graphene. Pushing on the topmost h-BN using an AFM rotates the layer and changes its crystal orientation relative to graphene. (I)–(III) The twisting heterojunctions. Reproduced from ref. 342 with permission from The American Association for the Advancement of Science, Copyright 2018. (IV) and (V) AFM image and SHG image of h-BN rotators dialled to different twist angles. Scale bars in (IV) and (V) are 3 μm.[343] Adapted from ref. 343 according to Creative Commons Attribution 4.0 International License (CC BY NC 4.0). (b) The quantum twist microscope (QTM). The QTM can allow the *in situ* twist and measurement of bi-layer graphene. Reproduced from ref. 346 with permission from Springer Nature, Copyright 2023. (c) The MEMS-based twist protocol. (I)–(V) SHG power map of an as-fabricated MEGA2D device with different contact status. (VI) Raman spectroscopy of a MEGA2D h-BN sample when the twisted h-BN flakes are air-spaced by 0.8 μm (up) and in contact (down). Lines with different colours were taken at different twist angles. The dashed lines denote the centre of the E_{2g} peak fit with a Lorentzian. Reproduced from ref. 347 with permission from Springer Nature, Copyright 2024.

holders and control firmware, aiming to lower the entry threshold.

Strict operational requirements: the *in situ* twist technology has strict requirements in terms of alignment and force

Open Access Article. Published on 06 January 2026. Downloaded on 1/16/2026 12:17:14 PM. This article is licensed under a Creative Commons Attribution-NonCommercial 3.0 Unported Licence.

control, so operators need to have proficient skills. Different operation rates, contact pressures *etc.* can also cause human-induced deviations, resulting in poor repeatability and large fluctuations in device data. Promoting automated control, standardized processes, *etc.*, addresses the limitations of manual operation.

Bottlenecks in scalability and scale: although the AFM probe method can be extended to a QTM microscope, it cannot meet the requirements of large areas and large scales. MEMS provides a parallel approach, but its compatibility with other fields has not yet been verified. In the future, arrayable MEMS driving devices will need to be developed and rapid twisting solutions to improve efficiency will need to be explored.

As these technologies evolve toward higher precision, automation, and accessibility, they will play an essential role in realizing the full potential of programmable quantum materials and multifunctional devices.

7. All-transfer strategies: transfer will be all you need

As the semiconductor industry moves toward the next generation of miniaturized, high-performance electronics and optoelectronics, 2D materials are poised to play a pivotal role, owing to their atomically thin nature, outstanding physical properties, and exceptional potential for integration with advanced device platforms. Notably, the IEEE International Roadmap for Devices and Systems (IRDS) now formally anticipates the integration of 2D materials into high-volume manufacturing, specifically as channel materials in ultra-scaled and low-power devices within the next decade. The IRDS highlights the promise of 2D TMDCs to complement silicon for transistors and other beyond-CMOS applications, potentially as early as 2028.[348–351] This formal inclusion marks a global consensus that 2D materials are a key enabler in the future of semiconductor technology.

A core technological driver in this transition is the emergence of the all-transfer strategy, a paradigm in which every component of an advanced device, from the active 2D semiconductor layer to metal electrodes, dielectric layers, and even the complete device stack, is assembled by transfer rather than traditional fabrication. This all-transfer approach offers several compelling advantages. Firstly, it bypasses the need for complex lithography, vacuum deposition, and aggressive etching processes, enabling rapid, low-cost, and lithography-free device fabrication—even outside a cleanroom environment. Second, transfer-based assembly minimizes chemical disorder, contamination, strain, and physical damage that often arise from standard fabrication steps, ensuring that the intrinsic quality of each component is preserved throughout the process. Perhaps most crucially, interface quality, especially at the metal–semiconductor junction, is dramatically improved. Transfer-assembled vdW contacts are free from chemical bonding, disorder, and Fermi-level pinning, allowing device performance to approach the fundamental limits predicted by ideal physics. This stands in stark contrast to traditional top-down approaches, where interfacial damage and chemical interactions frequently degrade device behaviour. Collectively, the all-transfer strategy provides new opportunities for scalable, high-quality device manufacturing, paving the way for next generation 2D electronics and optoelectronics.

Beyond improving the contact and interface quality, the all-transfer strategy also unlocks new design freedoms. Metal contacts, high-κ dielectrics, and even pre-patterned 2D layers can be precisely placed or stacked with minimal restrictions, facilitating complex device architectures and 3D vertical integration. This is particularly relevant as the field moves toward monolithic 3D integration, where reducing the physical connection length and stacking multiple functional layers become essential for overcoming scaling bottlenecks.

In this chapter, we provide a comprehensive overview of the all-transfer strategy. We begin by discussing the transfer of individual device components, such as metals and dielectric layers, with an emphasis on their role in interface engineering and their influence on overall device performance. We then turn to transfer-enabled patterning techniques for 2D materials, which offer a lithography-free pathway to large-area and high-resolution device fabrication.

7.1. Transfer of critical components: metal electrodes and high-κ dielectric layers

The all-transfer fabrication protocol offers a transformative approach for constructing high-performance 2D devices by directly assembling prefabricated metal electrodes and dielectric layers onto semiconductor channels, rather than relying on conventional lithography, etching, or direct deposition. Standard fabrication techniques (such as lithography, solvent washing, wet/dry etching, and high-energy metal deposition) often introduce contamination, induce strain, cause cracks or wrinkles, and result in suboptimal contact quality. In contrast, transfer-based methods largely circumvent these issues, providing a cleaner, simpler, and more scalable route to device integration.

7.1.1. Transfer of prefabricated metals for 2D device contact engineering. A broad suite of metal transfer protocols have emerged to address the interfacial and scalability challenges of 2D device integration. These strategies aim to address the intrinsic drawbacks of conventional metal deposition, including interfacial disorder, Fermi level pinning, and structural damage caused by high-energy processing. By laminating prefabricated, atomically clean metal electrodes directly onto the semiconductor surface, they preserve interfacial integrity, maintain the intrinsic electronic structure, and enable reproducible device performance.

One landmark method, pioneered by Liu *et al.* involves fabricating metal electrodes of varying work functions on a donor silicon substrate, coating them with a PMMA support, and then physically laminating these metals onto MoS_2 layers that have been mechanically exfoliated and prepared with dielectrics. Alignment is achieved under a microscope, and final PMMA removal yields metal–semiconductor contacts that

 This journal is © The Royal Society of Chemistry 2025

Open Access Article. Published on 06 January 2026. Downloaded on 1/16/2026 12:17:14 PM.
This article is licensed under a Creative Commons Attribution-NonCommercial 3.0 Unported Licence.

strictly obey the Schottky-Mott rule: the barrier height is determined by the metal's work function, not by interface states or pinning.[352] Devices fabricated in this manner achieve electron and hole mobilities close to theoretical limits, offering a decisive demonstration of the advantages of transfer-based vdW contacts.

To scale up and expand the compatibility of this approach, graphene-assisted metal transfer processes have been introduced.[353] Here, large-area single-crystal graphene, grown by CVD on Ge(110), serves as a weakly bound, atomically flat support for metals deposited by evaporation. A PVA film is then laminated on top and mechanically peeled off, carrying the metal film nearly defect-free, thanks to the weak vdW interaction at the metal–graphene interface. Once dissolved in water, the metal–PVA film can be transferred to a variety of substrates, including fragile 2D crystals. This process is gentle enough to maintain the integrity of both the metal and the semiconductor, but does rely on the eventual removal of the sacrificial PVA, which can present residue challenges.

Further advances have tackled both the residue problem and process flexibility. For example, vertical metal-assisted vdW integration leverages Bi_2O_3-assisted CVD to vertically grow single-crystal nanosheets (*e.g.*, Pd, Cu, and Au), which can then be mechanically transferred and used as templates for ALD growth of ultra-thin, uniform high-κ dielectrics (such as Al_2O_3 or HfO_2) without the need for seeding.[89] Similarly, hydrogenated diamond substrates offer extremely low adhesion for metal films, allowing for the clean pick-up and transfer of prefabricated metal patterns by PC or PPC stamps.[354] These reusable diamond substrates support standard lithography and enable transfer of a wide range of metals, including those difficult to manipulate by conventional dry transfer.

Another innovative route is the ice-assisted *in situ* transfer, in which a thin layer of amorphous water ice acts as a buffer during metal deposition.[355] After the desired metal thickness is evaporated onto the cold sample, the ice is sublimed in a vacuum, causing the metal film to collapse gently onto the underlying 2D material, leaving behind a pristine, undamaged metal-semiconductor interface. This approach also removes adsorbed contaminants, producing a high-quality device interface.

In parallel, high-pressure extrusion methods are pushing the boundaries of 2D metal fabrication. For example, metal powders are melted and pressed between anvils in the presence of monolayer MoS_2, yielding atomically flat, large area (>100 μm) 2D metals that can be mechanically exfoliated and encapsulated for further studies.[226] Such contacts are inherently non-bonding, minimizing gap states and maximizing surface smoothness, with physical isolation inhibiting metal-induced gap states (MIGS) and reducing Fermi level pinning.

Each of these methods, including physical lamination, graphene or diamond-assisted transfer, ice buffering, and vdW extrusion, highlights the importance of achieving clean, residue-free, and atomically precise interfaces in 2D device engineering. The formation of van der Waals metal-semiconductor contacts enable the Fermi level to align closely with the work function of the selected metal, thereby avoiding the interfacial disorder and electronic traps that often limit the performance of conventional contacts.

Nevertheless, practical challenges remain. The mechanical transfer process can introduce non-uniformities at the vdW interface, leading to local tunnelling barriers and increased contact resistance. In addition, sacrificial layers (PMMA and PVA) may leave behind residues that, if not carefully managed, could degrade device performance. Continuous improvement in transfer media, alignment strategies, and cleaning protocols will be crucial for the widespread adoption of these techniques in high-yield, wafer-scale device manufacturing.

7.1.2. Transfer of a high-κ dielectric layer for 2D device miniaturization. As transistor scaling continues to push the boundaries of device miniaturization, achieving ultrathin, high-quality gate dielectrics becomes increasingly crucial for performance and energy efficiency. Reducing the gate length, channel thickness, and equivalent oxide thickness (EOT) of the dielectric is essential for faster switching, lower power consumption, and tighter electrostatic control. However, conventional semiconductor channel materials, such as silicon, strained SiGe, and III-V compounds, face significant challenges at atomic scales: their volume properties degrade with thickness, and interface impurities introduce Coulomb scattering, which reduces carrier mobility and undermines device reliability.

2D semiconductors, with their atomically thin profiles and inherent surface passivation, offer a compelling alternative. Their strong quantum confinement effectively suppresses short-channel effects and leakage current, enabling enhanced gate control. However, the integration of high-quality, ultrathin dielectric layers onto 2D materials presents its own set of challenges. Traditional ALD processes rely on surface chemical activity, which is often absent on inert 2D crystals and therefore necessitates the use of seeding or nucleation layers. These seed layers, while enabling dielectric growth, can introduce defects or ''dangling bonds'' that degrade interface quality and device mobility.

To circumvent these issues, the transfer of prefabricated, high-quality dielectrics using a vdW integration approach has emerged as a transformative solution. In this process, crystalline or amorphous dielectric films (*e.g.*, Al_2O_3, HfO_2, Y_2O_3) are first grown on sacrificial substrates (often buffered by a polymer or graphene interlayer), then picked up and laminated directly onto the 2D semiconductor *via* dry or wet transfer. This bypasses the need for nucleation on the channel surface, preserves atomic flatness, and creates a clean vdW gap at the interface, effectively reducing interface states and suppressing gate leakage. The presence of a few-angstrom-wide vdW gap further mitigates edge-induced barrier lowering and minimizes gate-induced carrier tunnelling, yielding superior gate control and device performance.

Several advanced protocols have been developed to realize these goals. For instance, Lu *et al.* introduced a dry dielectric transfer strategy, in which Al_2O_3 or HfO_2 is deposited atop a thin PVA buffer layer on silicon, then etched and laminated onto wafer-scale monolayer MoS_2 *via* heat-releasable tape and

Open Access Article. Published on 06 January 2026. Downloaded on 1/16/2026 12:17:14 PM.
This article is licensed under a Creative Commons Attribution-NonCommercial 3.0 Unported Licence.

mild plasma treatment.[88] This ensures atomic flatness and preserves surface cleanliness, with the thin PVA enabling subsequent ALD growth of uniform dielectrics.

Other innovations exploit graphene as a sacrificial buffer. Wang *et al.* deposited Y_2O_3 atop graphene on SiO_2, then annealed and oxygenated the film to form atomically flat Y_2O_3.[358] The structure is supported by PMMA, then the graphene is removed by plasma etching, and the dielectric is transferred to the device. Inheriting the flatness of graphene, this ''one-step lamination'' method enables the integration of complex device stacks onto arbitrary substrates.

While amorphous oxides such as SiO_2, Al_2O_3, and HfO_2 can effectively reduce leakage, they often harbour a high density of interface defects due to their structural disorder. To address this, researchers are exploring single-crystal dielectric materials, such as h-BN and CaF_2, which provide atomically smooth, lattice-matched interfaces and minimal defect densities. However, even ultra-thin h-BN may show high leakage at nanoscale thickness, motivating the search for new high-κ, large-band-gap crystalline dielectrics.

Recent breakthroughs include the use of perovskite oxides and single-crystal films. For example, ultrathin, transferable $SrTiO_3$ (STO) has been realized by growing STO on a water-soluble sacrificial $Sr_3Al_2O_6$ layer, supporting it with PDMS and then dissolving the sacrificial layer to release atomically flat STO for transfer.[359] Such single-crystal films achieve dielectric breakdown fields and low leakage comparable to or exceeding amorphous counterparts, though current implementations are mostly limited to back-gate FET architectures.

In another advance, layered perovskite oxides such as $Sr_2Nb_3O_{10}$ (SNO) have been assembled *via* Langmuir–Blodgett techniques or top-down liquid-phase exfoliation and then transferred using polymer stamps to form heterostructures.[360] These crystalline dielectrics offer high-κ, robust band gaps, and atomically sharp interfaces, resulting in FETs with steep subthreshold swings and high on/off ratios.

Furthermore, emerging ferroelectric dielectrics, such as transferred $Hf_{0.5}Zr_{0.5}O_2$ (HZO) films, enable integration of non-volatile memory and logic into 2D architectures, with recent work demonstrating wafer-scale transfer and high-yield device performance.[361]

In summary, transfer-based integration of high-κ dielectrics with 2D materials, *via* vdW lamination, crystalline oxide exfoliation, or sacrificial-buffer techniques, provides a pathway to ultra-scale, low-leakage, high-mobility devices. The approach overcomes the limitations of direct ALD or CVD growth, enabling the construction of pristine interfaces, minimizing defect densities, and expanding the palette of available dielectrics. As the toolkit for dielectric transfer expands, the prospects for all-transfer, wafer-scale, and three-dimensional integration of 2D devices become ever more promising, accelerating progress toward next-generation electronics and quantum technologies.

7.1.3. Transfer of whole 2D devices: toward fully modular and scalable integration. Beyond the transfer of individual components such as metal electrodes and dielectric layers, a transformative advance is the ability to transfer entire prefabricated 2D devices from one substrate to another. This ''device transfer'' approach enables modular assembly, multi-level device stacking, and integration onto unconventional substrates, thereby greatly expanding the flexibility, scalability, and complexity of 2D electronics.

The process begins by fabricating and patterning a large array of 2D devices (such as transistors, photodetectors, or logic gates) on a growth or donor substrate using established techniques. Once the devices are completed, a support layer (typically a polymer film) is laminated onto the surface. The underlying sacrificial substrate is then selectively etched or dissolved, releasing the entire device array, which can be picked up and precisely transferred to a target wafer or even stacked onto another 2D device layer (see Fig. 19c).

Crucially, this approach decouples fabrication from integration: devices can be batch-produced under ideal growth and patterning conditions and later reconfigured, relocated, or stacked as needed. The advantages are multifold: (1) fabrication efficiency, through modular and scalable assembly; (2) stacking and heterogeneous integration, enabling monolithic 3D logic, memory, and sensing architectures; (3) damage-free assembly, since no erosive processing is imposed post-transfer; and (4) substrate versatility, allowing integration onto flexible, transparent, or bio-compatible platforms. Liu *et al.* showcased the transformative potential of van der Waals (vdW) lamination as a low-temperature route to monolithic three-dimensional (M3D) integration (Fig. 19c(I)–(IV)).[357] By sequentially stacking entire prefabricated circuit layers, they realized a ten-tier vertical M3D system. Remarkably, the vdW-mediated process confined the integration temperature to only 120 °C—well below the thermal budget restrictions that undermine conventional silicon-based M3D integration and hinder its compatibility with back-end-of-line (BEOL) processes. Equally critical, vdW transfer circumvents the need for harsh lithography or etching directly on 2D lattices, thus preserving atomic integrity while maintaining device performance. In parallel, Tao *et al.* demonstrated that prefabricated MoS_2 transistors could be laminated onto vertical stacks using a T-shaped PDMS stamp, achieving a 60-device array without degradation.[362] This strategy effectively overcame the inherent planar constraints of conventional lithographic processes, bridging lateral device fabrication with vertical stacking and thereby expanding the dimensionality of integration.

In summary, the transfer of whole 2D devices represents the next logical step in the all-transfer strategy. By enabling modular, reconfigurable, and damage-free assembly of complex electronic and optoelectronic circuits, it holds great promise for future wafer-scale integration, high-density logic and memory, and novel multi-functional device concepts. As transfer protocols mature, fully transfer-based device engineering may become the foundation for future electronics beyond the limits of traditional top-down fabrication.

7.2. Transfer-enabled patterning towards lithography-free direct fabrication

Traditional photolithography, despite its ubiquity and industrial maturity, imposes substantial limitations on the

 This journal is © The Royal Society of Chemistry 2025

Open Access Article. Published on 06 January 2026. Downloaded on 1/16/2026 12:17:14 PM.
This article is licensed under a Creative Commons Attribution-NonCommercial 3.0 Unported Licence.

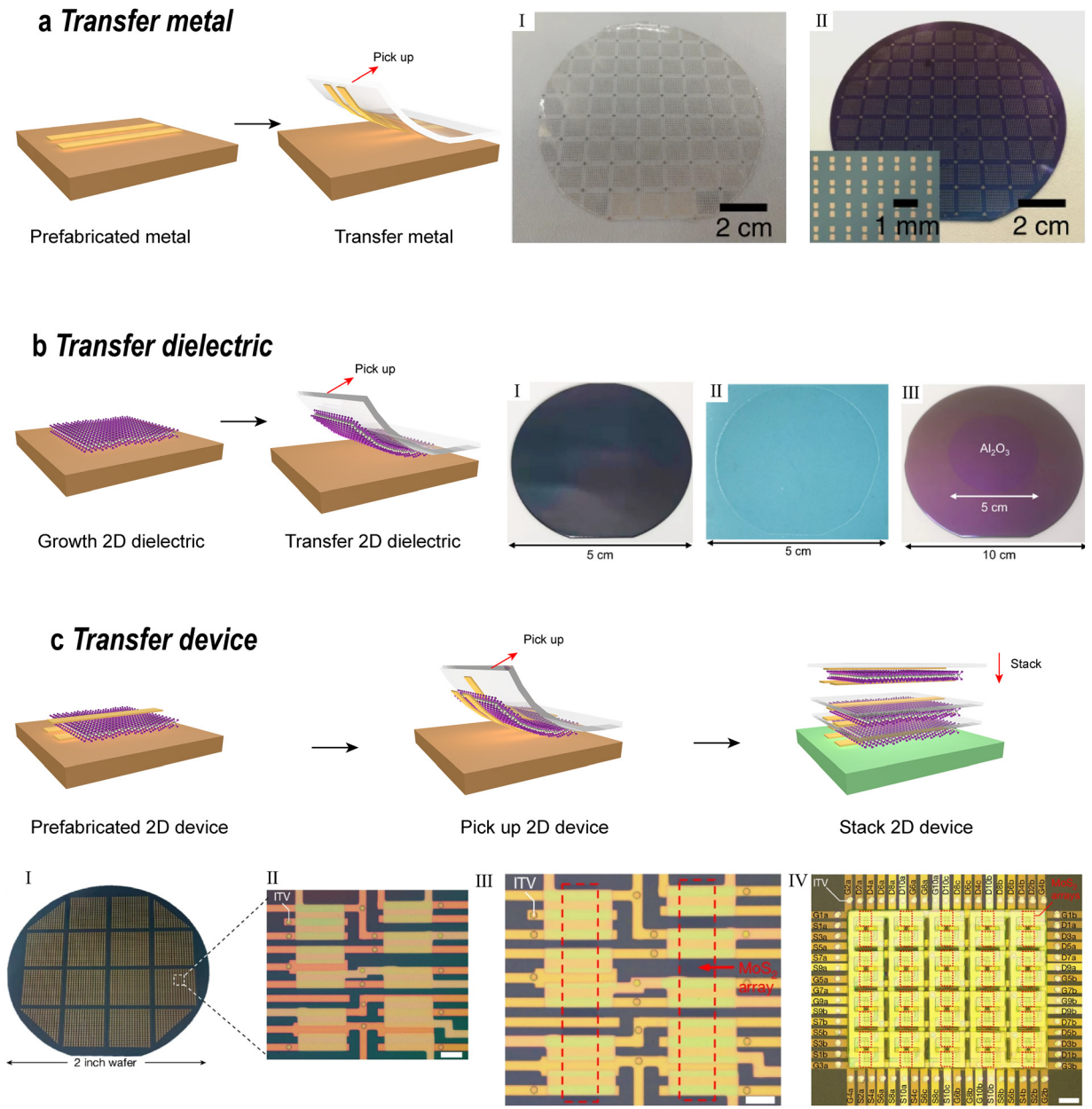

Fig. 19 All transfer strategies. (a) Transfer metal.[356] (I) Printing metal patterns on the target substrate. (II) The inset shows an optical image of the transferred Au pattern array. Reproduced from ref. 356 with permission from Springer Nature, Copyright 2022. (b) Transfer dielectrics. (I) Pre-deposition on a PVA sacrificial layer using the ALD process. (II) Dielectric dry peeling-off. (III) Dielectric lamination on top of a target substrate. Adapted from ref. 88 according to Creative Commons Attribution 4.0 International License (CC BY 4.0). (c) Transfer device. (I) Optical images of a prefabricated circuit tier on a 2-inch sacrificial substrate. (II) The zoomed-in image. (III) The optical image of the final device fabricated by laminating the circuit tier onto an MoS_2 substrate; the top patterned MoS_2 channel is highlighted by a red dashed box. (IV) The corresponding optical image of the 10-tier M3D systems. The MoS_2 substrates are grown using chemical vapour deposition within the 10-tier integration. Reproduced from ref. 357 with permission from Springer Nature, Copyright 2024.

fabrication of 2D materials and devices. The need for multiple chemical steps, mask alignment, and aggressive etching not only raises cost and complexity, but also introduces significant risks of surface contamination, non-uniform strain, pattern distortion, and interfacial disorder. These drawbacks are particularly acute for atomically thin materials, where interface cleanliness and damage-free processing are paramount for realizing their intrinsic properties in scalable devices.

Direct pattern transfer has thus emerged as a transformative solution, enabling the deterministic patterning and integration of 2D materials entirely without photolithography, masks, or solvents (Fig. 20). This paradigm shift is underpinned by several innovative approaches, each with its own unique technical merits and challenges.

A pioneering strategy is the MTP technique developed by Zhou Peng's group (Fig. 20a).[133] Here, a PDMS stamp patterned

Open Access Article. Published on 06 January 2026. Downloaded on 1/16/2026 12:17:14 PM.
This article is licensed under a Creative Commons Attribution-NonCommercial 3.0 Unported Licence.

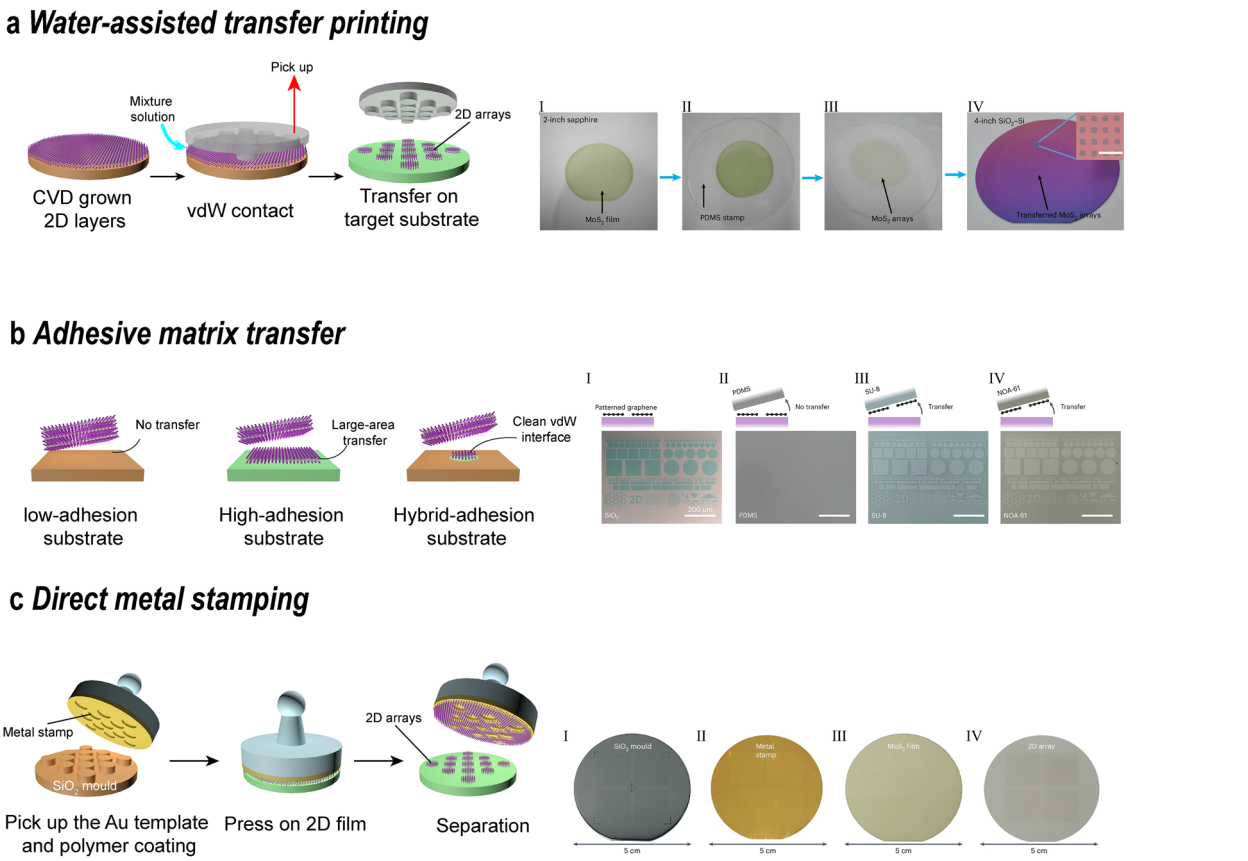

Fig. 20 Photolithography-free pattern transfer. (a) The water-assisted wafer-scale transfer printing technology. Reproduced from ref. 133 with permission from Springer Nature, Copyright 2025. (b) The adhesive matrix transfer method for wafer-scale patterned 2D material integration. Reproduced from ref. 363 with permission from Springer Nature, Copyright 2023. (c) The direct metal stamping method for wafer-scale fabrication. Reproduced from ref. 364 with permission from Springer Nature, Copyright 2025.

with an array of microcolumns is used to selectively contact and retrieve 2D materials from a growth substrate. During the process, a capillary-active mixed solution (ethanol/water) infiltrates the interface between the PDMS stamp and the substrate, enabling selective pick-up of contacted regions *via* capillary peeling. Subsequent alignment and mild heating allow the patterned 2D material array to be released onto the target substrate with high spatial precision. This method has been used to deterministically transfer 2-inch-scale monolayer MoS_2 arrays, achieving over one million functional devices per wafer, all while retaining their pristine electrical performance. MTP elegantly bypasses resist processing and chemical etching, making it exceptionally attractive for large-area, contamination-free 2D device fabrication. However, a critical bottleneck remains: the lateral resolution is fundamentally limited by the mechanical deformability of the PDMS microcolumns. As device dimensions approach the deep submicron regime, further progress will hinge on the development of stiffer, less deformable stamps or hybrid mechanical structures. Nevertheless, the high yield, process simplicity, and compatibility with scalable CVD-grown films render MTP a promising candidate for industrial 2D electronics.

To overcome the force limitations intrinsic to van der Waals pickup, adhesive matrix transfer has been developed by Farnaz Niroui's team (Fig. 20b).[363] In this approach, the receiving substrate (such as SiO_2) is embedded in an adhesion-tunable matrix (*e.g.*, patterned gold), enabling selective, high-strength interaction with the 2D material of interest. Unlike vdW stamping, the matrix can overcome weak interfacial adhesion, ensuring residue-free pickup and transfer of even the most challenging materials. This method enables one-step device integration, supports complex patterning, and preserves ultra-clean, exposed surfaces essential for subsequent functionalization or advanced quantum devices. Adhesive matrix transfer stands out for its exceptional interface cleanliness and its ability to break through vdW force limits. Notably, it eliminates the need for solvents, sacrificial layers, or thermal steps, thereby preserving the atomic flatness and electronic structure of transferred films. However, the method currently relies on precise matrix engineering for each material, and its extension to highly heterogeneous or flexible substrates is an open technical question. Nevertheless, the single-step process and mask-free patterning make it a valuable addition to the 2D device fabrication toolbox.

Recently, Li, *et al.* introduced a lithography-free patterning strategy by direct metal stamping (Fig. 20c).[364] Here, a pre-designed 3D metal stamp is pressed onto a continuous 2D material. Owing to the strong local metal-2D material

Open Access Article. Published on 06 January 2026. Downloaded on 1/16/2026 12:17:14 PM.
This article is licensed under a Creative Commons Attribution-NonCommercial 3.0 Unported Licence.

interaction, only the contact regions are picked up, while the non-contact areas remain on the growth substrate, resulting in cleanly patterned 2D arrays. The resulting devices, fabricated without any photoresist or chemical reagents, exhibit high performance and remarkable uniformity across large scales. This strategy is remarkable for its complete elimination of chemical patterning steps and post-transfer processing, offering the highest attainable cleanliness and structural integrity for 2D arrays. The main limitation lies in the design, cost, and reusability of the metal molds, especially for complex or fine-feature arrays. Future improvements in scalable, reconfigurable mold design could further enhance the practicality of this approach for industry.

In addition, a diverse suite of transfer-enabled, lithography-free patterning techniques, such as water-assisted transfer printing, single-lamination stacking, and one-step vdW integration, have rapidly expanded the design space for 2D devices and circuits. These methods enable high-yield, contamination-free fabrication across both planar and vertical architectures, support a wide range of substrates (including flexible and unconventional platforms), and deliver atomic interface quality unattainable by conventional lithography. While each approach has unique strengths and current technical limits, together they redefine scalable manufacturing in 2D electronics and bring modular, industrial-level device integration within reach.

In summary, transfer-enabled, lithography-free patterning is fundamentally redefining device manufacturing in 2D electronics. By circumventing the limitations of traditional photolithography and wet processing, these methods deliver new levels of scalability, yield, and interface quality for both planar and vertical device integration. As each approach continues to mature, a hybrid toolbox combining pattern transfer, adhesive engineering, and vertical stacking will likely emerge, paving the way for modular, high-performance, and industrial scale 2D electronics with truly clean and tunable interfaces.

8. Transfer for broader fields

While the transfer of 2D materials has been primarily developed for electronic and optoelectronic devices, its applicability extends far beyond these domains. Advances in precision transfer techniques now enable the deterministic positioning, stacking, and integration of 2D materials and nanostructures into a wide variety of functional platforms, opening transformative opportunities in chemistry,[24] polaritonic devices,[25] phonon polaritons,[26] tribology,[27] haptics,[28] thermal transport,[29,30] thermodynamic control,[31] quantum science,[169] neuromorphic computing,[32] electrocatalysts and energy.[33,34] By leveraging the ability to control interfacial properties, orientation, and symmetry at the atomic scale, transfer methods are increasingly becoming a cross-disciplinary tool for engineering novel functionalities that cannot be achieved through conventional fabrication routes. In this section, we review some of the most exciting and recent demonstrations where transfer-based assembly has enabled breakthroughs across these diverse fields, highlighting both the unique advantages and the current technical barriers.

8.1. Chemistry

The convergence of precision transfer techniques with electrochemical and synthetic chemistry platforms is redefining how interfacial charge transfer, catalytic activity, and supramolecular assembly can be engineered at the atomic and molecular levels. Beyond serving as a mechanical assembly tool, transfer now functions as a chemical design parameter by enabling deterministic control over lattice symmetry, registry, and moiré potential landscapes, which directly govern reaction thermodynamics and kinetics.

A notable example is provided by Yu *et al.*, who applied a deterministic dry transfer process to fabricate twisted bilayer graphene (TBG)/h-BN heterostructures with precisely controlled twist angles.[24] This approach revealed an unambiguous correlation between moiré geometry and interfacial electron-transfer kinetics: electrochemical measurements showed that reaction rates are maximized near the "magic angle" ($\sim 1.1^\circ$), where flat-band states localise carriers and amplify electronic density of states (Fig. 21a). This discovery positions the twist angle as a controllable degree of freedom for electrochemical reactivity, circumventing the stochasticity of dopant incorporation or defect engineering. Subsequent work extended this moiré-reactivity paradigm to transition metal dichalcogenides (TMDs), underscoring its potential impact on photoelectrochemistry and electrocatalysis, where band structure-driven reactivity tuning could complement or even supplant conventional catalyst modification strategies.

Equally transformative is the application of twist-controlled stacking to two-dimensional covalent organic frameworks (2D COFs), whose extended π-conjugation and tunable pore architectures make them attractive for catalysis, sensing, and energy storage.[291] Conventional COF synthesis typically yields rotationally disordered stacks due to the near-isoenergetic nature of different twist configurations, resulting in heterogeneous interlayer coupling. Recent advances, exemplified by Zhan *et al.*, have addressed this by directly synthesising bilayer COFs at a liquid–substrate interface under conditions that promote deterministic stacking control.[365] Through monomer structure design and mixed-solvent modulation, which can balance precursor solubility with low volatility, the authors achieved large-area moiré superlattices with a predominant twist angle ($\sim 9.2^\circ$) verified by atomic-resolution HRTEM and reciprocal-space mapping. This breakthrough not only extends moiré engineering beyond van der Waals solids into covalent molecular architectures, but also unlocks new opportunities to modulate electronic coupling, exciton dynamics, and host–guest chemistry through precise stacking symmetry control.

In summary, these studies exemplify how transfer-enabled twist engineering is evolving from a structural curiosity into a chemically actionable variable—capable of bridging solid-state physics and synthetic chemistry to create functional interfaces with unprecedented precision. Looking forward, integrating *in situ* spectroelectrochemical probes, operando microscopy,

Open Access Article. Published on 06 January 2026. Downloaded on 1/16/2026 12:17:14 PM.
This article is licensed under a Creative Commons Attribution-NonCommercial 3.0 Unported Licence.

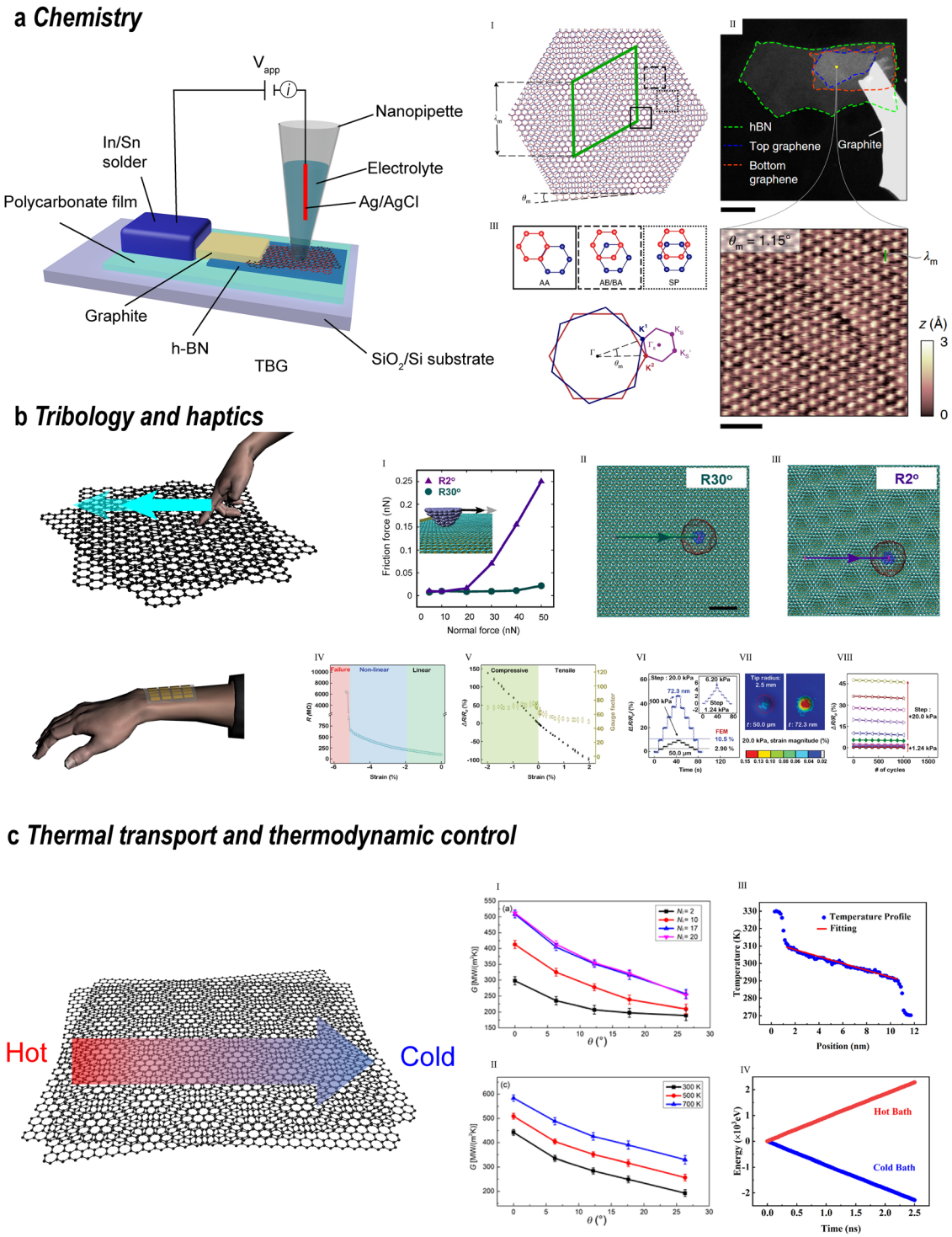

Fig. 21 Applications of 2D materials in other fields. (a) Chemistry. Reproduced from ref. 24 with permission from Springer Nature, Copyright 2022. (b) Tribology and haptics. Reproduced from ref. 27 with permission from American Chemical Society, Copyright 2023. Reproduced from ref. 28 with permission from Wiley-VCH, Copyright 2016. (c) Thermal transport and thermodynamic control. Reproduced from ref. 29 with permission from American Chemical Society, Copyright 2021. Reproduced from ref. 30 with permission from Elsevier, Copyright 2024.

and theory-guided twist-angle selection could yield predictive control over reactivity landscapes, accelerating the design of catalytic, photochemical, and sensing platforms based on moiré-tailored 2D materials.

8.2. Tribology and haptics

The interlayer twist degree of freedom offers an effective means of tuning friction and lubrication in vdW interfaces, giving rise to the emerging concept of superlubricity. Early studies by

Open Access Article. Published on 06 January 2026. Downloaded on 1/16/2026 12:17:14 PM.
This article is licensed under a Creative Commons Attribution-NonCommercial 3.0 Unported Licence.

Hirano *et al.* revealed that the frictional force between mica sheets varies with the twisting angle, which they initially attributed to shear forces within the basal planes.[366] Dienwiebel *et al.* later demonstrated that in graphite, rotating the top layer relative to the underlying lattice could dramatically reduce the interfacial shear strength, even approaching the near-zero friction regime, a phenomenon attributed to lattice incommensurability.[367]

More recent work has explicitly connected these effects to moiré superlattice engineering. Liu *et al*[27] showed that graphene grown on Pt exhibits moiré patterns due to partial lattice mismatch (Fig. 21b(I)–(III)) and that adjusting the twist angle allows for reversible switching between dissipative sliding and ultra-low-friction states. Here, both the moiré periodicity and the normal load threshold govern the transition: below the threshold, the interface remains in a constant superlubric state, while above it, the friction coefficient decreases systematically with increasing moiré period. These findings are supported by theoretical models linking twist-induced modulation of in-plane and out-of-plane deformation fields to energy dissipation pathways.

In the field of haptics, the exceptional thinness, mechanical compliance, and electromechanical sensitivity of 2D semiconductors have inspired a new generation of tactile sensors. Park *et al*[28] fabricated strain-gauge sensors based on monolayer MoS_2, achieving high gauge factors (GF), optical transparency, and mechanical flexibility (Fig. 21b(IV)–(VIII)). Devices maintained high sensitivity, uniformity, and linearity after 10 000 bending cycles, and their $\sim$75 nm total thickness allows direct integration onto non-planar and even skin-mounted substrates. These attributes make 2D-based tactile sensors attractive for wearable electronics, human-machine interfaces,[368–370] and prosthetic feedback systems.[371,372]

8.3. Thermal transport and thermodynamic control

At the nanoscale, thermal transport is dictated by phonon-mediated lattice vibrations, yet their propagation is readily disrupted by structural boundaries and defects that serve as dominant scattering centers. These scattering events drastically curtail the phonon mean free path, leading to a pronounced suppression of thermal conductivity. Recognizing this intrinsic sensitivity, the ability to deliberately tailor phonon transport—whether through defect engineering, interface design, or dimensional confinement—has emerged as a central pursuit in contemporary materials research.

Twist engineering in vdW heterostructures offers a powerful route to modulate phonon transport, providing a thermodynamic handle for heat management in nanoscale devices. By altering the interlayer registry, the twist angle can directly influence phonon spectra, scattering pathways, and mode coupling—parameters that govern both in-plane and cross-plane thermal conductivity.

Ren *et al.* demonstrated that in graphene/h-BN bilayers, the in-plane thermal conductivity decreases monotonically, by up to 50%, as the twist angle increases from 0° to 30° (Fig. 21c(I) and (II)).[29] This reduction was attributed to enhanced surface corrugation, which amplifies low-frequency (<10 THz) phonon scattering and suppresses interlayer phonon transmittance. Such a strong angular dependence reveals that even modest misalignment can be used to deliberately tune heat dissipation in vdW devices.

Extending this principle to hybrid heterostructures, Meng *et al.* employed non-equilibrium molecular dynamics (NEMD) simulations to study graphene/MoS_2/graphene stacks at varying twist angles (Fig. 21c(III) and (IV)).[30] They found that the in-plane thermal conductivity of the MoS_2 layer drops sharply with increasing twist angle, reaching a minimum at 10.893°, where it is only 47.3% of the untwisted value. This degradation stems from twist-induced lattice mismatch, which produces uneven stress fields and enhances phonon–phonon scattering. Interestingly, they also observed that increasing the number of graphene layers reduces the interfacial thermal resistance, as additional layers mitigate out-of-plane atomic displacement and improve structural stability.

In parallel, Ouyang *et al.* examined uniformly twisted graphite and h-BN multilayers, finding that the interfacial thermal resistance (ITR) increases markedly with the twist angle.[31] This behavior arises from reduced phonon mode coupling at misaligned interfaces, thereby lowering cross-plane thermal conductivity. Such control over interfacial thermal isolation is particularly relevant for applications requiring thermal shielding between an active layer and its substrate.

In summary, these studies position the twist angle as a versatile thermodynamic tuning parameter, enabling thermal conductivity suppression, directional heat management, and interfacial thermal isolation in 2D-based devices. By leveraging twist-induced phonon engineering, it is possible to co-optimize thermal transport with other functionalities such as friction modulation, mechanical stability, and optoelectronic performance.

8.4. Polaritonic devices and phonon polaritons

While moiré engineering in twisted vdW bilayers has gained prominence for enabling emergent electronic states such as superconductivity and correlated insulators, the same twist-angle degree of freedom is now recognised as a powerful lever for controlling light–matter interactions in the mid-infrared and terahertz regimes. In particular, phonon polaritons (PhPs), hybrid modes arising from strong coupling between infrared photons and optical phonons, can be dispersion-engineered by interlayer rotation, giving rise to the emerging field of twistnonics for phononics.[373–376] Analogous to twistronics in electronics, twistnonics allows precise modulation of interlayer atomic registry and potential energy landscapes, which in turn reshape polaritonic band structures and wavefront propagation.

One of the most striking phenomena accessible *via* twist engineering is the photonic ''magic angle'', a rotation configuration where the PhP isofrequency contours flatten, entering the canalization regime.[377,378] In this state, polaritons propagate in a highly collimated, unidirectional manner with negligible geometric spreading, enabling sub-diffractional information transport over extended distances.[379,380] The

Open Access Article. Published on 06 January 2026. Downloaded on 1/16/2026 12:17:14 PM.
This article is licensed under a Creative Commons Attribution-NonCommercial 3.0 Unported Licence.

canalization direction and wavelength are uniquely determined by the magic angle and material thickness, making twist control central to device functionality.[381]

α-Phase molybdenum trioxide (α-MoO_3), a naturally hyperbolic vdW crystal, provides an ideal platform for such studies due to its strong in-plane anisotropy and the ability to achieve clean rotational interfaces *via* all-dry viscoelastic stamping. Hu *et al.* demonstrated a topological transition of PhP dispersion in twisted bilayer α-MoO_3, tunable from hyperbolic to elliptical regimes by adjusting the rotation between layers along crystallographic [001] or [100] axes (Fig. 22a).[25] For a given frequency, only a single photonic magic angle exists, which confines canalization to a narrow set of directions and restricts all-angle tunability in bilayer geometries.

To overcome this constraint, Duan and co-workers introduced a reconfigurable twisted trilayer α-MoO_3 architecture (Fig. 22b).[26] Fabricated *via* sequential PDMS-assisted stacking of exfoliated α-MoO_3 flakes, the device features two independently set twist angles—θ_{1-2} (bottom-middle) and θ_{1-3} (bottom-top)—which can be reprogrammed by layer disassembly and reassembly. Near-field scanning optical microscope (s-SNOM) and full-wave simulations (Fig. 22b(I)–(IX)) revealed multiple photonic magic angles within a single device: for $\theta_{1-2} = 30^\circ$, canalization directions of 140°, 80°, and 50° were achieved at $\theta_{1-3} = -90^\circ$, -60°, and -40°, respectively. This multi-angle flexibility enables broadband canalization and all-directional polariton steering within the device plane—capabilities unattainable in bilayers. Importantly, these properties persist across a wide spectral range and for varying layer thicknesses, underscoring their robustness.[376]

By unlocking deterministic control over polaritonic dispersion, twist-engineered α-MoO_3 heterostructures open new frontiers for mid-IR nanophotonics, including compact waveguides, reconfigurable beam steering devices, and ultra-thin hyperlenses.[183] The ability to combine dry-transfer precision, multiple rotational degrees of freedom, and broadband robustness marks a significant step toward programmable polaritonic circuitry.

8.5. Quantum devices

Recent developments in 2D nonlinear materials have opened unprecedented opportunities for compact, integrable quantum light sources and nonlinear photonic devices. Guo *et al.* demonstrated that $NbOCl_2$ crystals exhibit vanishing interlayer

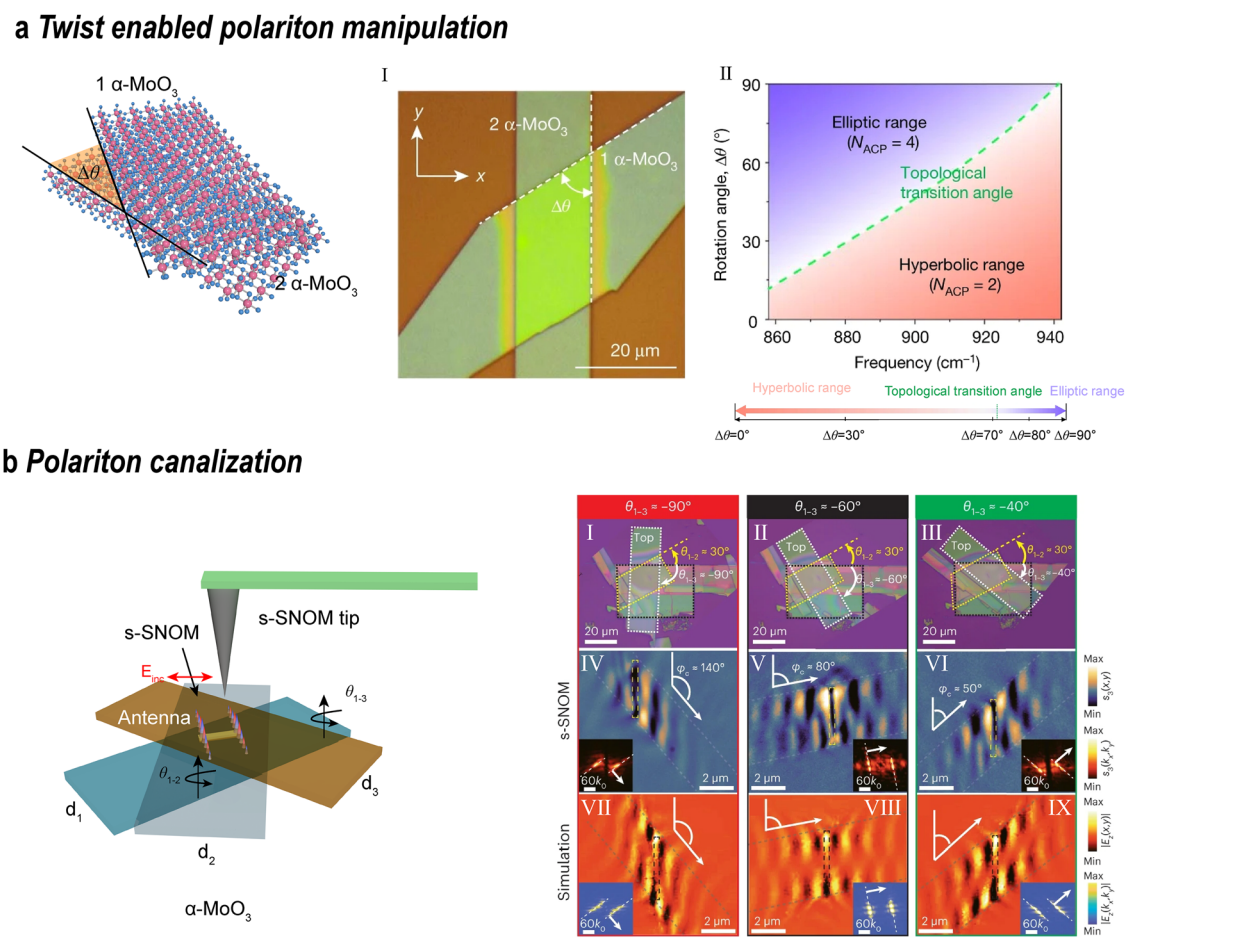

Fig. 22 Twist for optical devices. (a) Polariton dispersion is controlled by twisted bilayered α-MoO_3. Reproduced from ref. 25 with permission from Springer Nature, Copyright 2020. (b) Photonic magic angles and polariton canalization in reconfigurable trilayers. Reproduced from ref. 26 with permission from Springer Nature, Copyright 2023.

This journal is © The Royal Society of Chemistry 2025

Open Access Article. Published on 06 January 2026. Downloaded on 1/16/2026 12:17:14 PM.
This article is licensed under a Creative Commons Attribution-NonCommercial 3.0 Unported Licence.

electronic coupling and monolayer-like excitonic behavior even in bulk form, coupled with a large second order nonlinear coefficient (χ^2).[382] The SHG intensity scales quadratically with thickness, reaching values up to three orders of magnitude higher than monolayer WS_2. This exceptionally strong and scalable second-order nonlinearity enabled the first unambiguous demonstration of spontaneous parametric down-conversion (SPDC) in a 2D material, with correlated photon pairs generated in flakes as thin as 46 nm, currently the thinnest nonlinear quantum light source reported. The measured SPDC figure of merit ($\approx$ 9800 GHz W^{-1} m^{-1}) underscores its potential for on-chip quantum light sources compatible with integrated photonics.

Beyond intrinsic nonlinear properties, symmetry engineering has emerged as a powerful approach. Zhang *et al.* reported emergent SHG in otherwise centrosymmetric bilayer MoS_2 when stacked with monolayer graphene.[344] Interlayer charge transfer broke the inversion symmetry of MoS_2, producing SHG of comparable strength to monolayer MoS_2. This effect—absent before interlayer coupling was established—illustrates how charge transfer in van der Waals heterostructures can be exploited to tailor nonlinear optical responses and potentially activate SPDC processes in systems previously deemed inactive.

Control of nonlinear wave mixing can also be achieved *via* nonlinear geometric phase engineering. Hong *et al*. showed that twisting multilayer films by an optimal angle can induce a geometric phase that compensates phase mismatch, enabling high SHG conversion efficiencies ($\sim$8% in 3.2 μm-thick stacks) and tunable output polarization[383] (Fig. 23a(I)–(III)). The ''Twist-PM'' concept aligns the SHG contribution vectors from each layer to achieve constructive interference, offering a route to polarization- and phase-controlled quantum light emission in ultrathin platforms. In parallel, another twist stacking quasi-phase-matching strategy has been adapted to 3R-MoS_2. Tang *et al.* demonstrated that 3R-MoS_2 stacks with controlled 60° rotational offsets between successive layers create periodic modulation of the nonlinear polarization along the growth axis, surpassing the non- quasi-phase matching (QPM) SHG limit(Fig. 23a(IV)–(VI)).[384] Such QPM structures are promising for enhancing SPDC efficiency in atomically thin materials, enabling brighter entangled photon pair generation in ultra-compact geometries.

The concept of periodic poling, which is well established in nonlinear bulk crystals such as periodically poled lithium niobate (PPLN), has recently been translated into the realm of 2D materials, enabling unprecedented control over light-matter interactions at the atomic scale. In a landmark demonstration, Trovatello *et al.* realized periodically poled transition metal dichalcogenides (PPTMDCs) by fabricating multi-layer stacks of 3R-MoS_2 with alternating crystallographic orientations, which periodically invert the sign of the χ^2 along the stacking direction to implement QPM in an atomically thin platform (Fig. 23b).[385] This architecture supports both up-conversion SHG and SPDC with efficiencies far exceeding the non-QPM limit, and the phase mismatch between interacting waves can be precisely cancelled by tuning the thickness and periodicity of the 3R-MoS_2 domains. The monolithic 2D structure minimizes optical loss and allows seamless integration with photonic and quantum devices, offering a route to compact, chip-scale sources of entangled photons and wavelength-tunable light.[204,386] This atomically engineered periodic poling approach bridges bulk-crystal nonlinear optics and van der Waals nanophotonics, marking a decisive step toward scalable quantum photonic circuitry based on layered materials.

Taken together, these advances, from giant χ^2 2D ferroelectrics like $NbOX_2$[174,220,269,382] to symmetry-breaking heterostructures and twist- and QPM-engineered stacks, mark a pivotal step toward ultrathin, chip-integrable quantum photonic devices. The convergence of high nonlinearity, scalable thickness response, and engineered phase matching points to a future where deterministic entangled photon sources and reconfigurable quantum modulators are realized entirely within the van der Waals materials platform.

8.6. Neuromorphic computing

In the era of rapidly expanding global information volume, AI and information technology are developing rapidly, and there is a strong demand for low-power, high-efficiency hardware. Neuro-inspired computing is regarded by many researchers as a solution to the problems of big data and power consumption.

Since almost all atoms of 2D materials are exposed on the surface (or interface), this increases the coupling efficiency with electric fields, ions, or light, enabling small external fields to effectively modulate parameters such as device conductance/capacitance; this is the key to achieving low energy consumption and adjustable synaptic weights. Many 2D materials support fast electronic transport and reversible ion migration (*e.g.*, metal cations or protons) *via* defects, adsorption sites, or interlayer channels. This mixed ionic-electronic conduction provides the physical basis for synaptic behaviors: transient ionic redistribution gives rise to short-term plasticity (STP), whereas cumulative/partly irreversible ionic or electrochemical changes underpin long-term plasticity (LTP).[387] Furthermore, through factors such as layer thickness, phase transition, defect doping or strain, the conductive/electronic band structure of 2D materials can be controllably adjusted, thereby achieving multi-level tunable conductance levels. This is one of the core functions required by neuromorphic hardware.[388]

For instance, Qin *et al.* developed a molecular crystal memristor. The representative channel material Sb_2O_3 has a molecular crystal structure, in which the molecular cages are interconnected through van der Waals forces.[389] This unique structure enables ions to migrate through the molecular gaps with relatively low energy input, maintaining the integrity of the crystal structure even after numerous switching cycles. The energy consumption for a single operation is as low as 26 zJ. It completed 109 cycles and successfully fabricated a large cross-array on an 8-inch wafer, while also achieving single-chip integration with CMOS technology, demonstrating its significant industrialization potential. Teja Nibhanupudi *et al.* reported ultrafast memristors fabricated using 2D h-BN. They synthesized few-layer h-BN on copper foil using the CVD

Open Access Article. Published on 06 January 2026. Downloaded on 1/16/2026 12:17:14 PM.
This article is licensed under a Creative Commons Attribution-NonCommercial 3.0 Unported Licence.

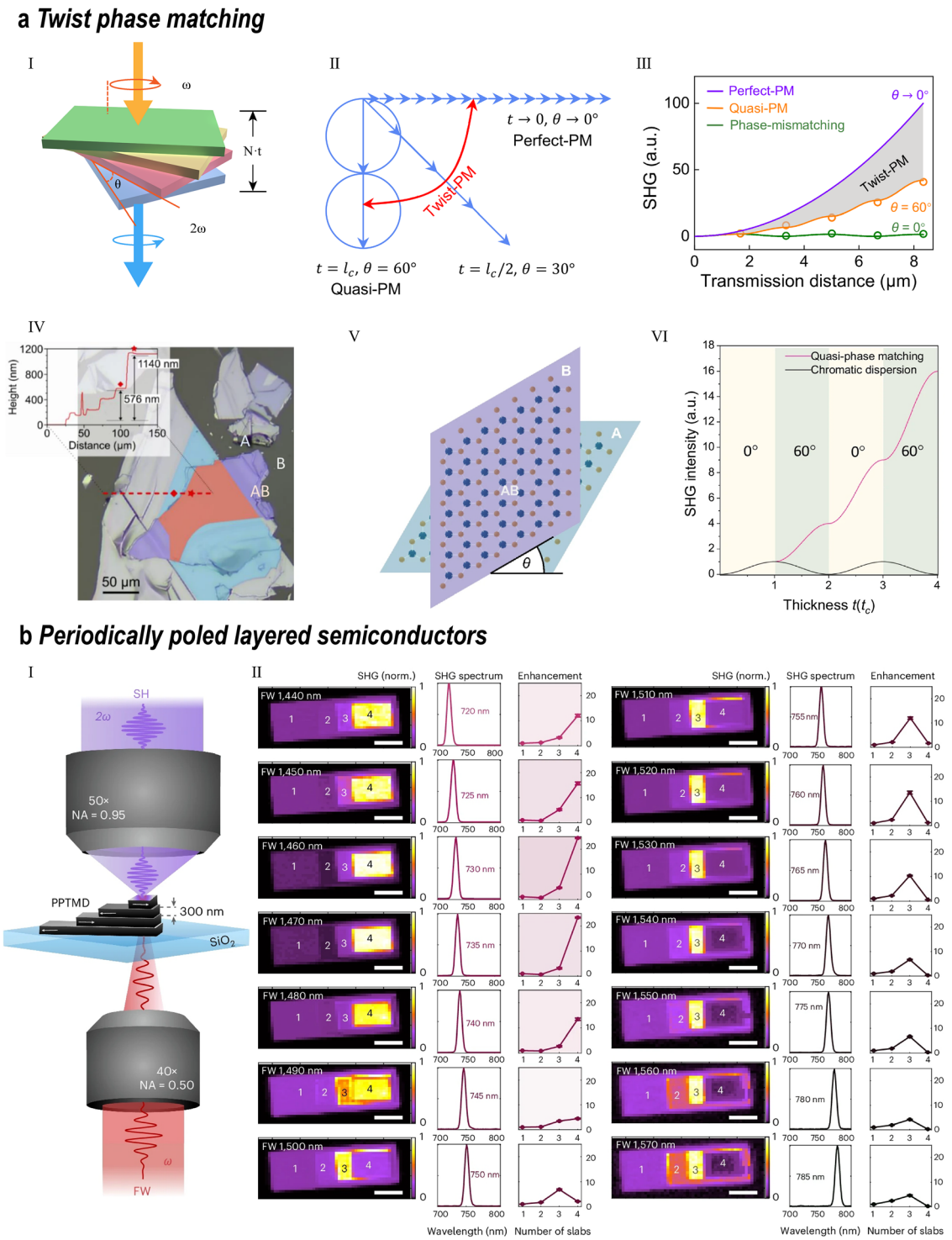

Fig. 23 (a) Twist phase matching. (I)–(III) The nonlinear geometric phase caused by the twist angle is used to compensate for the phase misfit in the SHG process. Reproduced from ref. 383 with permission from American Physical Society, Copyright 2023. (IV)–(VI) Theoretical model of a unique QPM enabled by van der Waals stacking. Adapted from ref. 384 according to Creative Commons Attribution 4.0 International License (CC BY NC ND 4.0). (b) Periodically poled layered semiconductors. (I) and (II) The quasi-phase-matched frequency conversion enabled by the χ^2 sign flip.[385] Reproduced from ref. 385 with permission from Springer Nature, Copyright 2025.

method and transferred it onto a Si/SiO_2 substrate to fabricate the memristors. The switching speed reached 120 ps, and the switching energy was extremely low, at 2 pJ.[390]

Looking ahead, moving from device demonstrations to system-level neuromorphic computing with 2D materials will require cross-layer co-design rather than merely "better

Open Access Article. Published on 06 January 2026. Downloaded on 1/16/2026 12:17:14 PM.
This article is licensed under a Creative Commons Attribution-NonCommercial 3.0 Unported Licence.

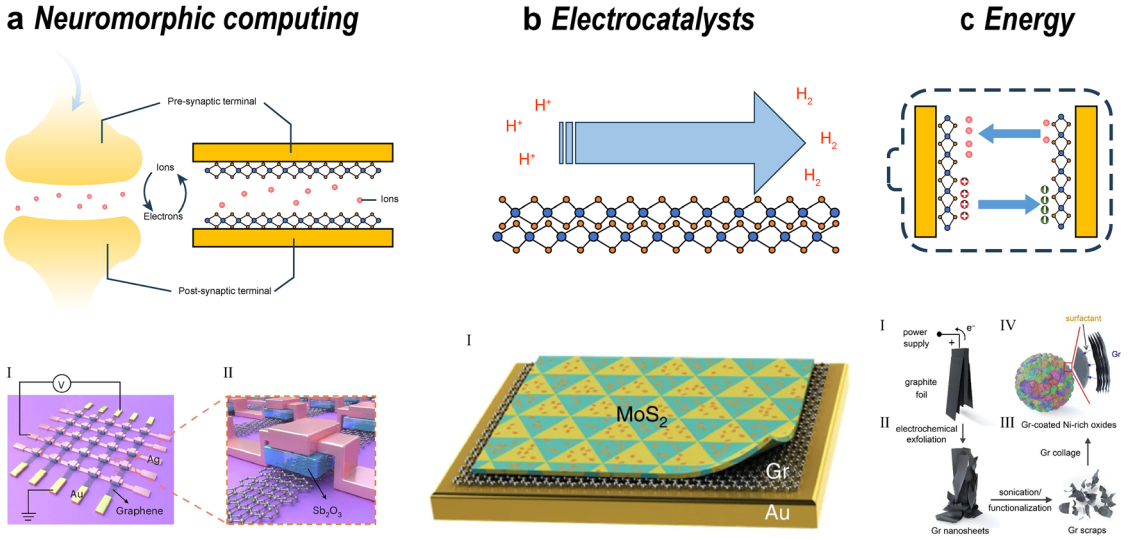

Fig. 24 (a) Neuromorphic computing. (I) and (II) Schematic of the molecular crystal memristor in the crossbar array architecture. Reproduced from ref. 389 with permission from Springer Nature, Copyright 2025. (b) Electrocatalysts. (I) The nonlinear geometric phase caused by the twist angle is used for high density of domain and phase boundaries. Adapted from ref. 33 according to Creative Commons Attribution 4.0 International License (CC BY 4.0). (c) Energy. (I)–(IV) Schematic structure of the multi-hierarchy MoS_2 catalysts. Adapted from ref. 34 according to Creative Commons Attribution 4.0 International License (CC BY 4.0).

heterostructures.'' At the materials level, vdW stacks must be engineered to deterministically gate ionic pathways and barriers, enabling on-demand switching between volatile and non-volatile responses while enhancing device stability and uniformity. At the architecture level, scalable three-dimensional integration of 2D devices requires addressing challenges related to endurance, retention, and transfer interfaces, as well as achieving ultra-low energy consumption at the system level rather than for individual devices. These advances will ultimately enable the realization of biologically realistic neural networks comprising synapses, dendrites, and somas, fully integrated within compact on-chip systems.

8.7. Electrocatalysts and energy

Since almost all atoms of 2D materials are exposed on the surface, they have an extremely high specific surface area, providing abundant electrochemical active sites, enhancing the adsorption of specific substances, and improving catalytic activity, enabling their application in the field of electrochemical sensing. Secondly, 2D layered materials exhibit excellent mechanical properties, such as high Young's modulus and elasticity, which can maintain stability under large stress and strain, serving as a mechanical support network for electrode materials.

Bae *et al.* developed a R2R transfer process for large-area graphene films, using them as transparent electrodes, laying a feasible path for large-area flexible energy storage devices.[200] Zhu *et al.* placed a single layer of MoS_2 on a conductive substrate (graphene/gold film) through a transfer process to form an electrocatalytic electrode and investigated the role of the boundary activation effect in the hydrogen evolution reaction.[33] In this study, the transfer engineering ensured that the large-area single-layer MoS_2 could serve as an actual electrocatalytic electrode. Park *et al.* coated the surface of high-nickel cathode particles with graphene layers, significantly reducing the reliance on conductive agents and binders. Graphene sheets were uniformly covered on the surface of the cathode particles through transfer/coating processes. This enhanced the volumetric energy density and cycle stability of the battery.[34]

For 2D materials to truly enter the field of energy applications, several issues need to be addressed, including large-scale controllable fabrication and transfer, long-term stability, and device-level integration. By developing low-cost, scalable synthesis and transfer methods, combined with interface and defect engineering, heterostructure design, and intelligent simulation and prediction, it is expected to achieve precise control over performance. At the same time, by further expanding 2D materials into new energy systems such as solid-state batteries and photocatalytic hydrogen production, it is possible to drive a qualitative leap in energy storage and conversion technologies (Fig. 24).

8.8. Summary and perspectives

In this section, we have discussed how transfer engineering of 2D materials has already enabled advances across a broad spectrum of fields, ranging from chemistry to polaritonic devices, phonon polaritons, tribology, haptics, thermal transport, thermodynamic control, quantum science, neuromorphic computing, electrocatalysts and energy. Looking ahead, the scope of applications is expected to expand even further, with particularly promising opportunities in quantum computing and other emerging domains. Each of these areas imposes unique demands, such as ultraclean and reconfigurable

Open Access Article. Published on 06 January 2026. Downloaded on 1/16/2026 12:17:14 PM.
This article is licensed under a Creative Commons Attribution-NonCommercial 3.0 Unported Licence.

interfaces for quantum devices, conformability and biocompatibility for bioelectronics, or scalable integration and chemical robustness for energy systems. By offering deterministic control over stacking order, interfacial cleanliness, and strain, transfer engineering provides a versatile pathway to address these requirements. Future progress will therefore depend on advancing transfer methods toward higher cleanliness, reconfigurability, and scalability, ultimately positioning 2D transfer engineering as a foundational technology for next-generation cross-disciplinary applications.

9. Conclusions and perspectives

At this stage of 2D material research, preparation, transfer, and post-transfer engineering are not auxiliary steps but central determinants of material quality, scalability, and device performance. As this review has outlined, advances from controlled growth and exfoliation to deterministic and reconfigurable transfer have enabled diverse applications, ranging from moiré superlattices in twisted structures to wrinkle- and bubble-mediated strain engineering and wafer-scale assembly for optoelectronic and quantum devices. These developments have transformed transfer into a cornerstone technology that connects chemistry, materials science, and device engineering.

Nevertheless, several grand challenges remain. Cleanliness and interface control continue to be the most critical bottlenecks. Conventional polymer-assisted protocols inevitably leave residues or interfacial defects that compromise transport and optical performance. Emerging concepts such as sacrificial mediator layers, intrinsically clean dry transfer, and dynamically tunable adhesion present promising solutions, but a universal, residue-free transfer process remains elusive. Equally urgent is the need for reconfigurability: current methods largely enable static stacking, whereas future directions should aim at reversible and *in situ* manipulation of twist angle, spacing, and domain registry. Such capabilities would open programmable device architectures, where 2D heterostructures can be dynamically tuned post-integration.

Scaling toward wafer-level integration is another frontier. While proof-of-concept demonstrations of large-area printing, stamp patterning, and R2R assembly exist, the uniformity, throughput, and CMOS compatibility remain limited. The convergence of robotics-assisted transfer, real-time metrology, and advanced adhesion engineering will be essential to bridge laboratory methods with industrial fabrication, ultimately enabling defect-free integration on 200–300 mm wafers. In parallel, *in situ* transfer concepts, where growth and relocation are integrated into continuous workflows, may eliminate stochasticity and reduce contamination, offering a seamless path to twist-controlled and multilayer heterostructures.

Looking forward, the scope of 2D transfer technology will extend beyond conventional electronics and photonics. Applications in tribology, haptics, wearable devices, chemistry, and thermal management are emerging, where controlled interfaces and ultrathin integration provide unique functionalities. Notably, twist-phase-matching and periodically poled 2D crystals point to a paradigm shift in nonlinear optics, enabling frequency conversion and quantum light generation in atomically thin platforms. Extending such concepts to wafer-scale, reconfigurable devices would open a new class of integrated nanophotonic and quantum technologies. Beyond these areas, the integration of ultraclean and reconfigurable 2D heterostructures may also provide decisive advantages for quantum computing, where atomic-scale control of interfaces and twist-dependent quantum phases can be harnessed to engineer qubits, quantum interconnects, and scalable architectures.

In conclusion, the future of 2D transfer lies in developing methods that are intrinsically clean, dynamically reconfigurable, and scalable to wafer-level integration. Achieving these milestones will not only overcome existing bottlenecks but also elevate transfer technology from a fabrication tool to a discipline in its own right, bridging chemistry, physics, and engineering while unlocking the full potential of low-dimensional materials in next-generation technologies.

Author contributions

All authors contributed to the preparation of the manuscript.

Conflicts of interest

The authors declare no conflict of interest.

Data availability

The data supporting this article have been included as part of the supplementary information.

The analyses are available within the supplementary information (SI). Supplementary information is available. See DOI: **https://doi.org/10.1039/d5cs00531k**.

Acknowledgements

This work was supported by the Scientific and Technological Development Project of Jilin Province, China (Grant No. 20240302035GX). Singapore RIE2025 Manufacturing, Trade, and Connectivity (MTC), Young Individual Research Grants (M23M7c0129); Individual Research Grant (M23M6c0104) administered by A*STAR; A*STAR Quantum Innovation Centre (Q. InC) core funding, the Hong Kong Research Grants Council (25228722 and T42-513/24-R), the National Natural Science Foundation of China (NSFC 12402115 and 22374074).

References

1 K. S. Novoselov, A. K. Geim, S. V. Morozov, D. Jiang, Y. Zhang, S. V. Dubonos, I. V. Grigorieva and A. A. Firsov, *Science*, 2004, **306**, 666–669.
2 Q. Zhang, M. Li, L. Li, D. Geng, W. Chen and W. Hu, *Chem. Soc. Rev.*, 2024, **53**, 3096–3133.

 This journal is © The Royal Society of Chemistry 2025

Open Access Article. Published on 06 January 2026. Downloaded on 1/16/2026 12:17:14 PM. This article is licensed under a Creative Commons Attribution-NonCommercial 3.0 Unported Licence.

3 S. Gbadamasi, M. Mohiuddin, V. Krishnamurthi, R. Verma, M. W. Khan, S. Pathak, K. Kalantar-Zadeh and N. Mahmood, *Chem. Soc. Rev.*, 2021, **50**, 4684–4729.
4 M. Yang, Z. Ye, Y. Ren, M. Farhat and P.-Y. Chen, *Micromachines*, 2023, **14**, 603.
5 Q. Deng, T. Zhao, J. Zhang, W. Yue, L. Li, S. Li, L. Zhu, Y. Sun, Y. Pan, T. Zheng, X. Liu, Y. Yan and N. Huo, *ACS Nano*, 2024, **18**, 23702–23710.
6 X. Ma, N. Youngblood, X. Liu, Y. Cheng, P. Cunha, K. Kudtarkar, X. Wang and S. Lan, *Nanophotonics*, 2021, **10**, 1031–1058.
7 P. V. Pham, S. C. Bodepudi, K. Shehzad, Y. Liu, Y. Xu, B. Yu and X. Duan, *Chem. Rev.*, 2022, **122**, 6514–6613.
8 X. Liu and M. C. Hersam, *Nat. Rev. Mater.*, 2019, **4**, 669–684.
9 A. Castellanos-Gomez, M. Buscema, R. Molenaar, V. Singh, L. Janssen, H. S. J. van der Zant and G. A. Steele, *2D Mater.*, 2014, **1**, 011002.
10 M. Lee, C. Kim, S.-Y. Kwon, K. Lee, G. Kwak, H. Lim and J. H. Seol, *Adv. Mater.*, 2025, **37**, 2418669.
11 Y. Wang, Y. Zheng, X. Xu, E. Dubuisson, Q. Bao, J. Lu and K. P. Loh, *ACS Nano*, 2011, **5**, 9927–9933.
12 F. Xiong, H. Wang, X. Liu, J. Sun, M. Brongersma, E. Pop and Y. Cui, *Nano Lett.*, 2015, **15**, 6777–6784.
13 L. Lin, B. Deng, J. Sun, H. Peng and Z. Liu, *Chem. Rev.*, 2018, **118**, 9281–9343.
14 J. Chen, J. Huang, T. Zheng, M. Yang, S. Chen, J. Ma, L. Jian, Y. Pan, Z. Zheng, N. Huo, W. Gao and J. Li, *ACS Appl. Mater. Interfaces*, 2024, **16**, 38231–38242.
15 Y. Y. Illarionov, T. Knobloch, M. Jech, M. Lanza, D. Akinwande, M. I. Vexler, T. Mueller, M. C. Lemme, G. Fiori, F. Schwierz and T. Grasser, *Nat. Commun.*, 2020, **11**, 3385.
16 D. Qi, P. Li, H. Ou, D. Wu, W. Lian, Z. Wang, F. Ouyang, Y. Chai and W. Zhang, *Adv. Funct. Mater.*, 2023, **33**, 2301704.
17 M. Ao, X. Zhou, X. Kong, S. Gou, S. Chen, X. Dong, Y. Zhu, Q. Sun, Z. Zhang, J. Zhang, Q. Zhang, Y. Hu, C. Sheng, K. Wang, S. Wang, J. Wan, J. Han, W. Bao and P. Zhou, *Nature*, 2025, **640**, 654–661.
18 S. Ghosh, Y. Zheng, M. Rafiq, H. Ravichandran, Y. Sun, C. Chen, M. Goswami, N. U. Sakib, M. U. K. Sadaf, A. Pannone, S. Ray, J. M. Redwing, Y. Yang, S. Sahay and S. Das, *Nature*, 2025, **642**, 327–335.
19 C. Liu, Y. Jiang, B. Shen, S. Yuan, Z. Cao, Z. Bi, C. Wang, Y. Xiang, T. Wang, H. Wu, Z. Liu, Y. Wang, S. Wang and P. Zhou, *Nature*, 2023, **6**, 981–990.
20 W. Wang, N. Clark, M. Hamer, A. Carl, E. Tovari, S. Sullivan-Allsop, E. Tillotson, Y. Gao, H. de Latour, F. Selles, J. Howarth, E. G. Castanon, M. Zhou, H. Bai, X. Li, A. Weston, K. Watanabe, T. Taniguchi, C. Mattevi, T. H. Bointon, P. V. Wiper, A. J. Strudwick, L. A. Ponomarenko, A. V. Kretinin, S. J. Haigh, A. Summerfield and R. Gorbachev, *Nat. Electron.*, 2023, **6**, 981–990.
21 M. Nakatani, S. Fukamachi, P. Solís-Fernández, S. Honda, K. Kawahara, Y. Tsuji, Y. Sumiya, M. Kuroki, K. Li, Q. Liu, Y.-C. Lin, A. Uchida, S. Oyama, H. G. Ji, K. Okada, K. Suenaga, Y. Kawano, K. Yoshizawa, A. Yasui and H. Ago, *Nat. Electron.*, 2024, **7**, 119–130.
22 D. Zeng, Z. Zhang, Z. Xue, M. Zhang, P. K. Chu, Y. Mei, Z. Tian and Z. Di, *Nature*, 2024, **632**, 788–794.
23 A. K. Geim and I. V. Grigorieva, *Nature*, 2013, **499**, 419–425.
24 Y. Yu, K. Zhang, H. Parks, M. Babar, S. Carr, I. M. Craig, M. Van Winkle, A. Lyssenko, T. Taniguchi, K. Watanabe, V. Viswanathan and D. K. Bediako, *Nat. Chem.*, 2022, **14**, 267–273.
25 G. Hu, Q. Ou, G. Si, Y. Wu, J. Wu, Z. Dai, A. Krasnok, Y. Mazor, Q. Zhang, Q. Bao, C.-W. Qiu and A. Alù, *Nature*, 2020, **582**, 209–213.
26 J. Duan, G. Álvarez-Pérez, C. Lanza, K. Voronin, A. I. F. Tresguerres-Mata, N. Capote-Robayna, J. Álvarez-Cuervo, A. Tarazaga Martín-Luengo, J. Martín-Sánchez, V. S. Volkov, A. Y. Nikitin and P. Alonso-González, *Nat. Mater.*, 2023, **22**, 867–872.
27 Z. Liu, J. G. Vilhena, A. Hinaut, S. Scherb, F. Luo, J. Zhang, T. Glatzel, E. Gnecco and E. Meyer, *Nano Lett.*, 2023, **23**, 4693–4697.
28 M. Park, Y. J. Park, X. Chen, Y.-K. Park, M.-S. Kim and J.-H. Ahn, *Adv. Mater.*, 2016, **28**, 2556–2562.
29 W. Ren, Y. Ouyang, P. Jiang, C. Yu, J. He and J. Chen, *Nano Lett.*, 2021, **21**, 2634–2641.
30 K. Meng, M. An, D. Chen, C. Chi, S. Li, J. Song and G. Zhang, *Surf. Interfaces*, 2024, **51**, 104525.
31 W. Ouyang, H. Qin, M. Urbakh and O. Hod, *Nano Lett.*, 2020, **20**, 7513–7518.
32 M. H. Pervez, E. Elahi, M. A. Khan, M. Nasim, M. Asim, A. Rehmat, M. A. Rehman, M. A. Assiri, S. Rehman, J. Eom and M. F. Khan, *Small Struct.*, 2025, **6**, 2400386.
33 J. Zhu, Z.-C. Wang, H. Dai, Q. Wang, R. Yang, H. Yu, M. Liao, J. Zhang, W. Chen, Z. Wei, N. Li, L. Du, D. Shi, W. Wang, L. Zhang, Y. Jiang and G. Zhang, *Nat. Commun.*, 2019, **10**, 1348.
34 C. W. Park, J.-H. Lee, J. K. Seo, W. Y. Jo, D. Whang, S. M. Hwang and Y.-J. Kim, *Nat. Commun.*, 2021, **12**, 2145.
35 X. Cai, Y. Luo, B. Liu and H.-M. Cheng, *Chem. Soc. Rev.*, 2018, **47**, 6224–6266.
36 M. Zhao, C. Casiraghi and K. Parvez, *Chem. Soc. Rev.*, 2024, **53**, 3036–3064.
37 T. Zhao, J. Guo, T. Li, Z. Wang, M. Peng, F. Zhong, Y. Chen, Y. Yu, T. Xu, R. Xie, P. Gao, X. Wang and W. Hu, *Chem. Soc. Rev.*, 2023, **52**, 1650–1671.
38 R. Mas-Ballesté, C. Gómez-Navarro, J. Gómez-Herrero and F. Zamora, *Nanoscale*, 2011, **3**, 20–30.
39 Y. Huang, Y.-H. Pan, R. Yang, L.-H. Bao, L. Meng, H.-L. Luo, Y.-Q. Cai, G.-D. Liu, W.-J. Zhao, Z. Zhou, L.-M. Wu, Z.-L. Zhu, M. Huang, L.-W. Liu, L. Liu, P. Cheng, K.-H. Wu, S.-B. Tian, C.-Z. Gu, Y.-G. Shi, Y.-F. Guo, Z. G. Cheng, J.-P. Hu, L. Zhao, G.-H. Yang, E. Sutter, P. Sutter, Y.-L. Wang, W. Ji, X.-J. Zhou and H.-J. Gao, *Nat. Commun.*, 2020, **11**, 2453.
40 B. Radisavljevic, A. Radenovic, J. Brivio, V. Giacometti and A. Kis, *Nat. Nanotechnol.*, 2011, **6**, 147–150.

Open Access Article. Published on 06 January 2026. Downloaded on 1/16/2026 12:17:14 PM. This article is licensed under a Creative Commons Attribution-NonCommercial 3.0 Unported Licence.

41 K. Kang, K.-H. Lee, Y. Han, H. Gao, S. Xie, D. A. Muller and J. Park, *Nature*, 2017, **550**, 229–233.
42 J.-Y. Moon, M. Kim, S.-I. Kim, S. Xu, J.-H. Choi, D. Whang, K. Watanabe, T. Taniguchi, D. S. Park, J. Seo, S. H. Cho, S.-K. Son and J.-H. Lee, *Sci. Adv.*, 2020, **6**, eabc6601.
43 H. Zhang, *ACS Nano*, 2015, **9**, 9451–9469.
44 Y. Huang, E. Sutter, N. N. Shi, J. Zheng, T. Yang, D. Englund, H.-J. Gao and P. Sutter, *ACS Nano*, 2015, **9**, 10612–10620.
45 F. Pizzocchero, L. Gammelgaard, B. S. Jessen, J. M. Caridad, L. Wang, J. Hone, P. Bøggild and T. J. Booth, *Nat. Commun.*, 2016, **7**, 11894.
46 A. Ambrosi and M. Pumera, *Chem. Soc. Rev.*, 2018, **47**, 7213–7224.
47 Y. Yang, H. Hou, G. Zou, W. Shi, H. Shuai, J. Li and X. Ji, *Nanoscale*, 2019, **11**, 16–33.
48 S. Yang, P. Zhang, A. S. Nia and X. Feng, *Adv. Mater.*, 2020, **32**, 1907857.
49 K. Verguts, K. Schouteden, C.-H. Wu, L. Peters, N. Vrancken, X. Wu, Z. Li, M. Erkens, C. Porret, C. Huyghebaert, C. Van Haesendonck, S. De Gendt and S. Brems, *ACS Appl. Mater. Interfaces*, 2017, **9**, 37484–37492.
50 H. Zhang, Q. Xiang, Z. Liu, X. Zhang, Y. Zhao and H. Tan, *Nat. Commun.*, 2024, **15**, 9329.
51 R. Morales Ibarra, M. Goto, J. García-Serna and S. M. García Montes, *Carbon Lett.*, 2021, **31**, 99–105.
52 Z. Sun, Q. Fan, M. Zhang, S. Liu, H. Tao and J. Texter, *Adv. Sci.*, 2019, **6**, 1901084.
53 X. Lu, M. Cai, X. Wu, Y. Zhang, S. Li, S. Liao and X. Lu, *Small*, 2023, **19**, 2206702.
54 Z. Lin, Y. Zhao, C. Zhou, R. Zhong, X. Wang, Y. H. Tsang and Y. Chai, *Sci. Rep.*, 2015, **5**, 18596.
55 J. Shim, S.-H. Bae, W. Kong, D. Lee, K. Qiao, D. Nezich, Y. J. Park, R. Zhao, S. Sundaram, X. Li, H. Yeon, C. Choi, H. Kum, R. Yue, G. Zhou, Y. Ou, K. Lee, J. Moodera, X. Zhao, J.-H. Ahn, C. Hinkle, A. Ougazzaden and J. Kim, *Science*, 2018, **362**, 665–670.
56 K. Wu, H. Wang, M. Yang, L. Liu, Z. Sun, G. Hu, Y. Song, X. Han, J. Guo, K. Wu, B. Feng, C. Shen, Y. Huang, Y. Shi, Z. Cheng, H. Yang, L. Bao, S. T. Pantelides and H.-J. Gao, *Adv. Mater.*, 2024, **36**, 2313511.
57 J.-Y. Moon, D.-H. Kim, S.-I. Kim, H.-S. Hwang, J.-H. Choi, S.-K. Hyeong, S. Ghods, H. G. Park, E.-T. Kim, S. Bae, S.-K. Lee, S.-K. Son and J.-H. Lee, *Matter*, 2022, **5**, 3935–3946.
58 H. Häkkinen, *Nat. Chem.*, 2012, **4**, 443–455.
59 M. Giza, M. Świniarski, A. P. Gertych, K. Czerniak-Łosiewicz, M. Rogala, P. J. Kowalczyk and M. Zdrojek, *ACS Appl. Mater. Interfaces*, 2024, **16**, 48556–48564.
60 G. Z. Magda, J. Pető, G. Dobrik, C. Hwang, L. P. Biró and L. Tapasztó, *Sci. Rep.*, 2015, **5**, 14714.
61 M. Velický, G. E. Donnelly, W. R. Hendren, S. McFarland, D. Scullion, W. J. I. DeBenedetti, G. C. Correa, Y. Han, A. J. Wain, M. A. Hines, D. A. Muller, K. S. Novoselov, H. D. Abruña, R. M. Bowman, E. J. G. Santos and F. Huang, *ACS Nano*, 2018, **12**, 10463–10472.
62 S. B. Desai, S. R. Madhvapathy, M. Amani, D. Kiriya, M. Hettick, M. Tosun, Y. Zhou, M. Dubey, J. W. Ager Iii, D. Chrzan and A. Javey, *Adv. Mater.*, 2016, **28**, 4053–4058.
63 T. H. Choudhury, X. Zhang, Z. Y. Al Balushi, M. Chubarov and J. M. Redwing, *Annu. Rev. Mater. Res.*, 2020, **50**, 155–177.
64 J. Dong, L. Zhang, X. Dai and F. Ding, *Nat. Commun.*, 2020, **11**, 5862.
65 Z. Zhang, X. Yang, K. Liu and R. Wang, *Adv. Sci.*, 2022, **9**, 2105201.
66 G. Xue, B. Qin, C. Ma, P. Yin, C. Liu and K. Liu, *Chem. Rev.*, 2024, **124**, 9785–9865.
67 C. Liu, T. Liu, Z. Zhang, Z. Sun, G. Zhang, E. Wang and K. Liu, *Nat. Nanotechnol.*, 2024, **19**, 907–918.
68 Y.-C. Lin, R. Torsi, R. Younas, C. L. Hinkle, A. F. Rigosi, H. M. Hill, K. Zhang, S. Huang, C. E. Shuck, C. Chen, Y.-H. Lin, D. Maldonado-Lopez, J. L. Mendoza-Cortes, J. Ferrier, S. Kar, N. Nayir, S. Rajabpour, A. C. T. van Duin, X. Liu, D. Jariwala, J. Jiang, J. Shi, W. Mortelmans, R. Jaramillo, J. M. J. Lopes, R. Engel-Herbert, A. Trofe, T. Ignatova, S. H. Lee, Z. Mao, L. Damian, Y. Wang, M. A. Steves, K. L. Knappenberger, Jr., Z. Wang, S. Law, G. Bepete, D. Zhou, J.-X. Lin, M. S. Scheurer, J. Li, P. Wang, G. Yu, S. Wu, D. Akinwande, J. M. Redwing, M. Terrones and J. A. Robinson, *ACS Nano*, 2023, **17**, 9694–9747.
69 X. Ling, Y.-H. Lee, Y. Lin, W. Fang, L. Yu, M. S. Dresselhaus and J. Kong, *Nano Lett.*, 2014, **14**, 464–472.
70 D. Moon, W. Lee, C. Lim, J. Kim, J. Kim, Y. Jung, H.-Y. Choi, W. S. Choi, H. Kim, J.-H. Baek, C. Kim, J. Joo, H.-G. Oh, H. Jang, K. Watanabe, T. Taniguchi, S. Bae, J. Son, H. Ryu, J. Kwon, H. Cheong, J. W. Han, H. Jang and G.-H. Lee, *Nature*, 2025, **638**, 957–964.
71 K. S. Kim, D. Lee, C. S. Chang, S. Seo, Y. Hu, S. Cha, H. Kim, J. Shin, J.-H. Lee, S. Lee, J. S. Kim, K. H. Kim, J. M. Suh, Y. Meng, B.-I. Park, J.-H. Lee, H.-S. Park, H. S. Kum, M.-H. Jo, G. Y. Yeom, K. Cho, J.-H. Park, S.-H. Bae and J. Kim, *Nature*, 2023, **614**, 88–94.
72 A. T. Hoang, L. Hu, B. J. Kim, T. T. N. Van, K. D. Park, Y. Jeong, K. Lee, S. Ji, J. Hong, A. K. Katiyar, B. Shong, K. Kim, S. Im, W. J. Chung and J.-H. Ahn, *Nat. Nanotechnol.*, 2024, **636**, 615–621.
73 J. Wang, X. Xu, T. Cheng, L. Gu, R. Qiao, Z. Liang, D. Ding, H. Hong, P. Zheng, Z. Zhang, Z. Zhang, S. Zhang, G. Cui, C. Chang, C. Huang, J. Qi, J. Liang, C. Liu, Y. Zuo, G. Xue, X. Fang, J. Tian, M. Wu, Y. Guo, Z. Yao, Q. Jiao, L. Liu, P. Gao, Q. Li, R. Yang, G. Zhang, Z. Tang, D. Yu, E. Wang, J. Lu, Y. Zhao, S. Wu, F. Ding and K. Liu, *Nat. Nanotechnol.*, 2022, **17**, 33–38.
74 J. Liang, X. Zhu, M. Chen, X. Duan, D. Li and A. Pan, *Acc. Mater. Res.*, 2022, **3**, 999–1010.
75 K. S. Kim, S. Seo, J. Kwon, D. Lee, C. Kim, J.-E. Ryu, J. Kim, J. M. Suh, H.-G. Jung, Y. Jo, J.-C. Shin, M.-K. Song, J. Feng, H. Ahn, S. Lee, K. Cho, J. Jeon, M. Seol, J.-H. Park, S. W. Kim and J. Kim, *Nature*, 2024, **636**, 615–621.

 This journal is © The Royal Society of Chemistry 2025

Open Access Article. Published on 06 January 2026. Downloaded on 1/16/2026 12:17:14 PM. This article is licensed under a Creative Commons Attribution-NonCommercial 3.0 Unported Licence.

76 Y. Li, S. Hao, J. G. DiStefano, A. A. Murthy, E. D. Hanson, Y. Xu, C. Wolverton, X. Chen and V. P. Dravid, *ACS Nano*, 2018, **12**, 8970–8976.
77 Y. Guo, P.-C. Shen, C. Su, A.-Y. Lu, M. Hempel, Y. Han, Q. Ji, Y. Lin, E. Shi, E. McVay, L. Dou, D. A. Muller, T. Palacios, J. Li, X. Ling and J. Kong, *Proc. Natl. Acad. Sci. U. S. A.*, 2019, **116**, 3437–3442.
78 G. H. Han, N. J. Kybert, C. H. Naylor, B. S. Lee, J. Ping, J. H. Park, J. Kang, S. Y. Lee, Y. H. Lee, R. Agarwal and A. T. C. Johnson, *Nat. Commun.*, 2015, **6**, 6128.
79 B. Qin, M. Z. Saeed, Q. Li, M. Zhu, Y. Feng, Z. Zhou, J. Fang, M. Hossain, Z. Zhang, Y. Zhou, Y. Huangfu, R. Song, J. Tang, B. Li, J. Liu, D. Wang, K. He, H. Zhang, R. Wu, B. Zhao, J. Li, L. Liao, Z. Wei, B. Li, X. Duan and X. Duan, *Nat. Commun.*, 2023, **14**, 304.
80 L. Huang, Z. Hu, H. Jin, J. Wu, K. Liu, Z. Xu, J. Wan, H. Zhou, J. Duan, B. Hu and J. Zhou, *Adv. Funct. Mater.*, 2020, **30**, 1908486.
81 J. Zhou, J. Lin, X. Huang, Y. Zhou, Y. Chen, J. Xia, H. Wang, Y. Xie, H. Yu, J. Lei, D. Wu, F. Liu, Q. Fu, Q. Zeng, C.-H. Hsu, C. Yang, L. Lu, T. Yu, Z. Shen, H. Lin, B. I. Yakobson, Q. Liu, K. Suenaga, G. Liu and Z. Liu, *Nature*, 2018, **556**, 355–359.
82 S. Zeng, C. Liu and P. Zhou, *Nat. Rev. Electr. Eng.*, 2024, **1**, 335–348.
83 K.-K. Liu, W. Zhang, Y.-H. Lee, Y.-C. Lin, M.-T. Chang, C.-Y. Su, C.-S. Chang, H. Li, Y. Shi, H. Zhang, C.-S. Lai and L.-J. Li, *Nano Lett.*, 2012, **12**, 1538–1544.
84 K. Zhang, Y. She, X. Cai, M. Zhao, Z. Liu, C. Ding, L. Zhang, W. Zhou, J. Ma, H. Liu, L.-J. Li, Z. Luo and S. Huang, *Nat. Nanotechnol.*, 2023, **18**, 448–455.
85 M. Kang, H. B. Jeong, Y. Shim, H.-J. Chai, Y.-S. Kim, M. Choi, A. Ham, C. Park, M.-K. Jo, T. S. Kim, H. Park, J. Lee, G. Noh, J. Y. Kwak, T. Eom, C.-W. Lee, S.-Y. Choi, J. M. Yuk, S. Song, H. Y. Jeong and K. Kang, *ACS Nano*, 2024, **18**, 819–828.
86 J. Zhu, J.-H. Park, S. A. Vitale, W. Ge, G. S. Jung, J. Wang, M. Mohamed, T. Zhang, M. Ashok, M. Xue, X. Zheng, Z. Wang, J. Hansryd, A. P. Chandrakasan, J. Kong and T. Palacios, *Nat. Nanotechnol.*, 2023, **18**, 456–463.
87 M. Leskelä and M. Ritala, *Thin Solid Films*, 2002, **409**, 138–146.
88 Z. Lu, Y. Chen, W. Dang, L. Kong, Q. Tao, L. Ma, D. Lu, L. Liu, W. Li, Z. Li, X. Liu, Y. Wang, X. Duan, L. Liao and Y. Liu, *Nat. Commun.*, 2023, **14**, 2340.
89 L. Zhang, Z. Liu, W. Ai, J. Chen, Z. Lv, B. Wang, M. Yang, F. Luo and J. Wu, *Nat. Electron.*, 2024, **7**, 662–670.
90 **https://irds.ieee.org/editions/2024**.
91 Y. H. Kim, D. Lee, W. Huh, J. Lee, D. Lee, G. Wang, J. Park, D. Ha and C.-H. Lee, *Nat. Electron.*, 2025, **8**, 770–783.
92 J. Dong, Y. Liu and F. Ding, *npj Comput. Mater.*, 2022, **8**, 109.
93 H. Kum, D. Lee, W. Kong, H. Kim, Y. Park, Y. Kim, Y. Baek, S.-H. Bae, K. Lee and J. Kim, *Nat. Electron.*, 2019, **2**, 439–450.
94 A. Koma, K. Sunouchi and T. Miyajima, *Microelectronic Eng.*, 1984, **2**, 129–136.
95 J. M. Wofford, S. Nakhaie, T. Krause, X. Liu, M. Ramsteiner, M. Hanke, H. Riechert and J. M. J. Lopes, *Sci. Rep.*, 2017, **7**, 43644.
96 Y. Zhang, L. Zhang and C. Zhou, *Acc. Chem. Res.*, 2013, **46**, 2329–2339.
97 X. Li, W. Cai, J. An, S. Kim, J. Nah, D. Yang, R. Piner, A. Velamakanni, I. Jung, E. Tutuc, S. K. Banerjee, L. Colombo and R. S. Ruoff, *Science*, 2009, **324**, 1312–1314.
98 C. Berger, Z. Song, X. Li, X. Wu, N. Brown, C. Naud, D. Mayou, T. Li, J. Hass, A. N. Marchenkov, E. H. Conrad, P. N. First and W. A. de Heer, *Science*, 2006, **312**, 1191–1196.
99 Q. Yu, J. Lian, S. Siriponglert, H. Li, Y. P. Chen and S.-S. Pei, *Appl. Phys. Lett.*, 2008, **93**, 113103.
100 Z. Zhang, Y. Liu, Y. Yang and B. I. Yakobson, *Nano Lett.*, 2016, **16**, 1398–1403.
101 Y. Shi, W. Zhou, A.-Y. Lu, W. Fang, Y.-H. Lee, A. L. Hsu, S. M. Kim, K. K. Kim, H. Y. Yang, L.-J. Li, J.-C. Idrobo and J. Kong, *Nano Lett.*, 2012, **12**, 2784–2791.
102 Y. Gao, Y.-L. Hong, L.-C. Yin, Z. Wu, Z. Yang, M.-L. Chen, Z. Liu, T. Ma, D.-M. Sun, Z. Ni, X.-L. Ma, H.-M. Cheng and W. Ren, *Adv. Mater.*, 2017, **29**, 1700990.
103 A. Aljarb, Z. Cao, H.-L. Tang, J.-K. Huang, M. Li, W. Hu, L. Cavallo and L.-J. Li, *ACS Nano*, 2017, **11**, 9215–9222.
104 D. Dumcenco, D. Ovchinnikov, K. Marinov, P. Lazić, M. Gibertini, N. Marzari, O. L. Sanchez, Y.-C. Kung, D. Krasnozhon, M.-W. Chen, S. Bertolazzi, P. Gillet, A. Fontcuberta i Morral, A. Radenovic and A. Kis, *ACS Nano*, 2015, **9**, 4611–4620.
105 X. Feng, S. Li, S. L. Wong, S. Tong, L. Chen, P. Zhang, L. Wang, X. Fong, D. Chi and K.-W. Ang, *ACS Nano*, 2021, **15**, 1764–1774.
106 L. Wang, X. Xu, L. Zhang, R. Qiao, M. Wu, Z. Wang, S. Zhang, J. Liang, Z. Zhang, Z. Zhang, W. Chen, X. Xie, J. Zong, Y. Shan, Y. Guo, M. Willinger, H. Wu, Q. Li, W. Wang, P. Gao, S. Wu, Y. Zhang, Y. Jiang, D. Yu, E. Wang, X. Bai, Z.-J. Wang, F. Ding and K. Liu, *Nature*, 2019, **570**, 91–95.
107 P. Yang, S. Zhang, S. Pan, B. Tang, Y. Liang, X. Zhao, Z. Zhang, J. Shi, Y. Huan, Y. Shi, S. J. Pennycook, Z. Ren, G. Zhang, Q. Chen, X. Zou, Z. Liu and Y. Zhang, *ACS Nano*, 2020, **14**, 5036–5045.
108 T. Li, W. Guo, L. Ma, W. Li, Z. Yu, Z. Han, S. Gao, L. Liu, D. Fan, Z. Wang, Y. Yang, W. Lin, Z. Luo, X. Chen, N. Dai, X. Tu, D. Pan, Y. Yao, P. Wang, Y. Nie, J. Wang, Y. Shi and X. Wang, *Nat. Nanotechnol.*, 2021, **16**, 1201–1207.
109 Y. Cao, V. Fatemi, S. Fang, K. Watanabe, T. Taniguchi, E. Kaxiras and P. Jarillo-Herrero, *Nature*, 2018, **556**, 43–50.
110 C. R. Dean, L. Wang, P. Maher, C. Forsythe, F. Ghahari, Y. Gao, J. Katoch, M. Ishigami, P. Moon, M. Koshino, T. Taniguchi, K. Watanabe, K. L. Shepard, J. Hone and P. Kim, *Nature*, 2013, **497**, 598–602.
111 M. Angeli and A. H. MacDonald, *Proc. Natl. Acad. Sci. U. S. A.*, 2021, **118**, e2021826118.
112 Q. Wang, J. Tang, X. Li, J. Tian, J. Liang, N. Li, D. Ji, L. Xian, Y. Guo, L. Li, Q. Zhang, Y. Chu, Z. Wei, Y. Zhao, L. Du,

Open Access Article. Published on 06 January 2026. Downloaded on 1/16/2026 12:17:14 PM.
This article is licensed under a Creative Commons Attribution-NonCommercial 3.0 Unported Licence.

H. Yu, X. Bai, L. Gu, K. Liu, W. Yang, R. Yang, D. Shi and G. Zhang, *Nat. Sci. Rev.*, 2022, **9**, nwac077.
113 X. Zhang, H. Nan, S. Xiao, X. Wan, X. Gu, A. Du, Z. Ni and K. Ostrikov, *Nat. Commun.*, 2019, **10**, 598.
114 B. Kalanyan, W. A. Kimes, R. Beams, S. J. Stranick, E. Garratt, I. Kalish, A. V. Davydov, R. K. Kanjolia and J. E. Maslar, *Chem. Mater.*, 2017, **29**, 6279–6288.
115 A. T. Hoang, A. K. Katiyar, H. Shin, N. Mishra, S. Forti, C. Coletti and J.-H. Ahn, *ACS Appl. Mater. Interfaces*, 2020, **12**, 44335–44344.
116 M. A. Islam, J. H. Kim, A. Schropp, H. Kalita, N. Choudhary, D. Weitzman, S. I. Khondaker, K. H. Oh, T. Roy, H.-S. Chung and Y. Jung, *Nano Lett.*, 2017, **17**, 6157–6165.
117 H. Heo, J. H. Sung, G. Jin, J.-H. Ahn, K. Kim, M.-J. Lee, S. Cha, H. Choi and M.-H. Jo, *Adv. Mater.*, 2015, **27**, 3803–3810.
118 M.-Y. Li, Y. Shi, C.-C. Cheng, L.-S. Lu, Y.-C. Lin, H.-L. Tang, M.-L. Tsai, C.-W. Chu, K.-H. Wei, J.-H. He, W.-H. Chang, K. Suenaga and L.-J. Li, *Science*, 2015, **349**, 524–528.
119 N. Choudhary, J. Park, J. Y. Hwang, H.-S. Chung, K. H. Dumas, S. I. Khondaker, W. Choi and Y. Jung, *Sci. Rep.*, 2016, **6**, 25456.
120 Y. Gong, J. Lin, X. Wang, G. Shi, S. Lei, Z. Lin, X. Zou, G. Ye, R. Vajtai, B. I. Yakobson, H. Terrones, M. Terrones, B. K. Tay, J. Lou, S. T. Pantelides, Z. Liu, W. Zhou and P. M. Ajayan, *Nat. Mater.*, 2014, **13**, 1135–1142.
121 F. Li, Y. Feng, Z. Li, C. Ma, J. Qu, X. Wu, D. Li, X. Zhang, T. Yang, Y. He, H. Li, X. Hu, P. Fan, Y. Chen, B. Zheng, X. Zhu, X. Wang, X. Duan and A. Pan, *Adv. Mater.*, 2019, **31**, 1901351.
122 J. Shen, X. Xu, W. Li, T. Jiang, X. Sun, H. Chen, C. Ji, L. Yu, J. Dong, T. Wei, H. Zhu and W. Kong, *Adv. Mater.*, 2025, 2504223.
123 X. Zheng, L. Han, S. Fatima, S. Khan, Y. Sun, Z. Li, Y. Ning, K. Leifer, G. Zhu, H. Li and A. Song, *Nano Lett.*, 2025, **25**, 9967–9975.
124 X. Ma, Q. Liu, D. Xu, Y. Zhu, S. Kim, Y. Cui, L. Zhong and M. Liu, *Nano Lett.*, 2017, **17**, 6961–6967.
125 Y. Zhang, Q. Liu and B. Xu, *Ext. Mech. Lett.*, 2017, **16**, 33–40.
126 K. Kinoshita, R. Moriya, M. Onodera, Y. Wakafuji, S. Masubuchi, K. Watanabe, T. Taniguchi and T. Machida, *npj 2D Mater. Appl.*, 2019, **3**, 22.
127 D. G. Purdie, N. M. Pugno, T. Taniguchi, K. Watanabe, A. C. Ferrari and A. Lombardo, *Nat. Commun.*, 2018, **9**, 5387.
128 R. K. Mech, J. Spièce, K. Watanabe, T. Taniguchi, B. P. Kesavan, Z. Sofer and P. Gehring, *Phys. Rev. B*, 2025, **111**, 195406.
129 P. J. Zomer, S. P. Dash, N. Tombros and B. J. van Wees, *Appl. Phys. Lett*, 2011, **99**, 232104.
130 T. Uwanno, Y. Hattori, T. Taniguchi, K. Watanabe and K. Nagashio, *2D Mater.*, 2015, **2**, 041002.
131 A. Reina, H. Son, L. Jiao, B. Fan, M. S. Dresselhaus, Z. Liu and J. Kong, *J. Phys. Chem. C*, 2008, **112**, 17741–17744.
132 H. Li, J. Wu, X. Huang, Z. Yin, J. Liu and H. Zhang, *ACS Nano*, 2014, **8**, 6563–6570.
133 L. Liu, Z. Cai, S. Xue, H. Huang, S. Chen, S. Gou, Z. Zhang, Y. Guo, Y. Yao, W. Bao and P. Zhou, *Nat. Electron.*, 2025, **8**, 135–146.
134 R. S. Weatherup, B. Dlubak and S. Hofmann, *ACS Nano*, 2012, **6**, 9996–10003.
135 N. Petrone, C. R. Dean, I. Meric, A. M. van der Zande, P. Y. Huang, L. Wang, D. Muller, K. L. Shepard and J. Hone, *Nano Lett.*, 2012, **12**, 2751–2756.
136 Y. Han, K. C. Lai, A. Lii-Rosales, M. C. Tringides, J. W. Evans and P. A. Thiel, *Surf. Sci.*, 2019, **685**, 48–58.
137 W. S. Leong, H. Wang, J. Yeo, F. J. Martin-Martinez, A. Zubair, P.-C. Shen, Y. Mao, T. Palacios, M. J. Buehler, J.-Y. Hong and J. Kong, *Nat. Commun.*, 2019, **10**, 867.
138 Z.-Q. Xu, Y. Zhang, S. Lin, C. Zheng, Y. L. Zhong, X. Xia, Z. Li, P. J. Sophia, M. S. Fuhrer, Y.-B. Cheng and Q. Bao, *ACS Nano*, 2015, **9**, 6178–6187.
139 T. Nasir, B. J. Kim, K.-W. Kim, S. H. Lee, H. K. Lim, D. K. Lee, B. J. Jeong, H. C. Kim, H. K. Yu and J.-Y. Choi, *Nanoscale*, 2018, **10**, 21865–21870.
140 S. J. Chae, F. Güneş, K. K. Kim, E. S. Kim, G. H. Han, S. M. Kim, H.-J. Shin, S.-M. Yoon, J.-Y. Choi, M. H. Park, C. W. Yang, D. Pribat and Y. H. Lee, *Adv. Mater.*, 2009, **21**, 2328–2333.
141 G. F. Schneider, V. E. Calado, H. Zandbergen, L. M. K. Vandersypen and C. Dekker, *Nano Lett.*, 2010, **10**, 1912–1916.
142 T. Zhang, K. Fujisawa, T. Granzier-Nakajima, F. Zhang, Z. Lin, E. Kahn, N. Perea-López, A. L. Elías, Y.-T. Yeh and M. Terrones, *ACS Appl. Nano Mater.*, 2019, **2**, 5320–5328.
143 H. Van Ngoc, Y. Qian, S. K. Han and D. J. Kang, *Sci. Rep.*, 2016, **6**, 33096.
144 R. Zhou, V. Ostwal and J. Appenzeller, *Nano Lett.*, 2017, **17**, 4787–4792.
145 X. Li, Y. Zhu, W. Cai, M. Borysiak, B. Han, D. Chen, R. D. Piner, L. Colombo and R. S. Ruoff, *Nano Lett.*, 2009, **9**, 4359–4363.
146 Z. Zhang, J. Du, D. Zhang, H. Sun, L. Yin, L. Ma, J. Chen, D. Ma, H.-M. Cheng and W. Ren, *Nat. Commun.*, 2017, **8**, 14560.
147 L. A. Belyaeva, W. Fu, H. Arjmandi-Tash and G. F. Schneider, *ACS Cent. Sci.*, 2018, **4**, 661.
148 D. Zhang, J. Du, Y.-L. Hong, W. Zhang, X. Wang, H. Jin, P. L. Burn, J. Yu, M. Chen, D.-M. Sun, M. Li, L. Liu, L.-P. Ma, H.-M. Cheng and W. Ren, *ACS Nano*, 2019, **13**, 5513–5522.
149 L. Gao, W. Ren, H. Xu, L. Jin, Z. Wang, T. Ma, L.-P. Ma, Z. Zhang, Q. Fu, L.-M. Peng, X. Bao and H.-M. Cheng, *Nat. Commun.*, 2012, **3**, 699.
150 D. Ma, J. Shi, Q. Ji, K. Chen, J. Yin, Y. Lin, Y. Zhang, M. Liu, Q. Feng, X. Song, X. Guo, J. Zhang, Y. Zhang and Z. Liu, *Nano Res.*, 2015, **8**, 3662–3672.
151 B. Jiang, D. Liang, Z. Sun, H. Ci, B. Liu, Y. Gao, J. Shan, X. Yang, M. H. Rümmeli, J. Wang, T. Wei, J. Sun and Z. Liu, *Adv. Funct. Mater.*, 2022, **32**, 2200428.

 This journal is © The Royal Society of Chemistry 2025

Open Access Article. Published on 06 January 2026. Downloaded on 1/16/2026 12:17:14 PM. This article is licensed under a Creative Commons Attribution-NonCommercial 3.0 Unported Licence.

152 C. J. Brennan, J. Nguyen, E. T. Yu and N. Lu, *Adv. Mater. Interfaces*, 2015, **2**, 1500176.
153 A. Borók, K. Laboda and A. Bonyár, *Biosensors*, 2021, **11**, 292.
154 A. Jain, P. Bharadwaj, S. Heeg, M. Parzefall, T. Taniguchi, K. Watanabe and L. Novotny, *Nanotechnology*, 2018, **29**, 265203.
155 A. Dalla Monta, F. Razan, J.-B. Le Cam and G. Chagnon, *Sens. Actuators A: Phys.*, 2018, **280**, 107–113.
156 L. Tao, H. Li, Y. Gao, Z. Chen, L. Wang, Y. Deng, J. Zhang and J.-B. Xu, *Adv. Mater. Technol.*, 2018, **3**, 1700282.
157 P. J. Zomer, M. H. D. Guimarães, J. C. Brant, N. Tombros and B. J. van Wees, *Appl. Phys. Lett.*, 2014, **105**, 013101.
158 J. I. J. Wang, Y. Yang, Y.-A. Chen, K. Watanabe, T. Taniguchi, H. O. H. Churchill and P. Jarillo-Herrero, *Nano Lett.*, 2015, **15**, 1898–1903.
159 A. S. Mayorov, R. V. Gorbachev, S. V. Morozov, L. Britnell, R. Jalil, L. A. Ponomarenko, P. Blake, K. S. Novoselov, K. Watanabe, T. Taniguchi and A. K. Geim, *Nano Lett.*, 2011, **11**, 2396–2399.
160 C. R. Dean, A. F. Young, I. Meric, C. Lee, L. Wang, S. Sorgenfrei, K. Watanabe, T. Taniguchi, P. Kim, K. L. Shepard and J. Hone, *Nat. Nanotechnol.*, 2010, **5**, 722–726.
161 S. J. Haigh, A. Gholinia, R. Jalil, S. Romani, L. Britnell, D. C. Elias, K. S. Novoselov, L. A. Ponomarenko, A. K. Geim and R. Gorbachev, *Nat. Mater.*, 2012, **11**, 764–767.
162 W. Zhou, J. Zuo, X. Zhang and A. Zhou, *J. Compos. Mater.*, 2013, **48**, 2517–2526.
163 D. Golberg, Y. Bando, Y. Huang, T. Terao, M. Mitome, C. Tang and C. Zhi, *ACS Nano*, 2010, **4**, 2979–2993.
164 Z. Zhang, S. Hu, J. Chen and B. Li, *Nanotechnology*, 2017, **28**, 225704.
165 D. Xu, Q. Liu, B. Liang, N. Yu, X. Ma, Y. Xu, T. Taniguchi, C. Ding, R. K. Lake, R. Yan and M. Liu, *Sci. Adv.*, 2025, **11**, eadv7614.
166 R. Frisenda, E. Navarro-Moratalla, P. Gant, D. Pérez De Lara, P. Jarillo-Herrero, R. V. Gorbachev and A. Castellanos-Gomez, *Chem. Soc. Rev.*, 2018, **47**, 53–68.
167 X. Zhang, L. Zhou, S. Wang, T. Li, H. Du, Y. Zhou, J. Liu, J. Zhao, L. Huang, H. Yu, P. Chen, N. Li and G. Zhang, *Nat. Commun.*, 2025, **16**, 4468.
168 J. Liao, Y. Zhao, X. Chen, Z. Hu, S. Bu, Y. Zhu, Q. Lu, M. Shang, H. Wu, F. Li, Z. Shi, Q. Zhao, K. Jia, J. Hu, Z. Han, Q. Xie, X. Zhao, J. Yin, W. Wang, H. Peng, X. Qiu, Y. Zhang, L. Lin and Z. Liu, *Nat. Electron.*, 2025, **8**, 309–321.
169 L. Wang, I. Meric, P. Y. Huang, Q. Gao, Y. Gao, H. Tran, T. Taniguchi, K. Watanabe, L. M. Campos, D. A. Muller, J. Guo, P. Kim, J. Hone, K. L. Shepard and C. R. Dean, *Science*, 2013, **342**, 614–617.
170 C.-H. Liu, G. Clark, T. Fryett, S. Wu, J. Zheng, F. Hatami, X. Xu and A. Majumdar, *Nano Lett.*, 2017, **17**, 200–205.
171 J. Jing, F. Sun, Z. Wang, L. Ma, Y. Luo, Z. Du, T. Zhang, Y. Wang, F. Xu, T. Zhang, C. Chen, X. Ma, Y. He, Y. Zhu, H. Sun, X. Wang, Y. Zhou, J. K. H. Tsoi, J. Wrachtrup, N. Wong, C. Li, D.-K. Ki, Q. Wang, K. H. Li, Y. Lin and Z. Chu, *Nature*, 2024, **636**, 627–634.
172 J. Wang, J. Yang, B. Yu, Z. Wu, M. Jiang, C.-Y. Wu, Y. Wang, F.-X. Liang, X. Ma, L. Li and L.-B. Luo, *Adv. Opt. Mater.*, 2025, **13**, 2402463.
173 H. Yang, N. Liang, J. Wang, R. Chen, R. Tian, X. Xin, T. Zhai and J. Hou, *Nano Energy*, 2023, **112**, 108472.
174 W. Chen, S. Zhu, R. Duan, C. Wang, F. Wang, Y. Wu, M. Dai, J. Cui, S. H. Chae, Z. Li, X. Ma, Q. Wang, Z. Liu and Q. J. Wang, *Adv. Mater.*, 2024, **36**, 2400858.
175 H. Yang, D. Zhao, S. Chuwongin, J.-H. Seo, W. Yang, Y. Shuai, J. Berggren, M. Hammar, Z. Ma and W. Zhou, *Nat. Photonics*, 2012, **6**, 615–620.
176 Y. Zhao, J. Mao, Z. Wu, W. F. Io, S.-Y. Pang, Y. Zhao and J. Hao, *Nat. Commun.*, 2024, **15**, 6795.
177 X. Xu, S. Thomas, T. Guo, L. Luo, Y. Khan, Y. Yuan, Y. A. Elhagrasy, M. Lanza, T. D. Anthopoulos, O. M. Bakr, O. F. Mohammed and H. N. Alshareef, *Adv. Mater.*, 2024, 2405214.
178 J. H. Cho, D. J. Kang, N.-S. Jang, K.-H. Kim, P. Won, S. H. Ko and J.-M. Kim, *ACS Appl. Mater. Interfaces*, 2017, **9**, 40905–40913.
179 X. Ma, K. Kudtarkar, Y. Chen, P. Cunha, Y. Ma, K. Watanabe, T. Taniguchi, X. Qian, M. C. Hipwell, Z. J. Wong and S. Lan, *Nat. Commun.*, 2022, **13**, 6916.
180 S. Wu, S. Buckley, J. R. Schaibley, L. Feng, J. Yan, D. G. Mandrus, F. Hatami, W. Yao, J. Vučković, A. Majumdar and X. Xu, *Nature*, 2015, **520**, 69–72.
181 I. Datta, S. H. Chae, G. R. Bhatt, M. A. Tadayon, B. Li, Y. Yu, C. Park, J. Park, L. Cao, D. N. Basov, J. Hone and M. Lipson, *Nat. Photonics.*, 2020, **14**, 256–262.
182 F. Peyskens, C. Chakraborty, M. Muneeb, D. Van Thourhout and D. Englund, *Nat. Commun.*, 2019, **10**, 4435.
183 Q. Liu, Z. Li, X. Ma, Q. Liu, F. Wei, S. L. Teo, R. Duan, A. M. D. Rachmawisista, Y. Zhang, C. J. J. Lee, J. Deng, A. Huang, P. Luo, H. K. Hui, S. L. K. Yap, M. Zhao, R. Ji, Y. Luo, Z. Liu and Q. Wang, *ACS Nano*, 2025, **19**, 21179–21188.
184 S.-X. Li, G.-Y. Huang, H. Xia, T. Fu, X.-J. Wang, X. Zeng, X. Liu, Y.-H. Yu, Q.-D. Chen, L. Lin and H.-B. Sun, *Nat. Commun.*, 2025, **16**, 3636.
185 M. Liu, X. Yin, E. Ulin-Avila, B. Geng, T. Zentgraf, L. Ju, F. Wang and X. Zhang, *Nature*, 2011, **474**, 64–67.
186 X. Sun, Y. Zhu, H. Qin, B. Liu, Y. Tang, T. Lü, S. Rahman, T. Yildirim and Y. Lu, *Nature*, 2022, **610**, 478–484.
187 U. Celano, D. Schmidt, C. Beitia, G. Orji, A. V. Davydov and Y. Obeng, *Nanoscale Adv.*, 2024, **6**, 2260–2269.
188 Q. Li, M. R. Vogt, H. Wang, C. Monticelli and A. Zanelli, *J. Clean. Prod.*, 2024, **468**, 143068.
189 J. Singh, N. A. Astarini, M.-L. Tsai, M. Venkatesan, C.-C. Kuo, C.-S. Yang and H.-W. Yen, *Adv. Sci.*, 2024, **11**, 2307839.
190 X. Feng, Y. Ma, T. Huang, S. Liu, L. Liu, E. Guo, K. Liu, Y. Li, X. Zhou, H. Li and T. Zhai, *InfoScience*, 2024, **1**, e12015.
191 C. Martin, Q. Zhao, A. Patel, E. Velasquez, D. Chen and W. Li, *J. Manuf. Sci. Eng.*, 2024, **147**, 041004.

Open Access Article. Published on 06 January 2026. Downloaded on 1/16/2026 12:17:14 PM. This article is licensed under a Creative Commons Attribution-NonCommercial 3.0 Unported Licence.

192 A. K. Katiyar, J. Choi and J.-H. Ahn, *Nano Convergence*, 2025, **12**, 11.
193 J. Jiang, K. Parto, W. Cao and K. Banerjee, *IEEE J. Electron Devices Soc.*, 2019, **7**, 878–887.
194 R. R. Das, T. R. Rajalekshmi and A. James, *IEEE Access*, 2024, **12**, 50556–50577.
195 X. Zheng, J. Wang, J. Jiang, T. Zhang, J. Zhu, T. Dang, P. Wu, A.-Y. Lu, D.-R. Chen, T. H. Yang, X. Zhang, K. Zhang, K. Y. Ma, Z. Wang, A. Yao, H. Liu, Y. Wan, Y.-P. Hsieh, V. Bulović, T. Palacios and J. Kong, *Nature*, 2025, **645**, 906–914.
196 N. Hong, D. Kireev, Q. Zhao, D. Chen, D. Akinwande and W. Li, *Adv. Mater.*, 2022, **34**, 2106615.
197 H. Xin, Q. Zhao, D. Chen and W. Li, *J. Micro Nano-Manuf.*, 2018, **6**, 031004.
198 Y. R. Lim, J. K. Han, S. K. Kim, Y. B. Lee, Y. Yoon, S. J. Kim, B. K. Min, Y. Kim, C. Jeon, S. Won, J.-H. Kim, W. Song, S. Myung, S. S. Lee, K.-S. An and J. Lim, *Adv. Mater.*, 2018, **30**, 1705270.
199 B. N. Chandrashekar, B. Deng, A. S. Smitha, Y. Chen, C. Tan, H. Zhang, H. Peng and Z. Liu, *Adv. Mater.*, 2015, **27**, 5210–5216.
200 S. Bae, H. Kim, Y. Lee, X. Xu, J.-S. Park, Y. Zheng, J. Balakrishnan, T. Lei, H. Ri Kim, Y. I. Song, Y.-J. Kim, K. S. Kim, B. Özyilmaz, J.-H. Ahn, B. H. Hong and S. Iijima, *Nat. Nanotechnol.*, 2010, **5**, 574–578.
201 Y. Zhao, J. Liao, S. Bu, Z. Hu, J. Hu, Q. Lu, M. Shang, B. Guo, G. Chen, Q. Zhao, K. Jia, G. Wang, E. Errington, Q. Xie, Y. Zhang, M. Guo, B. Mao, L. Lin and Z. Liu, *Nat. Chem. Eng.*, 2025, **2**, 296–308.
202 T. Kobayashi, M. Bando, N. Kimura, K. Shimizu, K. Kadono, N. Umezu, K. Miyahara, S. Hayazaki, S. Nagai, Y. Mizuguchi, Y. Murakami and D. Hobara, *Appl. Phys. Lett.*, 2013, **102**, 023112.
203 M. C. Lemme, D. Akinwande, C. Huyghebaert and C. Stampfer, *Nat. Commun.*, 2022, **13**, 1392.
204 X. Ma, Y. Ma, P. Cunha, Q. Liu, K. Kudtarkar, D. Xu, J. Wang, Y. Chen, Z. J. Wong, M. Liu, M. C. Hipwell and S. Lan, *Laser Photonics Rev.*, 2022, **16**, 2100658.
205 B. Liang, D. Xu, N. Yu, Y. Xu, X. Ma, Q. Liu, M. S. Asif, R. Yan and M. Liu, *ACS Appl. Mater. Interfaces*, 2022, **14**, 27397–27404.
206 I. Gasparutti, S. H. Song, M. Neumann, X. Wei, K. Watanabe, T. Taniguchi and Y. H. Lee, *ACS Appl. Mater. Interfaces*, 2020, **12**, 7701–7709.
207 Z. Li, Y. Wang, A. Kozbial, G. Shenoy, F. Zhou, R. McGinley, P. Ireland, B. Morganstein, A. Kunkel, S. P. Surwade, L. Li and H. Liu, *Nat. Mater.*, 2013, **12**, 925–931.
208 A. Kozbial, Z. Li, J. Sun, X. Gong, F. Zhou, Y. Wang, H. Xu, H. Liu and L. Li, *Carbon*, 2014, **74**, 218–225.
209 P. Cao, K. Xu, J. O. Varghese and J. R. Heath, *Nano Lett.*, 2011, **11**, 5581–5586.
210 F. R. Bagsican, A. Winchester, S. Ghosh, X. Zhang, L. Ma, M. Wang, H. Murakami, S. Talapatra, R. Vajtai, P. M. Ajayan, J. Kono, M. Tonouchi and I. Kawayama, *Sci. Rep.*, 2017, **7**, 1774.
211 F. K. Perkins, A. L. Friedman, E. Cobas, P. M. Campbell, G. G. Jernigan and B. T. Jonker, *Nano Lett.*, 2013, **13**, 668–673.
212 B. Cho, M. G. Hahm, M. Choi, J. Yoon, A. R. Kim, Y.-J. Lee, S.-G. Park, J.-D. Kwon, C. S. Kim, M. Song, Y. Jeong, K.-S. Nam, S. Lee, T. J. Yoo, C. G. Kang, B. H. Lee, H. C. Ko, P. M. Ajayan and D.-H. Kim, *Sci. Rep.*, 2015, **5**, 8052.
213 F. Urban, F. Giubileo, A. Grillo, L. Iemmo, G. Luongo, M. Passacantando, T. Foller, L. Madauß, E. Pollmann, M. P. Geller, D. Oing, M. Schleberger and A. Di Bartolomeo, *2D Mater.*, 2019, **6**, 045049.
214 A. Favron, E. Gaufrès, F. Fossard, A.-L. Phaneuf-L'Heureux, N. Y. W. Tang, P. L. Lévesque, A. Loiseau, R. Leonelli, S. Francoeur and R. Martel, *Nat. Mater.*, 2015, **14**, 826–832.
215 S. McDonnell, R. Addou, C. Buie, R. M. Wallace and C. L. Hinkle, *ACS Nano*, 2014, **8**, 2880–2888.
216 D. M. Sim, M. Kim, S. Yim, M.-J. Choi, J. Choi, S. Yoo and Y. S. Jung, *ACS Nano*, 2015, **9**, 12115–12123.
217 S. Park, A. T. Garcia-Esparza, H. Abroshan, B. Abraham, J. Vinson, A. Gallo, D. Nordlund, J. Park, T. R. Kim, L. Vallez, R. Alonso-Mori, D. Sokaras and X. Zheng, *Adv. Sci.*, 2021, **8**, 2002768.
218 S. Sovizi, S. Tosoni and R. Szoszkiewicz, *Nanoscale Adv.*, 2022, **4**, 4517–4525.
219 L. Peng, N. Abbasi, Y. Xiao and Z. Xie, *Adv. Mater. Interfaces*, 2020, **7**, 2001538.
220 L. Bai, M. Jiang, L. Qu, P. Zhu, W. Wu, Q. Li, Z. Guo, X. Sun, Z. Huang, M. Xie, W. Cai, S. Wang, X. Ma, M. Ren and J. Xu, *Adv. Opt. Mater.*, 2025, e01588.
221 A. Quellmalz, X. Wang, S. Sawallich, B. Uzlu, M. Otto, S. Wagner, Z. Wang, M. Prechtl, O. Hartwig, S. Luo, G. S. Duesberg, M. C. Lemme, K. B. Gylfason, N. Roxhed, G. Stemme and F. Niklaus, *Nat. Commun.*, 2021, **12**, 917.
222 D. I. Yakubovsky, Y. V. Stebunov, R. V. Kirtaev, G. A. Ermolaev, M. S. Mironov, S. M. Novikov, A. V. Arsenin and V. S. Volkov, *Adv. Mater. Interfaces*, 2019, **6**, 1900196.
223 M. S. Mironov, D. I. Yakubovsky, G. A. Ermolaev, I. A. Khramtsov, R. V. Kirtaev, A. S. Slavich, G. I. Tselikov, A. A. Vyshnevyy, A. V. Arsenin, V. S. Volkov and K. S. Novoselov, *Nano Lett.*, 2024, **24**, 16270–16275.
224 Y. Xu, J. Zhang, X. Han, X. Wang, C. Ye, W. Mu, Z. Jia and K. Qian, *ACS Appl. Mater. Interfaces*, 2023, **15**, 25831–25837.
225 V. Kochat, A. Samanta, Y. Zhang, S. Bhowmick, P. Manimunda, S. A. S. Asif, A. S. Stender, R. Vajtai, A. K. Singh, C. S. Tiwary and P. M. Ajayan, *Sci. Adv.*, 2018, **4**, e1701373.
226 J. Zhao, L. Li, P. Li, L. Dai, J. Dong, L. Zhou, Y. Wang, P. Zhang, K. Ji, Y. Zhang, H. Yu, Z. Wei, J. Li, X. Li, Z. Huang, B. Wang, J. Liu, Y. Chen, X. Zhang, S. Wang, N. Li, W. Yang, D. Shi, J. Pan, S. Du, L. Du and G. Zhang, *Nature*, 2025, **639**, 354–359.
227 R. Mirzayev, K. Mustonen, M. R. A. Monazam, A. Mittelberger, T. J. Pennycook, C. Mangler, T. Susi, J. Kotakoski and J. C. Meyer, *Sci. Adv.*, 2017, **3**, e1700176.
228 M. Gyeon, J. E. Seo, S. Oh, G. Noh, C. Lee, M. Choi, S. Kwon, T. S. Kim, H. Y. Jeong, S. Song, J. Chang and K. Kang, *ACS Nano*, 2024, **18**, 33977–33987.

 This journal is © The Royal Society of Chemistry 2025

Open Access Article. Published on 06 January 2026. Downloaded on 1/16/2026 12:17:14 PM. This article is licensed under a Creative Commons Attribution-NonCommercial 3.0 Unported Licence.

229 E. J. Telford, A. Benyamini, D. Rhodes, D. Wang, Y. Jung, A. Zangiabadi, K. Watanabe, T. Taniguchi, S. Jia, K. Barmak, A. N. Pasupathy, C. R. Dean and J. Hone, *Nano Lett.*, 2018, **18**, 1416–1420.

230 H. Y. Lee, Z. Wang, G. Chen, L. N. Holtzman, X. Yan, J. Amontree, A. Zangiabadi, K. Watanabe, T. Taniguchi, K. Barmak, P. Kim and J. C. Hone, *ACS Nano*, 2024, **18**, 17111–17118.

231 A. Pirkle, J. Chan, A. Venugopal, D. Hinojos, C. W. Magnuson, S. McDonnell, L. Colombo, E. M. Vogel, R. S. Ruoff and R. M. Wallace, *Appl. Phys. Lett*, 2011, **99**, 122108.

232 J. W. Suk, W. H. Lee, J. Lee, H. Chou, R. D. Piner, Y. Hao, D. Akinwande and R. S. Ruoff, *Nano Lett.*, 2013, **13**, 1462–1467.

233 S. W. Tong, M. Chen, X. Ju, J. Chai, J.-Y. Kim, J. Kim, H. K. Ng, B. Y. H. Tan and D. Chi, *Nanoscale*, 2025, **17**, 21554–21564.

234 H. Liu, Y. Li, K. Yang, L. Guo, Z. Zeng and Y. Yao, *J. Mater. Chem. C*, 2025, **13**, 19606–19614.

235 A. Gurarslan, Y. Yu, L. Su, Y. Yu, F. Suarez, S. Yao, Y. Zhu, M. Ozturk, Y. Zhang and L. Cao, *ACS Nano*, 2014, **8**, 11522–11528.

236 D. Marinov, J.-F. de Marneffe, Q. Smets, G. Arutchelvan, K. M. Bal, E. Voronina, T. Rakhimova, Y. Mankelevich, S. El Kazzi, A. Nalin Mehta, P.-J. Wyndaele, M. H. Heyne, J. Zhang, P. C. With, S. Banerjee, E. C. Neyts, I. Asselberghs, D. Lin and S. De Gendt, *npj 2D Mater. Appl.*, 2021, **5**, 17.

237 W. Zhu, T. Low, V. Perebeinos, A. A. Bol, Y. Zhu, H. Yan, J. Tersoff and P. Avouris, *Nano Lett.*, 2012, **12**, 3431–3436.

238 Y. Zhao, Y. Song, Z. Hu, W. Wang, Z. Chang, Y. Zhang, Q. Lu, H. Wu, J. Liao, W. Zou, X. Gao, K. Jia, L. Zhuo, J. Hu, Q. Xie, R. Zhang, X. Wang, L. Sun, F. Li, L. Zheng, M. Wang, J. Yang, B. Mao, T. Fang, F. Wang, H. Zhong, W. Liu, R. Yan, J. Yin, Y. Zhang, Y. Wei, H. Peng, L. Lin and Z. Liu, *Nat. Commun.*, 2022, **13**, 4409.

239 H. Li, A. W. Contryman, X. Qian, S. M. Ardakani, Y. Gong, X. Wang, J. M. Weisse, C. H. Lee, J. Zhao, P. M. Ajayan, J. Li, H. C. Manoharan and X. Zheng, *Nat. Commun.*, 2015, **6**, 7381.

240 R. Zhang, Y. Lai, W. Chen, C. Teng, Y. Sun, L. Yang, J. Wang, B. Liu and H.-M. Cheng, *ACS Nano*, 2022, **16**, 6309–6316.

241 A. P. Rooney, Z. Li, W. Zhao, A. Gholinia, A. Kozikov, G. Auton, F. Ding, R. V. Gorbachev, R. J. Young and S. J. Haigh, *Nat. Commun.*, 2018, **9**, 3597.

242 E. Wang, Z. Xiong, Z. Chen, Z. Xin, H. Ma, H. Ren, B. Wang, J. Guo, Y. Sun, X. Wang, C. Li, X. Li and K. Liu, *Nat. Commun.*, 2023, **14**, 4324.

243 S. Hwang, Y. Hwang, B. Park, J. Ah Lee, D.-H. Choi, A. Ra Kim, S.-K. Lee, J.-D. Kwon, S.-H. Kwon and Y. Kim, *Appl. Surf. Sci.*, 2022, **604**, 154523.

244 H. Chou, A. Ismach, R. Ghosh, R. S. Ruoff and A. Dolocan, *Nat. Commun.*, 2015, **6**, 7482.

245 X. Ma, Y. Zhu, N. Yu, S. Kim, Q. Liu, L. Apontti, D. Xu, R. Yan and M. Liu, *Nano Lett.*, 2019, **19**, 100–107.

246 P. V. Pham, T.-H. Mai, S. P. Dash, V. Biju, Y.-L. Chueh, D. Jariwala and V. Tung, *ACS Nano*, 2024, **18**, 14841–14876.

247 R. Tilmann, C. Bartlam, O. Hartwig, B. Tywoniuk, N. Dominik, C. P. Cullen, L. Peters, T. Stimpel-Lindner, N. McEvoy and G. S. Duesberg, *ACS Nano*, 2023, **17**, 10617–10627.

248 J. J. Schwartz, H.-J. Chuang, M. R. Rosenberger, S. V. Sivaram, K. M. McCreary, B. T. Jonker and A. Centrone, *ACS Appl. Mater. Interfaces*, 2019, **11**, 25578–25585.

249 X. Ma, Y. Zhu, S. Kim, Q. Liu, P. Byrley, Y. Wei, J. Zhang, K. Jiang, S. Fan, R. Yan and M. Liu, *Nano Lett.*, 2016, **16**, 6896–6902.

250 H. Y. Lee, S. Sarkar, K. Reidy, A. Kumar, J. Klein, K. Watanabe, T. Taniguchi, J. M. LeBeau, F. M. Ross and S. Gradečak, *Nat. Commun.*, 2022, **13**, 5000.

251 N. P. Lockyer, S. Aoyagi, J. S. Fletcher, I. S. Gilmore, P. A. W. van der Heide, K. L. Moore, B. J. Tyler and L.-T. Weng, *Nat. Rev. Methods Primers*, 2024, **4**, 32.

252 Z. Cheng, Q. Zhou, C. Wang, Q. Li, C. Wang and Y. Fang, *Nano Lett.*, 2011, **11**, 767–771.

253 H. J. Jeong, H. Y. Kim, S. Y. Jeong, J. T. Han, K.-J. Baeg, J. Y. Hwang and G.-W. Lee, *Carbon*, 2014, **66**, 612–618.

254 W. Fu, J. Chai, H. Kawai, T. Maddumapatabandi, F. Bussolotti, D. Huang, R. Lee, S. L. Teo, H. R. Tan, C. P. Y. Wong, A. Sng, Y. Chen, C. S. Lau, M. Zhang, H. Medina, M. Lin, M. Bosman and K. E. J. Goh, *Nat. Commun.*, 2025, **16**, 8488.

255 W. J. Choi, Y. J. Chung, S. Park, C.-S. Yang, Y. K. Lee, K.-S. An, Y.-S. Lee and J.-O. Lee, *Adv. Mater.*, 2014, **26**, 637–644.

256 N. Peltekis, S. Kumar, N. McEvoy, K. Lee, A. Weidlich and G. S. Duesberg, *Carbon*, 2012, **50**, 395–403.

257 J. Sun, H. O. Finklea and Y. Liu, *Nanotechnology*, 2017, **28**, 125703.

258 R. Jalilian, L. A. Jauregui, G. Lopez, J. Tian, C. Roecker, M. M. Yazdanpanah, R. W. Cohn, I. Jovanovic and Y. P. Chen, *Nanotechnology*, 2011, **22**, 295705.

259 X. Sun, M. Suriyage, A. R. Khan, M. Gao, J. Zhao, B. Liu, M. M. Hasan, S. Rahman, R. S. Chen, P. K. Lam and Y. Lu, *Chem. Rev.*, 2024, **124**, 1992–2079.

260 H. Tian, E. Codecido, D. Mao, K. Zhang, S. Che, K. Watanabe, T. Taniguchi, D. Smirnov, E.-A. Kim, M. Bockrath and C. N. Lau, *Nat. Phys.*, 2024, **20**, 1407–1412.

261 Y. Li, C. Shi, F. Zhang, X. Liu, Y. Xue, V.-A. Ha, Q. Gao, C. Dong, Y.-C. Lin, L. N. Holtzman, N. Morales-Durán, H. Kim, Y. Jiang, M. Holbrook, J. Hone, K. Barmak, J. A. Robinson, X. Li, F. Giustino, E. Khalaf, Y. Han and C.-K. Shih, *Nat. Phys.*, 2025, **21**, 1085–1092.

262 Q. Fu, P. Wang, C. Huang, Y. V. Kartashov, L. Torner, V. V. Konotop and F. Ye, *Nat. Photonics.*, 2020, **14**, 663–668.

263 V. E. Calado, G. F. Schneider, A. M. M. G. Theulings, C. Dekker and L. M. K. Vandersypen, *Appl. Phys. Lett*, 2012, **101**, 103116.

264 M. Ishigami, J. H. Chen, W. G. Cullen, M. S. Fuhrer and E. D. Williams, *Nano Lett.*, 2007, **7**, 1643–1648.

Open Access Article. Published on 06 January 2026. Downloaded on 1/16/2026 12:17:14 PM. This article is licensed under a Creative Commons Attribution-NonCommercial 3.0 Unported Licence.

265 P. Sutter, J. T. Sadowski and E. Sutter, *Phys. Rev. B:Condens. Matter Mater. Phys.*, 2009, **80**, 245411.
266 F. Guinea, B. Horovitz and P. Le Doussal, *Phys. Rev. B:Condens. Matter Mater. Phys.*, 2008, **77**, 205421.
267 V. M. Pereira, A. H. Castro Neto, H. Y. Liang and L. Mahadevan, *Phys. Rev. Lett.*, 2010, **105**, 156603.
268 J. Lu, W. Wu, F. M. Colombari, A. Jawaid, B. Seymour, K. Whisnant, X. Zhong, W. Choi, N. Chalmpes, J. Lahann, R. A. Vaia, A. F. de Moura, D. Nepal and N. A. Kotov, *Nature*, 2024, **630**, 860–865.
269 I. Abdelwahab, B. Tilmann, Y. Wu, D. Giovanni, I. Verzhbitskiy, M. Zhu, R. Berté, F. Xuan, L. D. S. Menezes, G. Eda, T. C. Sum, S. Y. Quek, S. A. Maier and K. P. Loh, *Nat. Photonics*, 2022, **16**, 644–650.
270 W. Han, X. Zheng, K. Yang, C. S. Tsang, F. Zheng, L. W. Wong, K. H. Lai, T. Yang, Q. Wei, M. Li, W. F. Io, F. Guo, Y. Cai, N. Wang, J. Hao, S. P. Lau, C.-S. Lee, T. H. Ly, M. Yang and J. Zhao, *Nat. Nanotechnol.*, 2023, **18**, 55–63.
271 E. Blundo, T. Yildirim, G. Pettinari and A. Polimeni, *Phys. Rev. Lett.*, 2021, **127**, 046101.
272 D. A. Sanchez, Z. Dai and N. Lu, *Trends Chem.*, 2021, **3**, 204–217.
273 J. Xiong, Y. Cai, W. Dong, X. Luo, Z. Yu, B. Liu, L. Liu, T. Liang, Z. Wang, Y. Gao and B. Wang, *Chem. Catal.*, 2024, **4**, 16074–16085.
274 A. V. Tyurnina, D. A. Bandurin, E. Khestanova, V. G. Kravets, M. Koperski, F. Guinea, A. N. Grigorenko, A. K. Geim and I. V. Grigorieva, *ACS Photonics*, 2019, **6**, 516–524.
275 J. Feng, X. Qian, C.-W. Huang and J. Li, *Nat. Photonics.*, 2012, **6**, 866–872.
276 H. K. Ng, D. Xiang, A. Suwardi, G. Hu, K. Yang, Y. Zhao, T. Liu, Z. Cao, H. Liu, S. Li, J. Cao, Q. Zhu, Z. Dong, C. K. I. Tan, D. Chi, C.-W. Qiu, K. Hippalgaonkar, G. Eda, M. Yang and J. Wu, *Nat. Electron.*, 2022, **5**, 489–496.
277 G. Wang, Z. Dai, J. Xiao, S. Feng, C. Weng, L. Liu, Z. Xu, R. Huang and Z. Zhang, *Phys. Rev. Lett.*, 2019, **123**, 116101.
278 H. Schmidt, T. Lüdtke, P. Barthold, E. McCann, V. I. Fal'ko and R. J. Haug, *Appl. Phys. Lett*, 2008, **93**, 172108.
279 X. Du, Y. Lee, Y. Zhang, T. Yu, K. Kim and N. Liu, *ACS Appl. Mater. Interfaces*, 2021, **13**, 22819–22827.
280 H. Zhao, B. Wang, F. Liu, X. Yan, H. Wang, W. S. Leong, M. J. Stevens, P. Vashishta, A. Nakano, J. Kong, R. Kalia and H. Wang, *Adv. Funct. Mater.*, 2020, **30**, 1908691.
281 Y. Wakafuji, R. Moriya, S. Masubuchi, K. Watanabe, T. Taniguchi and T. Machida, *Nano Lett.*, 2020, **20**, 2486–2492.
282 L. Liu, Y. Chen, L. Chen, B. Xie, G. Li, L. Kong, Q. Tao, Z. Li, X. Yang, Z. Lu, L. Ma, D. Lu, X. Yang and Y. Liu, *Nat. Commun.*, 2024, **15**, 165.
283 W. Zhang, Z. Zhao, Y. Yang, Y. Zhang, H. Hao, L. Li, W. Xu, B. Peng, R. Long and N. Liu, *ACS Appl. Mater. Interfaces*, 2021, **13**, 40922–40931.
284 B. Wang, M. Huang, N. Y. Kim, B. V. Cunning, Y. Huang, D. Qu, X. Chen, S. Jin, M. Biswal, X. Zhang, S. H. Lee, H. Lim, W. J. Yoo, Z. Lee and R. S. Ruoff, *Nano Lett.*, 2017, **17**, 1467–1473.
285 W. Xu, Z. Qin, C.-T. Chen, H. R. Kwag, Q. Ma, A. Sarkar, M. J. Buehler and D. H. Gracias, *Sci. Adv.*, 2017, **3**, e1701084.
286 Z. Zhen and H. Zhu, *Graphene*, 2018, 1–12.
287 A. K. Geim, *Science*, 2009, **324**, 1530–1534.
288 G. Gui, J. Li and J. Zhong, *Phys. Rev. B:Condens. Matter Mater. Phys.*, 2008, **78**, 075435.
289 B. Aslan, M. Deng and T. F. Heinz, *Phys. Rev. B*, 2018, **98**, 115308.
290 L. Wang, A. Baumgartner, P. Makk, S. Zihlmann, B. S. Varghese, D. I. Indolese, K. Watanabe, T. Taniguchi and C. Schönenberger, *Commun. Phys.*, 2021, **4**, 147.
291 M. Farjam and H. Rafii-Tabar, *Phys. Rev. B:Condens. Matter Mater. Phys.*, 2009, **80**, 167401.
292 D. Zhan, J. Yan, L. Lai, Z. Ni, L. Liu and Z. Shen, *Adv. Mater.*, 2012, **24**, 4055–4069.
293 V. M. Pereira, A. H. Castro Neto and N. M. R. Peres, *Phys. Rev. B:Condens. Matter Mater. Phys.*, 2009, **80**, 045401.
294 Y. Zhang, Y. Jin, J. Liu, Q. Ren, Z. Chen, Y. Zhao and P. Zhao, *Nanoscale Adv.*, 2022, **4**, 5056–5061.
295 L. Gong, I. A. Kinloch, R. J. Young, I. Riaz, R. Jalil and K. S. Novoselov, *Adv. Mater.*, 2010, **22**, 2694–2697.
296 H. J. Conley, B. Wang, J. I. Ziegler, R. F. Haglund, Jr., S. T. Pantelides and K. I. Bolotin, *Nano Lett.*, 2013, **13**, 3626–3630.
297 Y. Guo, S. Yu, C. Lu, L. Hu, W. Su and L. Li, *Adv. Mater. Interfaces*, 2023, **10**, 2201531.
298 T. M. G. Mohiuddin, A. Lombardo, R. R. Nair, A. Bonetti, G. Savini, R. Jalil, N. Bonini, D. M. Basko, C. Galiotis, N. Marzari, K. S. Novoselov, A. K. Geim and A. C. Ferrari, *Phys. Rev. B:Condens. Matter Mater. Phys.*, 2009, **79**, 205433.
299 Y. Shin, S. Hong, Y. C. Hur, C. Lim, K. Do, J. H. Kim, D.-H. Kim and S. Lee, *Nat. Mater.*, 2024, **23**, 1411–1420.
300 J.-B. Qiao, L.-J. Yin and L. He, *Phys. Rev. B*, 2018, **98**, 235402.
301 Y. Cheng, Z. Fan, T. Zhang, M. Nomura, S. Volz, G. Zhu, B. Li and S. Xiong, *Mater. Today Phys.*, 2023, **35**, 101093.
302 Z. Hao, A. M. Zimmerman, P. Ledwith, E. Khalaf, D. H. Najafabadi, K. Watanabe, T. Taniguchi, A. Vishwanath and P. Kim, *Science*, 2021, **371**, 1133–1138.
303 X.-D. Chen, W. Xin, W.-S. Jiang, Z.-B. Liu, Y. Chen and J.-G. Tian, *Adv. Mater.*, 2016, **28**, 2563–2570.
304 K. He, N. Kumar, L. Zhao, Z. Wang, K. F. Mak, H. Zhao and J. Shan, *Phys. Rev. Lett.*, 2014, **113**, 026803.
305 J. W. Matthews and A. E. Blakeslee, *J. Cryst. Growth*, 1974, **27**, 118–125.
306 S. Roy, A. Joseph, X. Zhang, S. Bhattacharyya, A. B. Puthirath, A. Biswas, C. S. Tiwary, R. Vajtai and P. M. Ajayan, *Chem Rev.*, 2024, **124**, 9376–9456.
307 A. Luican, G. Li, A. Reina, J. Kong, R. R. Nair, K. S. Novoselov, A. K. Geim and E. Y. Andrei, *Phys. Rev. Lett.*, 2011, **106**, 126802.
308 A. Kerelsky, L. J. McGilly, D. M. Kennes, L. Xian, M. Yankowitz, S. Chen, K. Watanabe, T. Taniguchi, J. Hone,

Open Access Article. Published on 06 January 2026. Downloaded on 1/16/2026 12:17:14 PM. This article is licensed under a Creative Commons Attribution-NonCommercial 3.0 Unported Licence.

C. Dean, A. Rubio and A. N. Pasupathy, *Nature*, 2019, **572**, 95–100.
309 Y. Cao, D. Chowdhury, D. Rodan-Legrain, O. Rubies-Bigorda, K. Watanabe, T. Taniguchi, T. Senthil and P. Jarillo-Herrero, *Phys. Rev. Lett.*, 2020, **124**, 076801.
310 A. L. Sharpe, E. J. Fox, A. W. Barnard, J. Finney, K. Watanabe, T. Taniguchi, M. A. Kastner and D. Goldhaber-Gordon, *Science*, 2019, **365**, 605–608.
311 Y. Cao, V. Fatemi, A. Demir, S. Fang, S. L. Tomarken, J. Y. Luo, J. D. Sanchez-Yamagishi, K. Watanabe, T. Taniguchi, E. Kaxiras, R. C. Ashoori and P. Jarillo-Herrero, *Nature*, 2018, **556**, 80–84.
312 A. De Sanctis, J. D. Mehew, S. Alkhalifa, F. Withers, M. F. Craciun and S. Russo, *Nano Lett.*, 2018, **18**, 7919–7926.
313 B. Hunt, J. D. Sanchez-Yamagishi, A. F. Young, M. Yankowitz, B. J. LeRoy, K. Watanabe, T. Taniguchi, P. Moon, M. Koshino, P. Jarillo-Herrero and R. C. Ashoori, *Science*, 2013, **340**, 1427–1430.
314 D. R. Hofstadter, *Phys. Rev. B*, 1976, **14**, 2239–2249.
315 L. A. Ponomarenko, R. V. Gorbachev, G. L. Yu, D. C. Elias, R. Jalil, A. A. Patel, A. Mishchenko, A. S. Mayorov, C. R. Woods, J. R. Wallbank, M. Mucha-Kruczynski, B. A. Piot, M. Potemski, I. V. Grigorieva, K. S. Novoselov, F. Guinea, V. I. Fal'ko and A. K. Geim, *Nature*, 2013, **497**, 594–597.
316 K. P. Nuckolls, M. G. Scheer, D. Wong, M. Oh, R. L. Lee, J. Herzog-Arbeitman, K. Watanabe, T. Taniguchi, B. Lian and A. Yazdani, *Nature*, 2025, **639**, 60–66.
317 M. Yankowitz, J. Xue, D. Cormode, J. D. Sanchez-Yamagishi, K. Watanabe, T. Taniguchi, P. Jarillo-Herrero, P. Jacquod and B. J. LeRoy, *Nat. Phys.*, 2012, **8**, 382–386.
318 D. S. Lee, C. Riedl, T. Beringer, A. H. Castro Neto, K. von Klitzing, U. Starke and J. H. Smet, *Phys. Rev. Lett.*, 2011, **107**, 216602.
319 M. Serlin, C. L. Tschirhart, H. Polshyn, Y. Zhang, J. Zhu, K. Watanabe, T. Taniguchi, L. Balents and A. F. Young, *Science*, 2020, **367**, 900–903.
320 G. Chen, L. Jiang, S. Wu, B. Lyu, H. Li, B. L. Chittari, K. Watanabe, T. Taniguchi, Z. Shi, J. Jung, Y. Zhang and F. Wang, *Nat. Phys.*, 2019, **15**, 237–241.
321 G. Chen, A. L. Sharpe, P. Gallagher, I. T. Rosen, E. J. Fox, L. Jiang, B. Lyu, H. Li, K. Watanabe, T. Taniguchi, J. Jung, Z. Shi, D. Goldhaber-Gordon, Y. Zhang and F. Wang, *Nature*, 2019, **572**, 215–219.
322 Q. Tong, H. Yu, Q. Zhu, Y. Wang, X. Xu and W. Yao, *Nat. Phys.*, 2017, **13**, 356–362.
323 S. Lisi, X. Lu, T. Benschop, T. A. de Jong, P. Stepanov, J. R. Duran, F. Margot, I. Cucchi, E. Cappelli, A. Hunter, A. Tamai, V. Kandyba, A. Giampietri, A. Barinov, J. Jobst, V. Stalman, M. Leeuwenhoek, K. Watanabe, T. Taniguchi, L. Rademaker, S. J. van der Molen, M. P. Allan, D. K. Efetov and F. Baumberger, *Nat. Phys.*, 2021, **17**, 189–193.
324 A. C. Gadelha, D. A. A. Ohlberg, F. C. Santana, G. S. N. Eliel, J. S. Lemos, V. Ornelas, D. Miranda, R. B. Nadas, K. Watanabe, T. Taniguchi, C. Rabelo, P. P. D. M. Venezuela, G. Medeiros-Ribeiro, A. Jorio, L. G. Cançado and L. C. Campos, *ACS Appl. Nano Mater.*, 2021, **4**, 1858–1866.
325 A. A. Puretzky, L. Liang, X. Li, K. Xiao, B. G. Sumpter, V. Meunier and D. B. Geohegan, *ACS Nano*, 2016, **10**, 2736–2744.
326 K. Kim, M. Yankowitz, B. Fallahazad, S. Kang, H. C. P. Movva, S. Huang, S. Larentis, C. M. Corbet, T. Taniguchi, K. Watanabe, S. K. Banerjee, B. J. LeRoy and E. Tutuc, *Nano Lett.*, 2016, **16**, 1989–1995.
327 Q. Sun, J. Lin, P. L. Hernandez-Martine, T. Li, Y. Li, L. Li, C. Wan, N. Mao, H. Yu, P. Wang, H. V. Demir, Z. Hu, R. Su and W. Xu, *Nat. Commun.*, 2025, **16**, 2712.
328 Y. Hassan, B. Singh, M. Joe, B.-M. Son, T. D. Ngo, Y. Jang, S. Sett, A. Singha, R. Biswas, M. Bhakar, K. Watanabe, T. Taniguchi, V. Raghunathan, G. Sheet, Z. Lee, W. J. Yoo, P. K. Srivastava and C. Lee, *Adv. Mater.*, 2024, **36**, 2406290.
329 S. Du, W. Yang, H. Gao, W. Dong, B. Xu, K. Watanabe, T. Taniguchi, J. Zhao, F. Zheng, J. Zhou and S. Zheng, *Adv. Mater.*, 2024, **36**, 2404177.
330 M. Xu, H. Ji, L. Zheng, W. Li, J. Wang, H. Wang, L. Luo, Q. Lu, X. Gan, Z. Liu, X. Wang and W. Huang, *Nat. Commun.*, 2024, **15**, 562.
331 I. Cheliotis and I. Zergioti, *2D Mater.*, 2024, **11**, 022004.
332 C. N. Lau, M. W. Bockrath, K. F. Mak and F. Zhang, *Nature*, 2022, **602**, 41–50.
333 Q. Tao, R. Wu, Q. Li, L. Kong, Y. Chen, J. Jiang, Z. Lu, B. Li, W. Li, Z. Li, L. Liu, X. Duan, L. Liao and Y. Liu, *Nat. Commun.*, 2021, **12**, 1825.
334 Y. Yang, J. Li, J. Yin, S. Xu, C. Mullan, T. Taniguchi, K. Watanabe, A. K. Geim, K. S. Novoselov and A. Mishchenko, *Sci. Adv.*, 2020, **6**, eabd3655.
335 X. Ma, Q. Liu, N. Yu, D. Xu, S. Kim, Z. Liu, K. Jiang, B. M. Wong, R. Yan and M. Liu, *Nat. Commun.*, 2021, **12**, 6868.
336 Y. Zhu, S. Kim, X. Ma, P. Byrley, N. Yu, Q. Liu, X. Sun, D. Xu, S. Peng, M. C. Hartel, S. Zhang, V. Jucaud, M. R. Dokmeci, A. Khademhosseini and R. Yan, *Nano Res.*, 2021, **14**, 4294–4303.
337 Y. Kim and J. Kim, *Nanophotonics*, 2021, **10**, 3397–3415.
338 M. Nørgaard, T. Yezekyan, S. Rolfs, C. Frydendahl, N. A. Mortensen and V. A. Zenin, *Nanophotonics*, 2025, **14**, 2473–2483.
339 Q. Fu and X. Bao, *Chem. Soc. Rev.*, 2017, **46**, 1842–1874.
340 L. Sortino, J. Biechteler, L. Lafeta, L. Kühner, A. Hartschuh, L. D. S. Menezes, S. A. Maier and A. Tittl, *Nat. Photonics.*, 2025, **19**, 825–832.
341 S. Kim, N. Yu, X. Ma, Y. Zhu, Q. Liu, M. Liu and R. Yan, *Nat. Photonics.*, 2019, **13**, 636–643.
342 R. Ribeiro-Palau, C. Zhang, K. Watanabe, T. Taniguchi, J. Hone and C. R. Dean, *Science*, 2018, **361**, 690–693.
343 K. Yao, N. R. Finney, J. Zhang, S. L. Moore, L. Xian, N. Tancogne-Dejean, F. Liu, J. Ardelean, X. Xu, D. Halbertal, K. Watanabe, T. Taniguchi, H. Ochoa, A. Asenjo-Garcia, X. Zhu, D. N. Basov, A. Rubio, C. R. Dean, J. Hone and P. J. Schuck, *Sci. Adv.*, 2021, **7**, eabe8691.
344 M. Zhang, N. Han, J. Zhang, J. Wang, X. Chen, J. Zhao and X. Gan, *Sci. Adv.*, 2023, **9**, eadf4571.

Open Access Article. Published on 06 January 2026. Downloaded on 1/16/2026 12:17:14 PM. This article is licensed under a Creative Commons Attribution-NonCommercial 3.0 Unported Licence.

345 K. Bian, C. Gerber, A. J. Heinrich, D. J. Müller, S. Scheuring and Y. Jiang, *Nat. Rev. Methods Primers*, 2021, **1**, 36.
346 A. Inbar, J. Birkbeck, J. Xiao, T. Taniguchi, K. Watanabe, B. Yan, Y. Oreg, A. Stern, E. Berg and S. Ilani, *Nature*, 2023, **614**, 682–687.
347 H. Tang, Y. Wang, X. Ni, K. Watanabe, T. Taniguchi, P. Jarillo-Herrero, S. Fan, E. Mazur, A. Yacoby and Y. Cao, *Nature*, 2024, **632**, 1038–1044.
348 K. S. Kim, J. Kwon, H. Ryu, C. Kim, H. Kim, E.-K. Lee, D. Lee, S. Seo, N. M. Han and J. M. Suh, *Nat. Nanotechnol.*, 2024, **19**, 895–906.
349 S. Zeng, C. Liu and P. Zhou, *Nat. Rev. Electr. Eng.*, 2024, **1**, 335–348.
350 Y.-C. Lu, J.-K. Huang, K.-Y. Chao, L.-J. Li and V. P.-H. Hu, *Nat. Nanotechnol.*, 2024, **19**, 1066–1072.
351 Y. Liu, X. Duan, H.-J. Shin, S. Park, Y. Huang and X. Duan, *Nature*, 2021, **591**, 43–53.
352 Y. Liu, J. Guo, E. Zhu, L. Liao, S.-J. Lee, M. Ding, I. Shakir, V. Gambin, Y. Huang and X. Duan, *Nature*, 2018, **557**, 696–700.
353 Z. Zhang, G. Liu, S. Gou, W. Hong, H. Jiang, Z. Xue, M. Zhang, W. Bao, Z. Tian and Z. Di, *Adv. Funct. Mater.*, 2025, **35**, 2418615.
354 K. Xing, D. McEwen, Y. Yin, W. Zhao, A. Bake, D. Cortie, J. Liu, T.-H.-Y. Vu, Y.-H. Chen, J. Hone, A. Stacey, M. T. Edmonds, N. V. Medhekar, K. Watanabe, T. Taniguchi, Q. Ou, D.-C. Qi and M. S. Fuhrer, *ACS Nano*, 2025, **19**, 3579–3588.
355 H. Liu, Q. H. Thi, P. Man, X. Chen, T. Chen, L. W. Wong, S. Jiang, L. Huang, T. Yang, K. H. Leung, T. T. Leung, S. Gao, H. Chen, C.-S. Lee, M. Kan, J. Zhao, Q. Deng and T. H. Ly, *Adv. Mater.*, 2023, **35**, 2210503.
356 G. Liu, Z. Tian, Z. Yang, Z. Xue, M. Zhang, X. Hu, Y. Wang, Y. Yang, P. K. Chu, Y. Mei, L. Liao, W. Hu and Z. Di, *Nat. Electron.*, 2022, **5**, 275–280.
357 D. Lu, Y. Chen, Z. Lu, L. Ma, Q. Tao, Z. Li, L. Kong, L. Liu, X. Yang, S. Ding, X. Liu, Y. Li, R. Wu, Y. Wang, Y. Hu, X. Duan, L. Liao and Y. Liu, *Nature*, 2024, **630**, 340–345.
358 L. Wang, P. Wang, J. Huang, B. Peng, C. Jia, Q. Qian, J. Zhou, D. Xu, Y. Huang and X. Duan, *Nat. Nanotechnol.*, 2022, **17**, 1206–1213.
359 J.-K. Huang, Y. Wan, J. Shi, J. Zhang, Z. Wang, W. Wang, N. Yang, Y. Liu, C.-H. Lin, X. Guan, L. Hu, Z.-L. Yang, B.-C. Huang, Y.-P. Chiu, J. Yang, V. Tung, D. Wang, K. Kalantar-Zadeh, T. Wu, X. Zu, L. Qiao, L.-J. Li and S. Li, *Nature*, 2022, **605**, 262–267.
360 S. Li, X. Liu, H. Yang, H. Zhu and X. Fang, *Nat. Electron.*, 2024, **7**, 216–224.
361 C.-Y. Lin, B.-C. Chen, Y.-C. Liu, S.-F. Kuo, H.-C. Tsai, Y.-M. Chang, C.-Y. Kuo, C.-F. Chang, J.-H. Chen, Y.-H. Chu, M. Yamamoto, C.-H. Shen, Y.-L. Chueh, P.-W. Chiu, Y.-C. Chen, J.-C. Yang and Y.-F. Lin, *Nat. Electron.*, 2025, **8**, 560–570.
362 Q. Tao, R. Wu, X. Zou, Y. Chen, W. Li, Z. Lu, L. Ma, L. Kong, D. Lu, X. Yang, W. Song, W. Li, L. Liu, S. Ding, X. Liu, X. Duan, L. Liao and Y. Liu, *Nat. Commun.*, 2024, **15**, 5774.
363 P. F. Satterthwaite, W. Zhu, P. Jastrzebska-Perfect, M. Tang, S. O. Spector, H. Gao, H. Kitadai, A.-Y. Lu, Q. Tan, S.-Y. Tang, Y.-L. Chueh, C.-N. Kuo, C. S. Lue, J. Kong, X. Ling and F. Niroui, *Nat. Electron.*, 2024, **7**, 17–28.
364 Z. Li, X. Liu, J. Shi, X. Cai, Y. Zhang, W. Chen, Y. Jin, H. Jiang, S. Y. Kim, C. Zhu, Y. Deng, Y. Liu, X. R. Wang, T. Li, J. Li, Z. Liu, H. Cai and W. Gao, *Nat. Electron.*, 2025, **8**, 571–577.
365 G. Zhan, B. Koek, Y. Yuan, Y. Liu, V. Mishra, V. Lenzi, K. Strutyński, C. Li, R. Zhang, X. Zhou, H. S. Choi, Z.-F. Cai, J. Almarza, K. S. Mali, A. Mateo-Alonso, M. M. Franco, Y. Zhu, S. De Feyter and K. P. Loh, *Nat. Chem.*, 2025, **17**, 518–524.
366 M. Hirano and K. Shinjo, *Phys. Rev. B:Condens. Matter Mater. Phys.*, 1990, **41**, 11837–11851.
367 M. Dienwiebel, G. S. Verhoeven, N. Pradeep, J. W. M. Frenken, J. A. Heimberg and H. W. Zandbergen, *Phys. Rev. Lett.*, 2004, **92**, 126101.
368 X. Li, Y. Ma, C. Choi, X. Ma, S. Chatterjee, S. Lan and M. C. Hipwell, *Adv. Mater.*, 2021, **33**, 2008337.
369 C. Choi, Y. Ma, X. Li, X. Ma and M. C. Hipwell, *ACS Appl. Mater. Interfaces*, 2021, **13**, 3303–3310.
370 Y. Tang, J. Xu, Q. Liu, X. Hu, W. Xue, Z. Liu, Z. Lin, H. Lin, Y. Zhang, Z. Zhang, X. Ma, J. Wang, J. Zhong, D. Wang, H. Jiang and Y. Ma, *Device*, 2024, **2**, 100365.
371 W. Xue, Y. Ren, Y. Tang, Z. Gong, T. Zhang, Z. Chen, X. Dong, X. Ma, Z. Wang, H. Xu, J. Zhao and Y. Ma, *Nat. Rev. Electr. Eng.*, 2025, **2**, 425–439.
372 Y. Ma, X. Li, X. Ma, C. Choi, L. Kruse, S. Lan and M. Cynthia Hipwell, *Commun. Mater.*, 2025, **6**, 1.
373 G. Hu, A. Krasnok, Y. Mazor, C.-W. Qiu and A. Alù, *Nano Lett.*, 2020, **20**, 3217–3224.
374 M. Chen, X. Lin, T. H. Dinh, Z. Zheng, J. Shen, Q. Ma, H. Chen, P. Jarillo-Herrero and S. Dai, *Nat. Mater.*, 2020, **19**, 1307–1311.
375 M.-L. Lin, Q.-H. Tan, J.-B. Wu, X.-S. Chen, J.-H. Wang, Y.-H. Pan, X. Zhang, X. Cong, J. Zhang, W. Ji, P.-A. Hu, K.-H. Liu and P.-H. Tan, *ACS Nano*, 2018, **12**, 8770–8780.
376 C. Zheng, G. Hu, J. Wei, X. Ma, Z. Li, Y. Chen, Z. Ni, P. Li, Q. Wang and C.-W. Qiu, *Nat. Commun.*, 2024, **15**, 7047.
377 K. Dong, T. Zhang, J. Li, Q. Wang, F. Yang, Y. Rho, D. Wang, C. P. Grigoropoulos, J. Wu and J. Yao, *Phys. Rev. Lett.*, 2021, **126**, 223601.
378 C. Jiang, M. Baggioli and Q.-D. Jiang, *Phys. Rev. Lett.*, 2024, **132**, 166901.
379 M. Yankowitz, Q. Ma, P. Jarillo-Herrero and B. J. LeRoy, *Nat. Rev. Phys.*, 2019, **1**, 112–125.
380 L. Zhou, X. Ni, Z. Wang, E. M. Renzi, J. Xu, Z. Zhou, Y. Yin, Y. Yin, R. Song, Z. Zhao, K. Yu, D. Huang, Z. Wang, X. Cheng, A. Alù and T. Jiang, *Nat. Commun.*, 2025, **16**, 2953.
381 J. Duan, N. Capote-Robayna, J. Taboada-Gutiérrez, G. Álvarez-Pérez, I. Prieto, J. Martín-Sánchez, A. Y. Nikitin and P. Alonso-González, *Nano Lett.*, 2020, **20**, 5323–5329.
382 Q. Guo, X.-Z. Qi, L. Zhang, M. Gao, S. Hu, W. Zhou, W. Zang, X. Zhao, J. Wang, B. Yan, M. Xu, Y.-K. Wu,

 This journal is © The Royal Society of Chemistry 2025

Open Access Article. Published on 06 January 2026. Downloaded on 1/16/2026 12:17:14 PM.
This article is licensed under a Creative Commons Attribution-NonCommercial 3.0 Unported Licence.

G. Eda, Z. Xiao, S. A. Yang, H. Gou, Y. P. Feng, G.-C. Guo, W. Zhou, X.-F. Ren, C.-W. Qiu, S. J. Pennycook and A. T. S. Wee, *Nature*, 2023, **613**, 53–59.

383 H. Hong, C. Huang, C. Ma, J. Qi, X. Shi, C. Liu, S. Wu, Z. Sun, E. Wang and K. Liu, *Phys. Rev. Lett.*, 2023, **131**, 233801.

384 Y. Tang, K. Sripathy, H. Qin, Z. Lu, G. Guccione, J. Janousek, Y. Zhu, M. Hasan, Y. Iwasa, P. K. Lam and Y. Lu, *Nat. Commun.*, 2024, **15**, 9979.

385 C. Trovatello, C. Ferrante, B. Yang, J. Bajo, B. Braun, Z. H. Peng, X. Xu, P. K. Jenke, A. Ye, M. Delor, D. N. Basov, J. Park, P. Walther, C. R. Dean, L. A. Rozema, A. Marini, G. Cerullo and P. J. Schuck, *Nat. Photonics.*, 2025, **19**, 291–299.

386 Z. Li, X. Ma, F. Wei, D. Wang, Z. Deng, M. Jiang, A. Siddiquee, K. Qi, D. Zhu, M. Zhao, M. Shen, P. Canepa, S. Kou, J. Lin and Q. Wang, *Adv. Mater.*, 2023, **35**, 2302468.

387 T. Mei, F. Chen, T. Huang, Z. Feng, T. Wan, Z. Han, Z. Li, L. Hu, C.-H. Lin, Y. Lu, W. Cheng, D.-C. Qi and D. Chu, *ACS Nano*, 2025, **19**, 17140–17172.

388 R. A. Wells and A. W. Robertson, *Adv. Electron. Mater.*, 2024, **10**, 2400121.

389 L. Qin, P. Guan, J. Shao, Y. Xiao, Y. Yu, J. Su, C. Zhang, Y. Li, S. Liu, P. Li, D. Ouyang, W. He, F. Liu, K. Zhu, K. Liu, Z. Yao, J. Wu, Y. Zhao, H. Li, F. Hui, P. Lin, M. Lanza, Y. Li and T. Zhai, *Nat. Nanotechnol.*, 2025, **20**, 1641–1647.

390 S. S. Teja Nibhanupudi, A. Roy, D. Veksler, M. Coupin, K. C. Matthews, M. Disiena, Ansh, J. V. Singh, I. R. Gearba-Dolocan, J. Warner, J. P. Kulkarni, G. Bersuker and S. K. Banerjee, *Nat. Commun.*, 2024, **15**, 2334.